Study on Integrated Redox Image Sensor Employing Square Wave Voltammetry

ABSTRACT

In this dissertation, an integrated square wave voltammetry redox image sensor has been developed on the basis of a standard complementary metal-oxide-semiconductor process technology for 2-dimensional chemical imaging and high-scan speed in electrochemical analysis. The field of electrochemical analysis is combined with the semiconductor technology in this study. The square wave voltammetry is a voltammetric technique which can be possible the high speed and high sensitivity measurement compared with cyclic voltammetry. High scan speed is suitable for the array sensor.

For miniaturization and high functional sensor, integration of the electrochemical system is needed. Portable diagnosis and high speed measurement system are developed with the demands for the point of care testing, the simple detecting, and on-site measurements in agriculture, environmental field, and medical science. Bulky external instruments should be miniaturized for simple and fast measurement. Electrochemical sensors using square wave voltammetry based on complementary metal-oxide-semiconductor technology would be possible to solve these requirements.

Square wave voltammetric technology is not new, however so far there is no report about integrated square wave voltammetry circuit on a single chip. The reason is that the general square wave voltammetry technique has a bulky and expensive equipment, and complexity of the measuring equipment. The proposed sensor in this study is the first integrated sensor system of a square wave pulse generator circuit. Compared with conventional square wave voltammetry method, our integrated square wave voltammetry redox sensor system has the advantages of potable diagnosis, on-site analysis, and simple detection. The square wave pulse was observed as expected. We confirmed that the proposed sensor system can detect potassium ferricyanide with good performance by comparison with an electrochemical analyzer. The proposed sensor is designed to control the scan rate, square wave amplitude, and step increment as purposes of measurement. The sensor also shows a good linearity in the range of 0.6 to 6 mM and 20 to 500 Hz. We also successfully obtained the detection limit as low as 0.6 mM under the condition of a higher scan rate than cyclic voltammetry. This is the first objective of our research.

As the next step, array biosensor is considered for chemical imaging. If the electrochemical array sensor technique is established, we can analyze the location information and visualization of biomaterials in a 2-dimensional plane. The integrated square wave voltammetry redox sensor with an 8 x 8 array pixels was fabricated. An 8-bit shift resistor is used for readout signals. We confirmed that the 2-dimensional imaging of potassium ferricyanide was obtained. This result shows the possibility of real-time chemical imaging and has established the basis of the point of care testing.

CONTENTS

CHAPTER 1

Introduction

1.1   Background Studies

 The beginning of the electrochemistry is a discovery of an electricity from animal by Luigi Galvani (Italian physician, 1737 ~ 1798) in 1791. Galvani shows the possibility that electricity is related with chemical reaction. After that, in 1799 Alessandro Volta (Italian physician, 1745 ~ 1827) discovers the relation between chemical reaction and electricity. Volta created a battery called voltaic pile as the first electrochemical cell [1-2]. Figure 1.1 shows the voltaic pile. This consists of two electrodes. One is zinc, and the other is copper. The zinc reacts with the negative charges, and the positive charge captures electrons from the copper. He is the first person who successfully obtained the electric energy from chemical reaction using his voltaic pile.

 In 19th century, Faraday's law of electrolysis came out by Micheal Faraday (UK, 1791 ~ 1867). Faraday's law was enabled to discuss the chemical reaction more than before, and it is also discovered that electrochemical reaction is related with reduction and oxidation of the electrode and electrolyte from many researches [3].

 In 1879, Helmholtz (Germany, 1821 ~ 1894) proposed a simple model for the space charge region surrounding the electrode [4]. This model was based on a capacitor. In the late 19th century, Nernst (Germany, 1864 ~ 1941) explored a variety of electrochemical characteristics. The development of thermodynamics affects electrochemistry because Nernst equation is announced at that time. Because of this electrochemical reaction is

enabled to think within the field of general chemical reaction. Nernst equation says that the potential difference can take the electrochemical reaction [5-9].

Gouy and Chapman (1910) improved the space charge region model of Helmholtz [10-12]. The current model of the space charge region was introduced in 1947 by Graham, and it is known as the electrical double layer.

Figure 1.1 Volta's voltaic pile model [1-2].

1.2   Electrochemical Analysis

Electrochemistry is studies of chemical reaction which can obtain quantitative and qualitative information under the condition between the electrode and the electrolyte. Practical applications such as glass electrode and reference electrode came into general use in a medical field and industrial field as shown in figure 1.2 [13]. The electrodes are a direct implementation of the Nernst equation and are based on the measurement of the cell potential. This measuring technique is called potentiometry [14-15]. The basic

electrochemical cell consists of two electrodes and the electrolyte. We can get the information of target materials from potentiometry by obtaining the cell potential under the condition of no current flowing. Voltammetry is more general technique which can be defined as the measurement of current-voltage relation of an electrode immersed in a solution containing biomaterials [16-19]. Voltammetry can obtain the material information through the current by applying changed potential. This study of current-voltage relation began by Salomen in the late 19th century. The various electrochemical analysis are shown in table 1.1. In 1956, Clark developed an Amperometric sensor for the measurement of dissolved oxygen [20-21]. This device is called the Clark cell as shown in figure 1.3. The Clark cell was the source of inspiration for several other types of sensors based on the electrochemical reduction of oxygen. In combination with a glucose oxidase membrane, a glucose sensor can be made by Updike and Hicks in 1967 [22-24]. The early work on glucose sensors has now evolved into a world-wide interest in biosensors based on electrochemical detectors as an interface between the chemical and the electrical world and on enzymes or other biological components as highly selective modifiers.

Figure 1.2 Ag/AgCl reference electrode (left) and glass electrode (right).
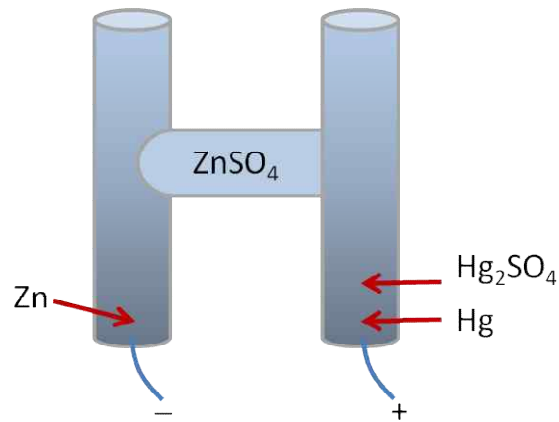
Figure 1.3 Structure of the Clark cell.

Ion-sensitive field effect transistor (ISFET) was discovered by Bergveld in 1970 [25]. The ISFET can easily be miniaturized and combined with electronic circuits on the same silicon chip. This ISFET has a simple structure of normal MOS transistor without a gate [26-27]. The electrolyte is in contact with the gate oxide, so the electrical parameters are modulated by variation of the chemical characteristics of the electrolyte.

Today the electrochemistry is widely used in energy conversion, analytical chemistry, biochemistry, and material chemistry. The research of energy conversion among the chemical, electrical, and light energy [28-29], applications of heavy metals [30-33], medical fields, studies of battery, a organic electro luminescence, electrophoresis [34-35], pH sensors [36-37], a gas sensors [38-39], an aluminum smelting [40] and so on, all of these applications of electrochemistry are closely related in our life. In this study, the integration and miniaturization of the electrochemical sensor on the basis of the silicon semiconductor technology is achieved. Portable diagnosis and high speed measurement system are developed with the demands for the point of care testing and a simple detecting. The on-chip redox (reduction-oxidation) sensor system is proposed by using the electrochemical analysis on the CMOS technology [41-42].

4

	Input signal	Output signal	Measurement method
Potentiometry	Current	Voltage	Measurement condition: Electrochemical cell (the electrolyte and two electrodes), No current flowing. Material information from measurement of a cell potential.
Voltammetry	Voltage	Current	Measurement condition: Elctrochemical cell. Changed potential at a constant rate. Material information from measurement of the current.
Amperometry	Voltage	Current	Measurement condition: Electrochemical cell. Constant potential value. Material information from measurement of the current which is flowed through the cell.
Conductometry	Voltage	Conductance	Measurement condition: Electrochemical cell. Applying AC potential. Material information from conductivity of electrolyte.

Table 1.1 Various electrochemical analysis.

1.3 The Development of the Integrated electrochemical array sensors

CMOS integrated sensors such as temperature sensors and light sensors and so on, already have been worked. However, the research of the integrated electrochemical sensor started 1987 by R. Turner who proposed the potentiostat with CMOS technology [43]. At that time, most of chemical sensors are pH sensors or voltage measured sensor of ISFET [44-45]. He described the potentiostat focusing on the current measurement which can measure the enzyme reaction. This research opened up the possibility of electrochemical sensor using silicon technology.
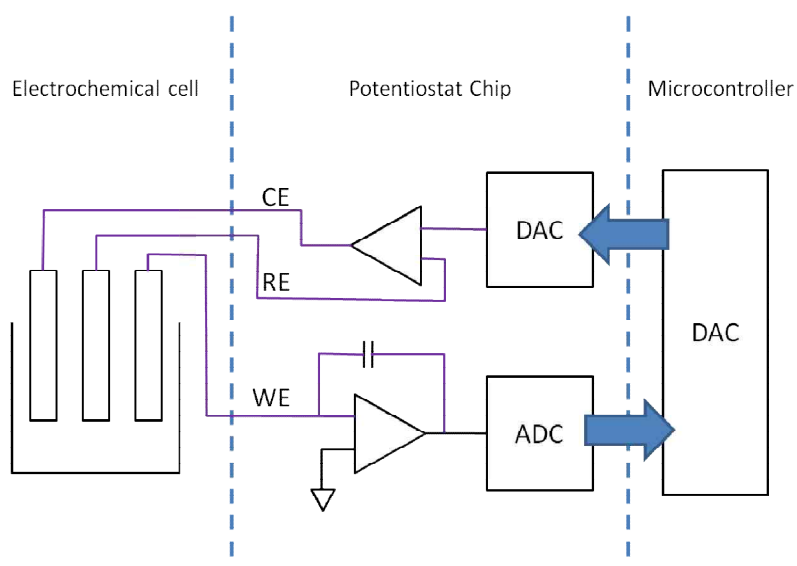
Figure 1.4 An integrated CMOS potentiostat [46].

In 1994 at the Center for integrated system, Stanford University, R. Reay et al studied the integration of CMOS potentiostat as shown in figure 1.4 [46]. The circuit which controls the potential between a working electrode and a reference electrode and measure the current of working electrode is integrated on a chip with CMOS technology. The research of Turner used two electrodes, but Reay used three electrodes such as working, reference,
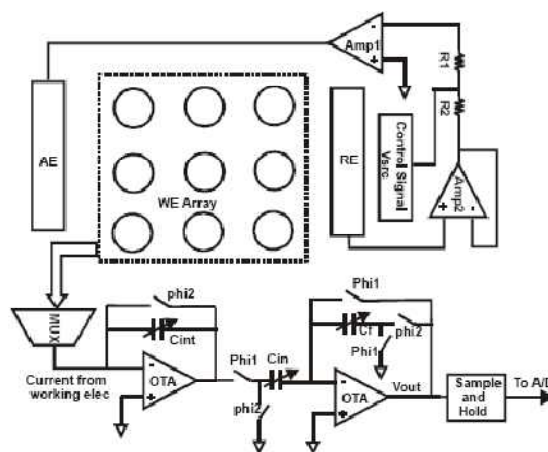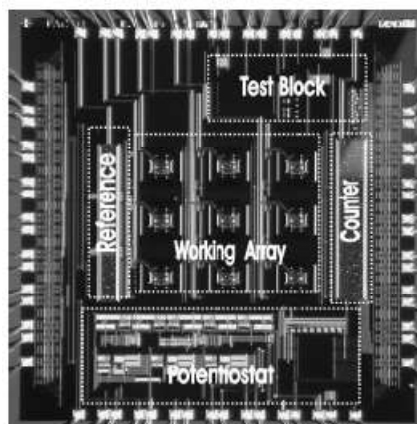
Figure 1.5 Electrochemical sensor system with integrated potentiostat and electrochemical cell (2005, J. Zhang et al.) [47].

7

and counter electrode. A current can flow through the counter electrode. However, the integration of microcontroller, battery, and electrochemical cell is still needed to miniaturization.

In 2005 and 2007, J. Zhang et al integrated an electrochemical cell which consists of working electrode, reference electrode, and counter electrode as shown in figure 1.5 and figure 1.6 [47-48]. Potentiostat is also integrated for operating electrodes. This chip is made to the need of protein based biomemetic sensors but applicable to a variety of electrochemical and current output sensors. This work also carried out post CMOS process for electrodes formation. However, since somewhat unstable of a reference electrode, electrochemical analysis is fulfilled using external systems. In 2007, P. Levine studied the DNA hybridization with integrated electrochemical sensor as shown in figure 1.7 [49]. This CMOS integrated electrochemical sensor for biomolecular detection eliminates the need for bulky and expensive optical equipment used in fluorescence based microarrays. It was also possible to detect of 4 x 4 array sensors.

Visual images of biomaterials are developed as a development of electrochemical analysis. The array sensor is needed for the visual images. The typical chemical image sensor is pH image sensor. The pH image sensor is based on the principle of a charge couple device (CCD). Figure 1.8 and figure 1.9 show the photograph of the ISFET image sensors [50-51]. A depth of the potential well is varied under the charge influence of sensing area. These sensors can visualize using various circuits such as readout and control circuits.

In 2012, K. Inoue et al has been worked the LSI based amperometric sensor for bioimaging as shown in figure 1.10 [52]. This sensor has 20 x 20 array sensing area, and the target material is detected using enzyme for high selectivity. The output current of each pixel shows good linearity by using CMOS technology. The scan rate per pixel is somewhat long because of measuring cyclic voltammetry technique.

This section was introduced the development of the integrated array sensors. If the electrochemical array sensor technique is established, the analysis of biomaterials is possible at the various points of view. The location information and amount of biomaterials which stimulate nerve cells and emit from the nerve cells can be monitored as in-vivo and in-vitro measurement. The high scan speed is important with respect to the array sensor, because biomaterials or neurotransmitter has the quite quick diffusion speed. Measurement with high scan speed is needed. Cyclic voltammetry technique which is conventional method takes a few minutes to scan of one pixel because of its capacitive current. Therefore, a new method which has high speed and high sensitivity is needed compared with cyclic voltammtrey. Square wave voltammetry technique is a good way to measure the array sensors. A detailed explanation of the square wave voltammetry will describe in the next chapter. The array sensor chip is also needed to detect various biomaterials simultaneously. At this point of view, different membrane on each pixel of the array chip is needed.
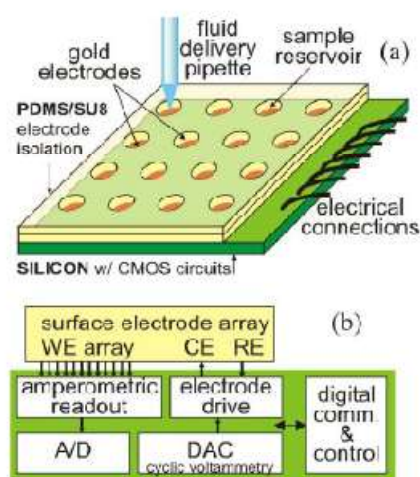
Figure 1.6 Electrochemical sensor system with electrode array and electrochemical cell

(2007, J. Zhang et al.) [48].

9
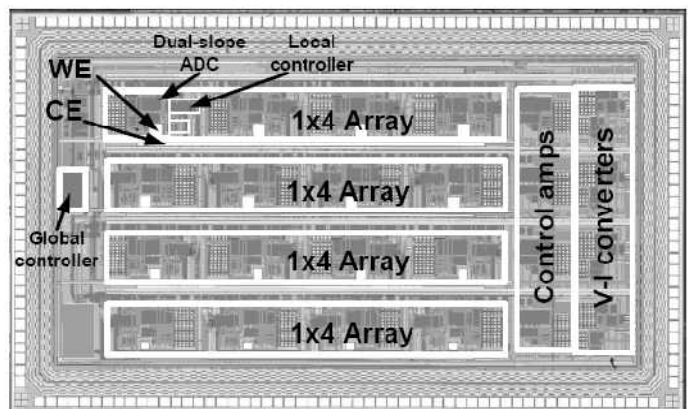
Figure 1.7 CMOS array chip [49].
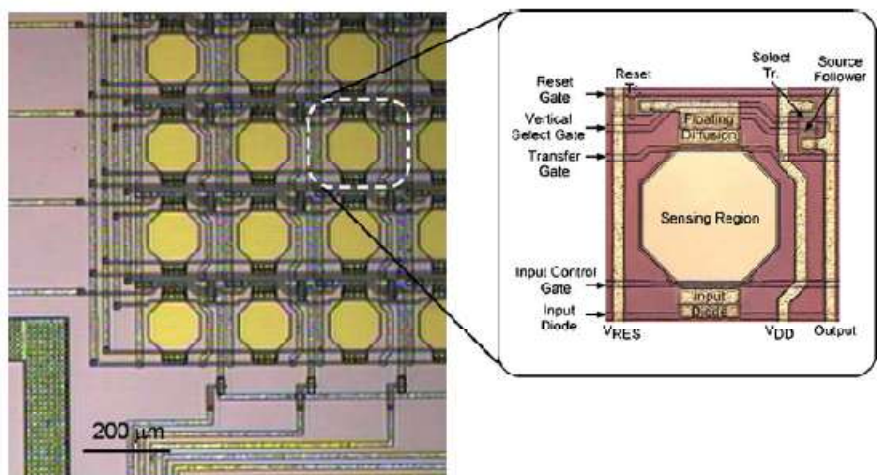
Figure 1.8 pH array sensor [50].
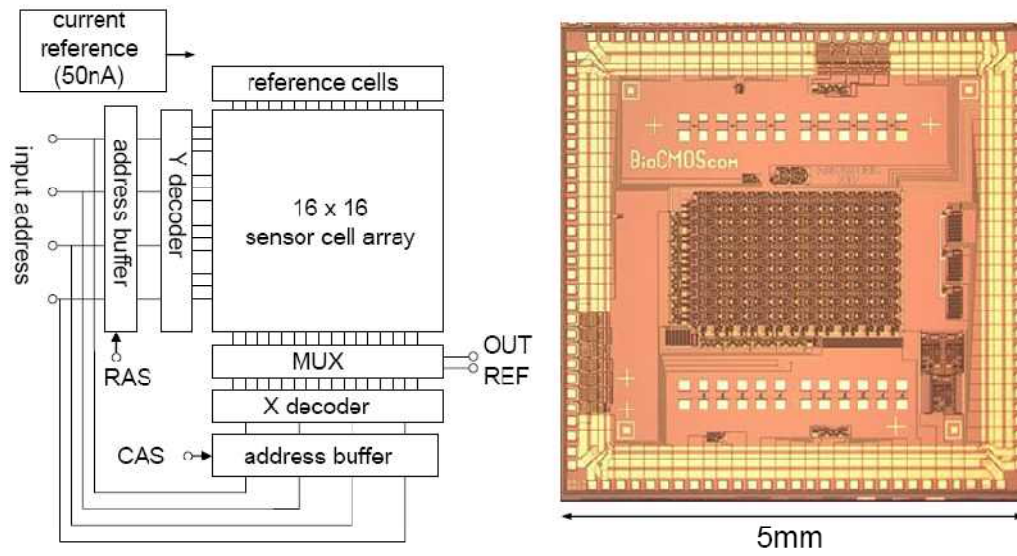
Figure 1.9 Integrated ISFET sensor array with peripheral circuits [51].
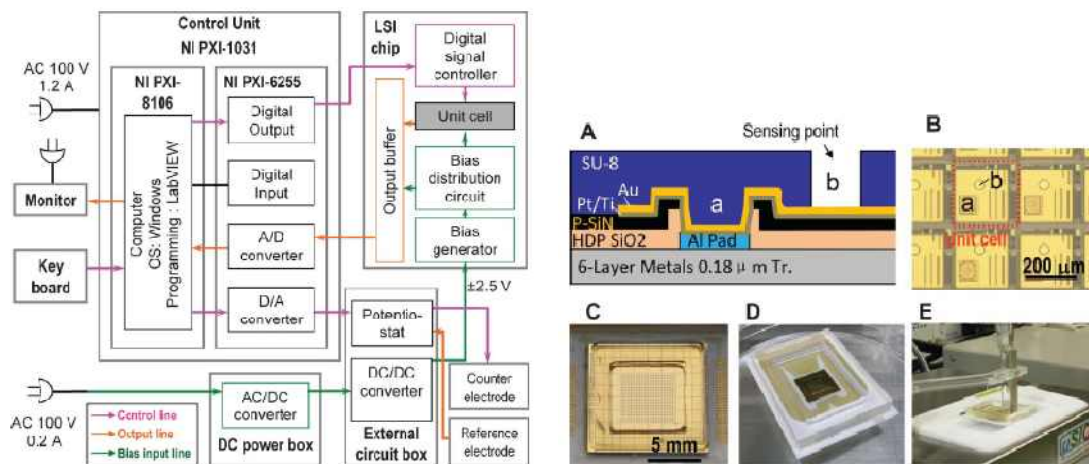
Figure 1.10 LSI based Amperometric sensor for bioimaging [52].

1.4　Redox Imaging and Microelectrode Array Sensor

Redox stands for reduction and oxidation. The redox measurement is important because the redox occurs in almost all living cells and organisms. Organisms use redox reaction to generate most of their energy for living. Using redox measurement, quantitative and qualitative information can be obtained.

In section 1.3, I described the development of the integrated electrochemical sensor and array sensor chip. Chemical imaging using redox (reduction-oxidation) reaction is developed with the demands for visualization of tissue and cell activities. The typical methods of redox imaging are the use of microelectrode array based on an electrochemical analysis [53-54] and a scanning electrochemical microscope (SECM) [55-56]. SECM is a technique that is used a scanning probe to measure the local redox current through the redox reaction at the surface of the sample and to monitor the biological activity and immobilized materials. Two-dimensional information can be acquired directly. The probe is scanned laterally on the substrate, and can analyze the reduction and oxidation in the vicinity of the probe. Figure 1.11 shows the structure of the SECM. Figure 1.12 and 1.13 shows the example of redox imaging using SECM. We use redox imaging to see the location information of cells, Al alloy, and to observe poisonous material extinction. Comparing with array sensor chips, SECM is difficult to detect simultaneous measurement because of the structural feature of SECM. Scan speed is also limited by the speed of the probe. It takes several minutes to tens of minutes per one frame, and we need to increase the scan rate for high resolution and detailed information of biomaterials.

Microelectrode array sensors based on the electrochemical analysis using Si technology have attracted attention for miniaturization of the sensor to conduct on-site monitoring [48-52]. Thus, this method has a potential of in vivo experiment, that is to say implantable chip. Microelectrode array sensors also have a simple detection way, just dropping the

sample solution onto the sensing area, and conduct not only multi-target detection but also simultaneous detection at the various points. It is also possible to detect unknown materials due to the sweep of input signal whereas SECM does not do sweep. For these reasons, there are recent reports in medical science and biological fields [58-59].
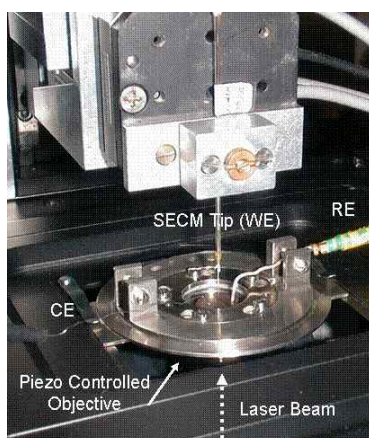
Figure 1.11 Structure of SECM.
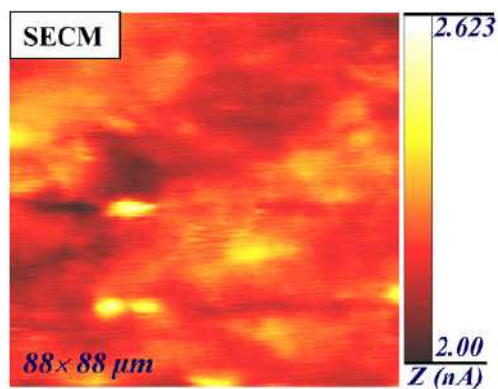
Figure 1.12 Example of the SECM imaging [56].
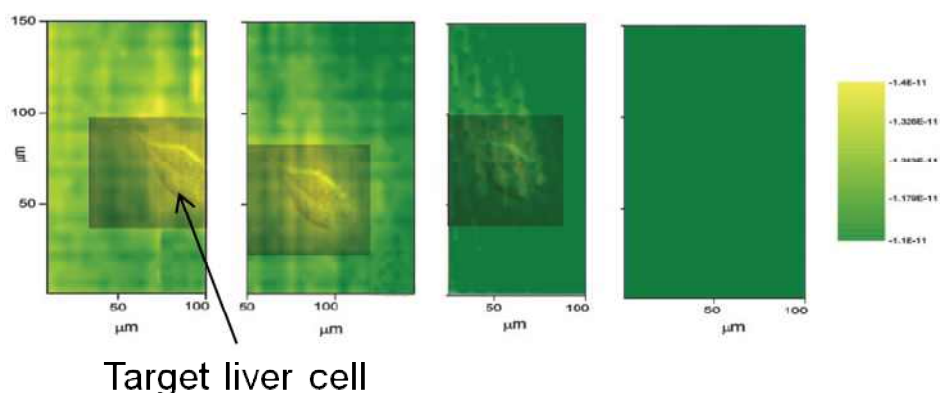
Figure 1.12 Example of the SECM imaging [57].

1.5   Research Objective

In this dissertation, an integrated square wave voltammetry redox image sensor has been developed on the basis of a standard complementary metal-oxide-semiconductor process technology for 2-dimensional chemical imaging and high scan speed in electrochemical analysis. High scan speed is suitable for the array sensor. Square wave voltammetry technology is not new, however so far there is no report about integrated square wave voltammetry. The reason is that the general square wave voltammetry technique has a bulky and expensive equipment, and complexity of the measuring equipment. If this square wave voltammetry technique is integrated on a chip, the development of a miniaturization and high-functional devices can be possible. We will describe the square wave voltammetry technique in the next chapter. When the technology of the miniaturization, the high-functional devices, and high scan rate measurement is established, on-site analysis and point of care testing can be possible in the medical and environment field.

References

[1] C. A. Russell, "The electrochemical theory of Sir Humphry Davy - park 1: The voltaic pile and electrolysis", Annals of Science, Vol. 15, Issue 1, pp. 1-13, 1959.

[2] J. Mertens, "Shocks and sparks: The voltaic pile as a demonstration device", Chicago Journals, Vol. 89, No. 2, pp. 300-311, 1998.

[3] M. F. Iskander, "Electromagnetic fields and waves (2nd edition)", Long Grove, IL: Waveland Press, 2013.

[4] D. M. Kolb, "An atomistic view of electrochemistry", Surface Science, Vol. 500, pp. 722-740, 2002.

[5] B. Hille, "Ion channels of excitable membranes (3rd edition)", Sunderland, Massachusetts, USA, 2001.

[6] A. P. Brown, and F. C. Anson, "Cyclic and differential pulse voltammetric behavior of reactants confined to the electrode surface", Analytical Chemistry, Vol. 49, No. 11, pp. 1589-1595, 1977.

[7] P. T. Kissinger and W. R. Heineman, "Cyclic voltammetry", Journal of Chemical Education, Vol 60, No. 9, p. 702, 1983.

[8] Mary M. Walczak, Deborah A. Dryer, Dana D. Jacobson, Michele G. Foss, and Nolan T. Flynn, "pH Dependent Redox Couple: An Illustration of the Nernst Equation", Journal of Chemical Education, Vol. 74, No. 10, p. 1195, 1997.

[9] Richard A. Durst, "Ion-selective electrodes", US Government Printing Office, Washington DC, 1969.

[10] A. Sridharan and M. S. Jayadeva, "Double layer theory and compressibility of clays", Geotechnique, Vol. 32, No. 2, pp. 133-144, 1982.

[11] G. H. Bolt, "Analysis of the validity of the Gouy-Chapman theory of the electric double layer", Journal of Colloid Science, Vol. 10, No. 2, pp. 206-218, 1955.

[12]S. McLaughlin, "The electrostatic properties of membranes", Annual Review of Biophysics and Biophysical Chemistry, Vol. 18, pp. 113-136, 1989.

[13]Richard P. Baldwin, Thomas J. Roussel, Jr., Mark M. Crain, Vijay Bathlagunda, Douglas J. Jackson, Jayadeep Gullapalli, John A. Conklin, Rekha Pai, John F. Naber, Kevin M. Walsh, and Robert S. Keynton, "Fully Integrated On-Chip Electrochemical Detection for Capillary Electrophoresis in a Microfabricated Device", Analytical Chemistry, Vol. 74, No. 15, pp. 3690-3697, 2002.

[14]Richard P. Buck, "Ion selective electrodes, potentiometry, and potentiometric titrations", Analytical Chemistry, Vol. 44, No. 5, pp. 270-295, 1972.

[15]Joseph Wang, "Electrochemical detection for microscale analytical systems: a review", Talanta, Vol. 56, No. 2, pp. 223-231, 2002.

[16]Kh. Z. Brainina, "Advances in voltammetry", Tantala, Vol. 34, No. 1, pp. 41-50, 1987.

[17]G. Osteryoung and M. M. Schreiner, "Recent advances in pulse voltammetry", Analytical Chemistry, vol.19, No. 1, pp. s1-s27, 1988.

[18]Marek Trojanowicz, "Analytical applications of carbon nanotubes: a review", TrAC Treds in Analytical Chemistry, Vol. 25, No. 6, pp 480-489, 2006.

[19]Jiri Barek, Arnold G. Fogg, Alexandr Muck, and Jiri Zima, "Polarography and Voltammetry at Mercury Electrodes", Analitical Chemistry, Vol. 31, No. 4, 2001.

[20]H. C. Budnikov, E. P. Medyantseva, and S.S. Babkina, "An enzyme amperometric sensor for toxicant determination", Journal of Electroanalytical Chemistry and Interfacial Electrochemistry, Vol. 310, No. 1-2, pp. 49-55, 1991.

[21]G. Jeanty and J. L. Marty, "Detection of paraoxon by continuous flow system based enzyme sensor", Biosensors and Bioelectronics, Vol. 13, No. 2, pp. 213-218, 1998.

[22]S. J. Updike and G. P. Hicks, "Reagentless Substrate Analysis with Immobilized Enzymes, Science, Vol. 158, No. 3798, pp. 270-272, 1967.

[23] S. Gernet, M. Koudelka, and N. F. De Rooij, "Fabrication and characterization of a planar electrochemical cell and its application as a glucose sensor, Sensors and Actuators, Vol. 18, No. 1, pp. 59-70, 1989.

[24] Ryohei Nagata, "A glucose sensor fabricated by the screen printing technique", Biosensors and Bioelectronics, Vol. 10, No. 3-4, pp. 261-267, 1995.

[25] P. Bergveld, "Development of an Ion-Sensitive Solid-State Device for Neurophysiological Measurements", IEEE Engineering in Medicine and Biology Society, Vol. BME-17, Issue. 1, pp. 70-71, 1970.

[26] Cecilia Jimenez-Jorquera, Jahir Orozco, and Antoni Baldi, "ISFET Based Microsensors for Environmental Monitoring", Sensors, Vol. 10, pp. 61-83, 2010.

[27] P. Bergveld, "ISFET, Theory and practice", IEEE Sensor Conference Toronto, pp.1-26, 2003

[28] S. R. Morrison, "Electrochemistry at semiconductor and oxidized metal electrodes", US, 1980.

[29] E. Gileadi, E. Kirowa-Eisner, and J. Penciner, "Interfacial electrochemistry: an experimental approach", US, 1975.

[30] Ha Na Kim, Wen Xiu Ren, Jong Seung Kim, and Juyoung Yoon, "Fluorescent and colorimetric sensors for detection of lead, cadmium, and mercury ions", Chemical Society Reviews, Vol. 41, pp. 3210-3244, 2012.

[31] Israel Biran, Reuven Babai, Klimentiy Levcov, Judith Rishpon, and Eliora Z. Ron, "Online and in situ monitoring of environmental pollutants: electrochemical biosensing of cadmium", Environmental Microbiology, Vol. 2, Issue 3, pp. 285-290, 2000.

[32] Richard J. Reaya, Anthony F. Flannerya, Christopher W. Stormenta, Samuel P. Kounavesb, and Gregory T.A. Kovacs, "Microfabricated electrochemical analysis system for heavy metal detection", Vol. 34, Issues 1-3, pp. 450-455, 1996.

[33] Yujun Zheng, Jhony Orbulescu, Xiaojun Ji, Fotios M. Andreopoulos, Si M. Pham, and Roger M. Leblanc, "Development of Fluorescent Film Sensors for the Detection of Divalent Copper", Vol. 125, No. 9, pp. 2680-2686, 2003.d

[34] M. A. Baldo, S. Lamansky, P. E. Burrows, M. E. Thompson, and S. R. Forrest, "Interfacial electrochemistry: an experimental approach", Applied Physics Letters, Vol 75, No. 4, 1999

[35] P. F. Gavin and A. G. Ewing, "Continuous Separations with Microfabricated Electrophoresis−Electrochemical Array Detection", Journal of the American Chemical Society, Vol. 118, No. 37, pp. 8932-8936, 1996.

[36] L. A. Saari and W. R. Seitz, "pH sensor based on immobilized fluoresceinamine", Analytical Chemistry, Vol. 54, No. 4, pp. 821-823, 1982.

[37] T. P. Jones and M. D. Porter, "Optical pH sensor based on the chemical modification of a porous polymer film", Analytical Chemistry, Vol. 60, No. 5, pp. 404-406, 1988.

[38] C. Hagleitner, A. Hierlemann, D. Lange, A. Kummer, N. Kerness, O. Brand, and H. Baltes, "Smart single-chip gas sensor microsystem", Nature, Vol. 414, pp. 293-296, 2001.

[39] G. S. Trivikrama Rao and D. Tarakarama Rao, "Gas sensitivity of ZnO based thick film sensor to NH3 at room temperature", Sensors and Actuators B, Vol. 55, Issues 2-3, pp. 166-169, 1999.

[40] P. Booth and K. Gribben, "A Review of the Formation, Environmental Fate, and Forensic Methods for PAHs from Aluminum Smelting Processes", Environmental Forensics, Vol. 6, Issue 2, pp. 133-142, 2005.

[41] T. Yamazaki, T. Ikeda, Y. Kano, H. Takao, M. Ishida, and K. Sawada, "Design and Fabrication of Complementary Metal–Oxide–Semiconductor Sensor Chip for Electrochemical Measurement", Japanese Journal of Applied Physics, Vol. 49, p. 04DL11, 2010.

[42] T. Yamazaki, T. Ikeda, M. Ishida, and K. Sawada, "Compact Electrochemical System Using On-Chip Sensor Electrodes and Integrated Devices", Japanese Journal of Applied Physics, Vol. 50, p. 04DL02, 2011.

[43] R. F. B. Turner, D. J. Harrison, and H. P. Baltes, "A CMOS potentiostat for Amperometric chemical sensors", IEEE Journal of Solid-State Circuits, Vol. 22, Issue 3, pp. 473-478, 1987.

[44] B. H. van der Schoot and P. Bergveld, "The pH-static enzyme sensor : An ISFET-based enzyme sensor, insensitive to the buffer capacity of the sample, Analytica Chimica Acta, Vol. 199, pp. 157-160, 1987.

[45] Y. Miyahara and T. Moriizumi, "Integrated enzyme fets for simultaneous detections of urea and glucose", Sensors and Actuators, Vol. 7, Issue 1, pp. 1-10, 1985.

[46] R. J. Reay, S. P. Kounaves, and G. T. A. Kovacs, "An integrated CMOS potentiostat for miniaturized electroanalytical instrumentation", Solid-State Circuits Conference, Digest of Technical Papers. 41st ISSCC., 1994 IEEE International, San Francisco, pp. 162-163, 1994

[47] J. Zhang, Y. Huang, N. Trombly, C. Yang, and A. Mason, "Electrochemical Array Microsystem with Integrated Potentiostat", IEEE Sensors, pp. 385-388, 2005.

[48] A. Mason, Y. Huang, C. Yang, and J. Zhang, "Amperometric Readout and Electrode Array Chip for Bioelectrochemical Sensors", IEEE international symposium on circuits and systems, New Orleans, LA, US, pp. 3562-3565, 2007.

[49] P. M. Levine, P. Gong, K. L. Shepard, and R. Levicky, "Active CMOS Array for Electrochemical Sensing of Biomolecules", IEEE 2007 Custom Intergrated Circuits Conference (CICC), San Jose, California, pp. 825-828, 2007.

[50] T. Hizawa, K. Sawada, H. Takao, and M. Ishida, "Fabrication of a two-dimensional pH image sensor using a charge transfer technique", Sensors and Actuators B, Vol. 117, pp. 509-515, 2006.

[51] K. Nakazato, M. Ohura, H. Ozawa, and S. Uno, "A BioCMOS LSI circuit with extended-gate FET sensor array", 2008 International Conference on Solid State Devices and Materials (SSDM 2008), Tsukuba, Japan, 2008.

[52] Kumi Y. Inoue, Masahki Matsudaira, Reyushi Kubo, Masanori Nakano, Shinya Yoshida, Sakae Matsuzaki, Atsushi Suda, Ryota Kunikata, Tatsuo Kimura, Ryota Tsurumi, Toshihito Shioya, Kosuke Ino, Hitoshi Shiku, Shiro Satoh, Masayoshi Esashi, and Tomokazu Matsue, "LSI-based amperometric sensor for bio-imaging and multi-point biosensing", Lab on a Chip, Vol. 12, pp. 3481-3490, 2012.

[53] J. Wang and Q. Chen, "Enzyme microelectrode array strips for glucose and lactate," Analytical Chemistry, Vol. 66, pp. 1007-1011, 1994.

[54] R. Hintsche, J. Albers, H. Bernt, and A. Eder, "Multiplexing of microelectrode arrays in voltammetric measurements," Electroanalysis, Vol. 12, No. 9, pp. 660-665, 2000.

[55] A. J. Bard, X. Li, and W. Zhan, "Chemically imaging living cells by scanning electrochemical microscopy," Biosensors and Bioelectronics, Vol. 22, pp. 461-472, 2006.

[56] A. Davoodi, J. Pan, C. Leygraf, and S. Norgren, " Integrated AFM and SECM for in situ studies of localized corrosion of Al alloys", Electrochimica Acta, Vol. 52, pp. 7697-7705, 2007.

[57] A. J. Bard, X. Li, and W. Zhan, "Chemically imaging living cells by sanning electrochemical microscopy", Biosensors and Bioelectronics, Vol. 22, pp. 461-472, 2006.

[58] M. Stanacevic, K. Murari, A. Rege, G. Cauwenberghs, and N. Thakor, "VLSI Potentiostat Array with Oversampling Gain Modulation for Wide-Range Neurotransmitter Sensing", IEEE Transactions on Biomedical Circuits and Systems, Vol. 1, Issue 1, pp. 63-72, 2007.

[59] R. A. Young, "Biomedical discovery with DNA arrays," Cell, Vol. 102, pp. 9-15, 2000.

CHAPTER 2

Overview of Electrochemical Analysis

2.1   Introduction

Electrochemical analysis is the analytic technique which is capable of obtaining quantitative and qualitative information of the materials based on electrochemical property. This analysis is based on an electrochemical cell which is composed of analyte and electrolyte. The advantages of electrochemical analysis are simple measurement, low limit of detection, inexpensive technique, and precise measurement. Therefore, it is widely used in medical application, environmental assessment, and biological fields.

2.2   Basic electrochemical principles

2.2.1   Electrochemical cells

An electrochemical cell consists of two electrodes and an electrolyte. The electrolyte is a phase through which charge is transferred by the movement of ions [1-3]. The electrode is a phase through which charge is transferred by electronic movement. Two electrodes are placed in an electrolyte. A potential difference appears and can be measured between a working electrode and a counter electrode. This cell potential is a sum of the differences in electrical potential between the various phases in the current path. The measurement and

control of this cell potential and cell current is the main topic of experimental electrochemistry. Figure 2.1 shows the electrochemical measurement using two electrodes, and figure 2.2 shows the potential windows of each electrode [4].
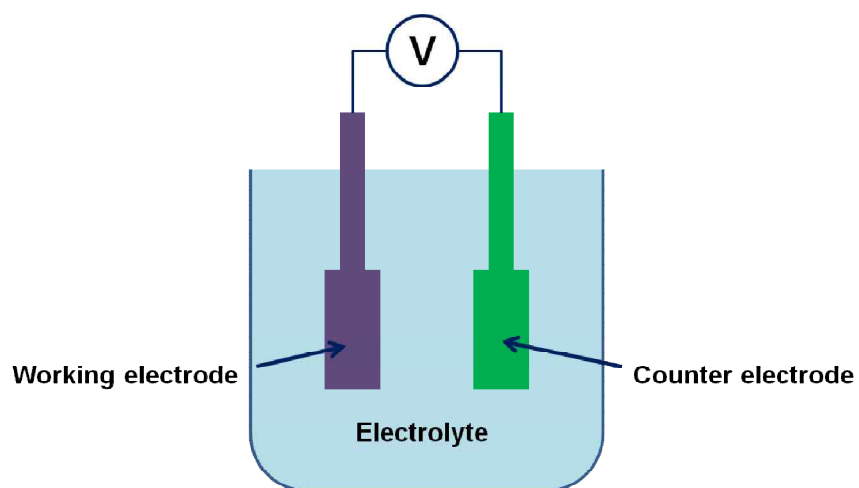
Figure 2.1 Measurement of electrode potential.
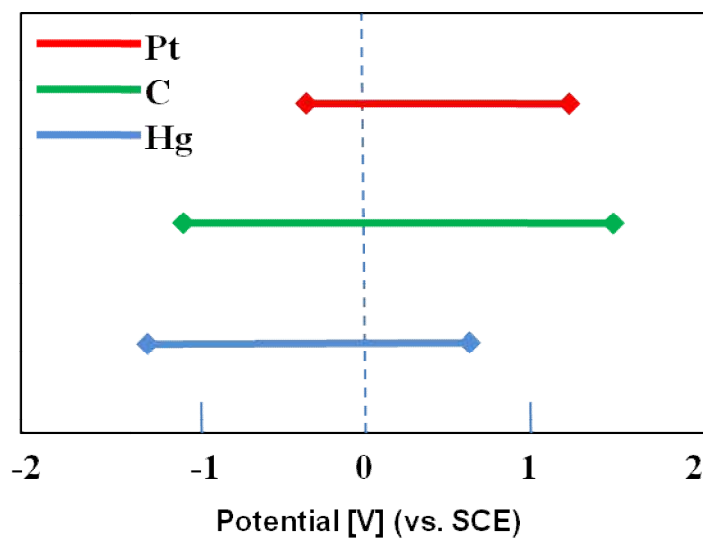
Figure 2.2 Potential windows of electrodes (in 1M $HClO_4$) [4].

2.2.2 Capacitive current

An electrode immersed in an electrolyte is surrounded by a space charge region, which is called the electric double layer. The electric double layer is built up at the interface between electrode and electrolyte when a voltage is applied, and is described by the double layer capacitance C_d. Figure 2.3 shows the concept of the electrical double layer.
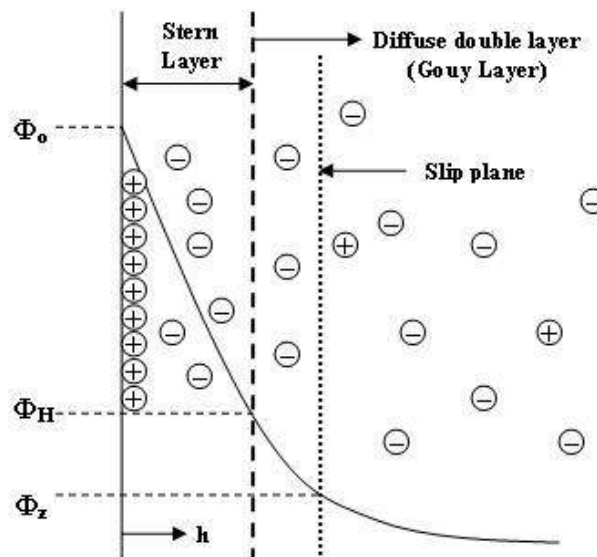
Figure 2.3 Electrical double layer.

This capacitance depends on the electrolyte composition and the applied potential. If a varying potential as a function of time is applied to an electrode, this layer has to be charged and discharged. This charging process gives rise to a capacitive current Ic

$$I_C = C_d \frac{dv}{dt} \tag{2.1}$$

The scan rate dv/dt is usually expressed in (mV sec^{-1}) and equals the slope of the triangular potential wave. The capacitive current is proportional to the scan rate. This capacitive current does not give valuable analytical information. Thus, it is an interfering current in electrochemical measurement. Capacitive current must be decreased for maintaining pure materials and a clean surrounding, and can be kept small by decreasing the scan rate.

2.2.3   Faradaic current

The faradaic current is a measure of the rate of the electrochemical reaction taking place at the electrode. Faradaic currents also produce a change in reduction/oxidation state of some material in the cell. The current is proportional to the concentration of reduced and oxidized species. The electrochemical reaction is determined by the mass transport and the charge transfer. The mass transport is the process that transports material from a bulk of the electrolyte to the electrode. The charge transfer is the process that transfers electrons from the electrode to the solution. Mass transport is the movement of the materials from high concentration to low concentration. This is called the diffusion. When the diffusion is occurred at the electrode surface, the current is described as,

$$I = \frac{nFA\,C_0\sqrt{D}}{\sqrt{\pi t}} \qquad\qquad (2.2)$$

This is the Cottrell equation [5-7]. It describes the change in electric current with respect to time. F is the faradaic constant (96.49 C/mol), n is a number of electrons, A is the area of the electrode (cm^2), C_0 is a bulk concentration of the oxidized analyte (mol/cm^3), D is a

diffusion coefficient for species (cm^2/s), and t is a time (sec).

2.2.4 Potentiometry method

Figure 2.1 show the electrode potential measurement using two electrodes measurement system. It can be measured between a reference electrode and a working electrode. Potentiometry can be defined as a direct analytical application of the Nernst equation through measurement of the potential. Reference electrode is important for electrochemical experiments. For reliable electrochemical measurement, a stable reference electrode is needed.

Reference electrode is based on the principles of the Nernst equation. In this study, an Ag/AgCl reference electrode is used. Requirements of the reference electrode are as in the following. 1) Good reproducibility of potential. 2) Nonpolarised electrodes under conditions of zero current. 3) No reaction with target materials. The Ag/AgCl reference electrode consists of a Ag wire coated with AgCl immersed in a saturated KCl solution. The following reaction takes place.

$$AgCl(s) + e^- \leftrightarrow Ag(s) + Cl^- \qquad\qquad (2.3)$$
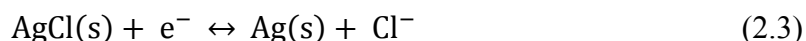
The potential of the saturated Ag/AgCl reference electrode is 197 mV with respect to the standard hydrogen electrode (SHE). The requirements of the working electrodes are potential window and chemical stability. The potential window is a potential range between which the material is neither oxidized nor reduced. This range is important for the electrochemical measurement. If the potential goes out of this range, water gets electrolysed. It is needed to be selected suitable working electrode for chemical reaction.

Platinum, gold, mercury, and palladium are widely known as materials of working electrodes. In this study, platinum working electrode is used which is well-established electrode formation and easy to integrated in a silicon chip.

The Nernst equation gives a relation between the potential at an electrode with respect to the solution and the concentration of the corresponding electroactive species in the solution. The Nernst equation is based on electrochemical thermodynamics. We can think about a half-cell reaction at the single electrode.

$$\mathrm{Ox} + n\mathrm{e}^- \leftrightarrow \mathrm{Red} \tag{2.4}$$

The Gibbs free energy change of the cell reaction in equilibrium is given from basic thermodynamics by,

$$\Delta G = \Delta G^0 + RT \ln \frac{[\mathrm{Red}]}{[\mathrm{Ox}]} \tag{2.5}$$

ΔG is a change in Gibbs free energy (J), ΔG^0 is standard change in Gibbs free energy (J), R is gas constant (8.3144 J mol^{-1} K^{-1}), and T is absolute temperature.

Moreover, we can also be derived that,

$$\Delta G = -nFE \tag{2.6}$$

and,

$$\Delta G^0 = -nF E^0 \tag{2.7}$$

Substituting (2.5) and (2.6) into (2.8),

$$E = E^0 - \frac{RT}{nF} \ln \frac{[Red]}{[Ox]} \tag{2.8}$$

We can realize the potential of a general reduction and oxidation electrode reaction as a function of the activities of Ox and Red from the above equation. This relation gives concentration of reductant and oxidant measuring reduction and oxidation potential, and control a concentration rate of reductant and oxidant nearby the electrode with controlling electrode potential.

2.3   Voltammetry

Voltammetry is the measurement of the current which flows at an electrode as a function of the potential applied to the electrode. As a result of a voltammetric experiment, the current-voltage plot is recorded. We can perform the qualitative and quantitative analysis from this plot. According to the applied potential waveform, different techniques can be distinguished. For example, in square wave voltammetry a square wave pulse is applied to the electrochemical cell, and in cyclic voltammetry a triangular potential wave is applied. Amperometry is a special case of voltammetry, as in this technique the potential is kept constant as a function of time. Each method has advantages and disadvantages. These are discussed in this section.

2.3.1   Square Wave Voltammetry

Square wave voltammetry is a general pulse voltammetric technique. The square wave voltammetry technique stemmed from the work of Barker's square wave polarography in the 1950s [8-9]. The applied waveform is shown in figure 2.4 [10-15]. A staircase wave is superimposed on a square wave pulse. The period of the square wave is identical to the time step of the staircase. Figure 2.5 shows the current response while entering the square wave.

The value of the pulse width is in the range of tens of Hz to hundreds of Hz. The current result is the difference between the current sampled at the end of the positive pulse and the current sampled at the end of the negative pulse. The capacitive current decreases much faster than the Faradaic current. Thus, the Faradaic current is measured at the end of the pulse. The capacitive current is a charging current of the electric double layer as already explained in section 2.2, this capacitive current decreases exponentially as a function of time. The Faradaic current decreases as an inverse of a square root ($t^{-1/2}$) of time, by the Cottrell equation in section 2.2.

Square wave voltammetry (SWV) is a favorable technique in high sensitivity and high speed measurement as following reasons: 1) SWV technique does not include the influence of capacitive current because the technique was developed to discriminate the capacitive current. This results more sensitive to faradaic current than the cyclic voltammetry. 2) This method obtained rejection of background currents because the output current comes from differential value between reduction and oxidation current. 3) Amount of peak current and the sensitivity is higher than cyclic voltammetry. Electrons are not stacked up on the electrode surface because of an alternate with reduction and oxidation during the reaction. Therefore, high speed measurement is possible, and sensitivity is increased as compared with conventional method.
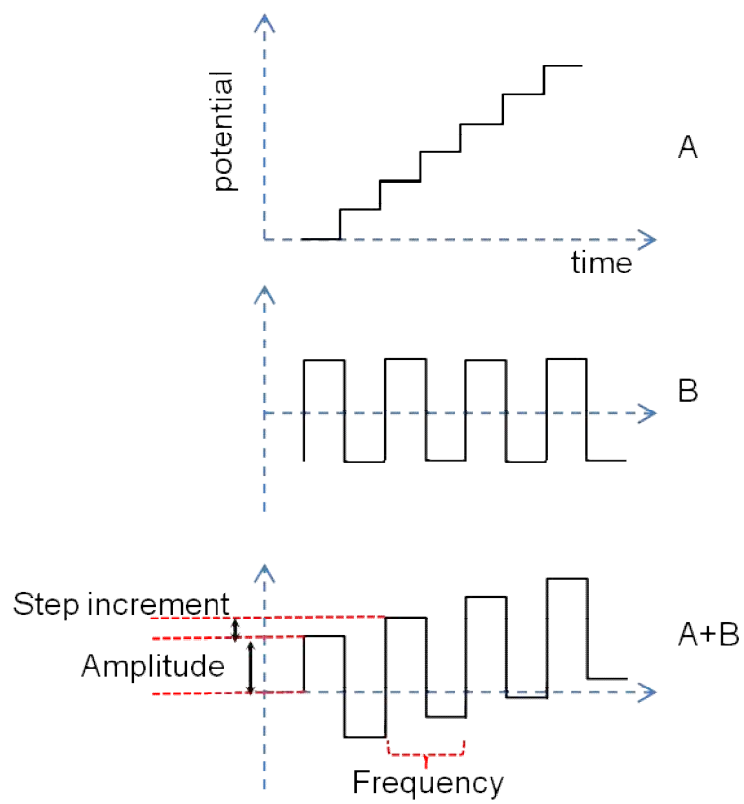
Figure 2.4 The applied potential waveform of square wave voltammetry.
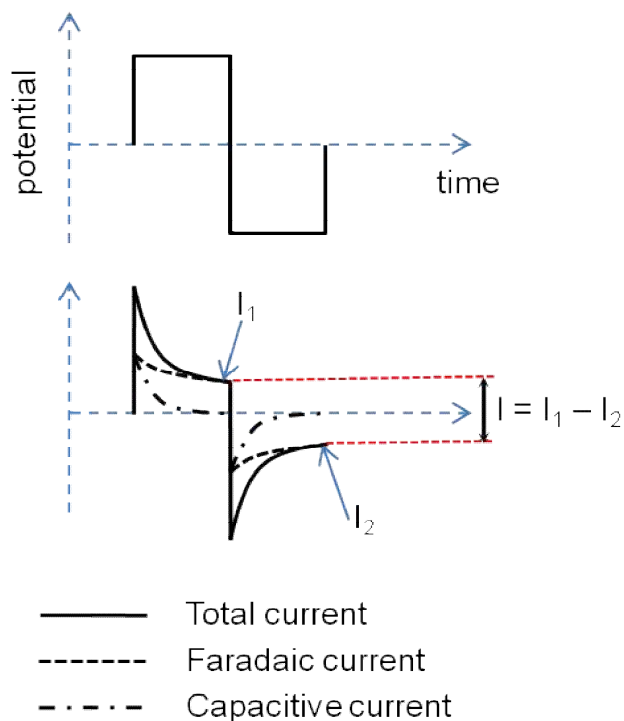
Figure 2.5 Measured current response of the square wave voltammetry.

Figure 2.5 shows a general square wave voltammetric experiment, the differential current response as a function of potential of the square wave pulse. The height of the peak is directly propotional to the concentration of the biomaterial. Peak faraday current depends linearly on the square root of SW frequency and the concentration of materials according to the following current equation of square wave voltammetry

.

$$I = nFA\,D^{1/2}f^{1/2}C\Psi \qquad\qquad (2.9)$$

where I is a peak current, n is the number of electrons transferred, F is the Faraday constant, A is the area of the electrode, D is the reactant diffusion constant, f is the square wave frequency, C is the bulk concentration of the reactant, and Ψ is the dimensionless peak current which depends on the square-wave amplitude and the step increment [10]. A characteristic of a potassium ferricyanide is present as shown in figure 2.6. The peak current is clearly seen. Because of the separated peak currents, square wave voltammetry allows the analysis of systems with multiple biomaterials. Square wave voltammetry is characterized by a square wave frequency, amplitude, a step increment, and an initial potential. The frequency and the amplitude have an important influence on peak height and peak separation. By increasing the step height, the sensitivity increases but the peak separation decreases.
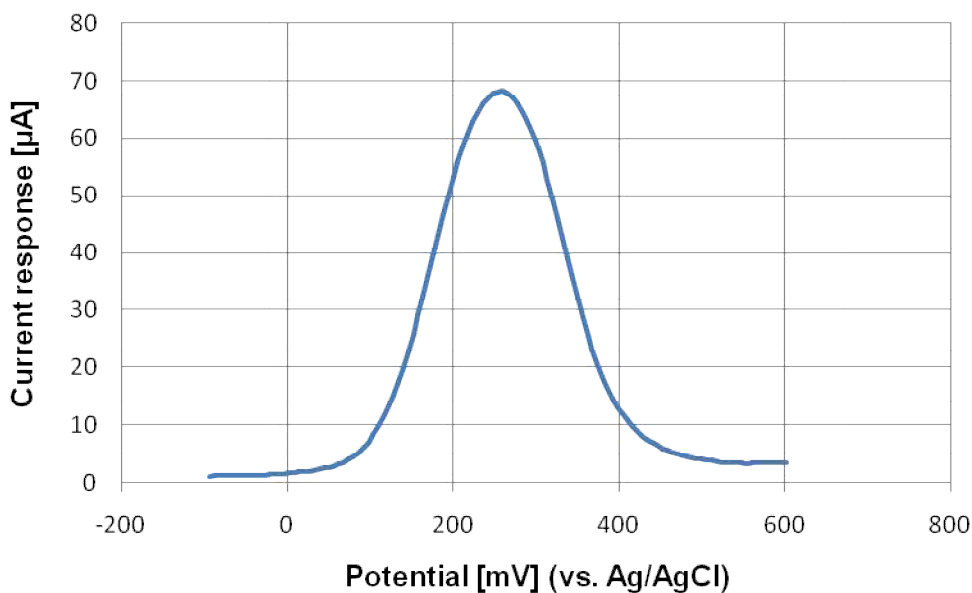
Figure 2.6 Current-potential plot of the square wave voltammetry.

2.3.2   Other Voltammetric Techniques

2.3.2.1   Cyclic voltammetry

In cyclic voltammetry, the applied potential is changed linearly with time, starting from a potential where no electrode reaction occurs and moving to a potential where reduction or oxidation of the materials involved occurs. After increasing the potential region where the electrode reactions take place, the scan direction is reversed. A triangular waveform of potential is applied as shown in figure 2.7 (b). Cyclic voltammetry is characterized by a scan rate, initial potential, and switching potential. The initial potential usually equals the final potential. The measured current result is shown in figure 2.7 (b). The current-potential plot is also shown in figure 2.7 (b). The cathodic and anodic peak potentials, the cathodic and anodic peak currents are the important parameters in the cyclic voltammetry. Compare to square wave voltammetry, a scan rate of the cyclic voltammetry is slower than square wave voltammetry technique. Fast scanning measurements using cyclic voltammtery cannot be operated because of an influence of charge currents on electric double layer capacitance.

2.3.2.2   Differential pulse voltammetry

Differential pulse voltammetry is also a pulsed voltammetric technique like a square wave voltammetry. The applied potential waveform is shown in figure 2.7 (c). Pulse is superimposed on a staircase wave. The current is measured twice. One is before the pulse and the other is at the end of the pulse. The signal current is obtained by subtraction of the

two measured current so the differential pulse is a plot of the differential current versus the applied potential. In general, square wave voltammetry technique has faster, higher output current, and higher sensitivity than differential pulse voltammetry [16-17]. The current response and current-potential plot are shown in figure 2.7 (c).

	Applied potential waveform	Current response	Current-potential plot
(a)			
(b)			
(c)			
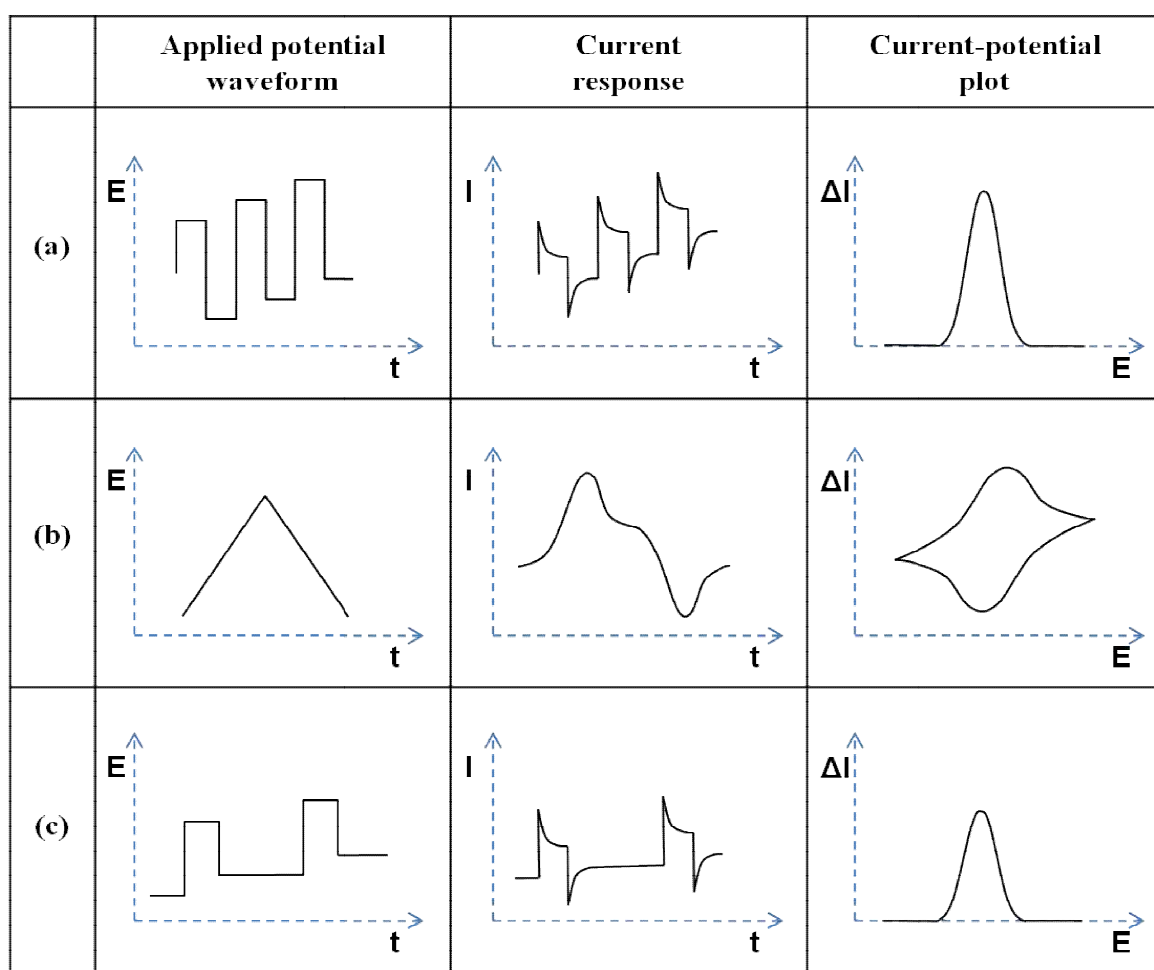
Figure 2.7 The various voltammetry techniques. (a) Square wave voltammetry. (b) Cyclic voltammetry. (c) Differential pulse voltammetry.

2.4 Conclusion

In this chapter, we described the basic electrochemical principles and the techniques of electrochemical analysis. Among the voltammetric techniques, square wave voltammetry is suitable for high-sensitivity and high-speed measurement compared with conventional methods. In the next chapter, we will describe the experiment of square wave voltammetry using integrated Si technique for miniaturization and point of care testing of electrochemical analysis.

References

[1] E. Bakker, "Electrochemical sensors", Analytical Chemistry, Vol. 76, No. 12, pp. 3285-3298, 2004.

[2] J. Wang, G. Rivas, X. Cai, E. Palecek, P. Nielsen, H. Shiraishi, N. Dontha, D. Luo, C. Parrado, M. Chicharro, P.A.M. Farias, F.S. Valera, D.H. Grant, M. Ozsoz, and M.N. Flair, "DNA electrochemical biosensors for environmental monitoring. A review", Analytica Chimica Acta, Vol. 347, Issues 1-2, pp. 1-8, 1997.

[3] D. Tyler McQuade , Anthony E. Pullen , and Timothy M. Swager, "Conjugated Polymer-Based Chemical Sensors", Chemical Reviews, Vol. 100, No. 7, pp. 2537-2574, 2000.

[4] Donald T. Sawyer and Julian L. Roberts, "Experimental electrochemistry for chemists", Wiley, New York, US, 1974.

[5] F. G. Cottrell, "Application of the Cottrell equation to chronoamperometry", Zeitschrift Physics Chemistry, Vol. 42, p. 385, 1902.

[6] T. Pajkossy, "Electrochemistry at fractal surfaces", Journal of Electroanalytical Chemistry and Interfacial Electrochemistry, Vol. 300, Issues 1-2, pp. 1-11, 1991.

[7] D. Grujicic and B. Pesic, "Electrodeposition of copper: the nucleation mechanisms", Electrochimica Acta, Vol. 47, Issue 18, pp. 2901-2912, 2002.

[8] V. Mirceski, S. Komorsky-Lovric, and M. Lovric, "Square-Wave Voltammetry: Theory and application", Springer-Verlag Berlin Heidelberg, 2007.

[9] L. Ramaley, and M. S. Krause Jr, "Theory of square wave voltammetry", Analytical Chemistry, Vol. 41, No. 11, pp. 1362-1365, 1969.

[10] M. Lovric, "Theory of Square-Wave Voltammetry of a Reversible Redox Reaction Complicated by the Reactant Adsorption", Electroanalysis, Vol. 14, No. 6, pp. 405-414, 2002.

[11]M. Jakubowska, "Signal processing in electrochemistry", Electroanalysis, Vol. 23, No. 3, pp. 553-572, 2011.

[12]Dario Omanovi, Cedric Garnierb, Yoann Louisb, Veronique Lenobleb, Stephane Mounierb, and Ivanka Pizeta, "Significance of data treatment and experimental setup on the determination of copper complexing parameters by anodic stripping voltammetry", Analytica Chimica Acta, Vol. 664, pp. 136-143, 2010.

[13]I. Pizeta, D. Omanovic, and M. Branica, "The influence of data treatment on the interpretation of experimental results in voltammetry", Analytica Chimica Acta, Vol. 401, pp. 163-172, 1999.

[14]D. Omanovic and M. Branica, "Pseudopolarography of trace metals Part I. The automatic ASV measurements of reversible electrode reactions", Journal of Electroanalytical Chemistry, Vol. 543, pp. 83-92, 2003.

[15]V. Mirceski and M. Lovric, "Ohmic drop effects in square-wave voltammetry", Journal of Electroanalytical Chemistry, Vol. 497, pp. 114-124, 2001.

[16]L. Codognoto, S. A. S. Machado, and L. A. Avaca, "Square wave voltammetry on boron-doped diamond electrodes for analytical determinations," Diamond and Related Materials, Vol. 11, pp. 1670-1675, 2002.

[17]D. D. Souza, S. A. S. Machado, and R. C. Pires, "Multiple square wave voltammetry for analytical determination of paraquat in natural water, food, and beverages using microelectrodes," Talanta, Vol. 69, pp. 1200-1207, 2006.

CHAPTER 3

Studies on Integrated Square Wave Voltammetry Redox Sensor

3.1   Introduction

A new technique has arisen which, in our view, surpasses and thus will soon supplant differential pulse voltammetry as the ultimate voltammetric technique. This technique, square wave voltammetry, capitalizes on the present revolution in electronics, particularly the capability of performing on-line computer-controlled experiments with both mini- and microcomputer systems. Square wave voltammetry has attracted attention over the recent decades. The square wave voltammetry technique stemmed from the work of Barker's square wave polarography in the 1950s. Square wave voltammetry is a suitable configuration for high-speed and high-sensitivity measurement. The advantage of Square wave voltammetry is its capability to discriminate capacitive currents and background currents [1-6]. This results in more sensitivity to Faradaic currents than cyclic voltammetry, which is a conventional method. Recently, integrated electrochemical sensors using semiconductor technology for miniaturizing sensor systems have been fabricated, which are widely used in many fields [7-8].

3.2 Design and Fabrication of Integrated Square Wave Voltammetry Redox Sensor

3.2.1 Overview of the Chip

Figure 3.1 shows the photograph and the layout of the integrated square wave voltammetric redox sensor. At the center of the chip there are seven working electrodes and a counter electrode which is needed for electrochemical measurement. Each size of working electrodes is 500 x 500 μm^2, 200 x 200 μm^2, 100 x 100 μm^2, 50 x 50μm^2, 20 x 20 μm^2, 10 x 10 μm^2, and 5 x 5 μm^2. The size of counter electrode is 2.5 mm^2 which is 100 times larger than working electrode of 500 x 500 μm^2. Counter electrode has a wider area compared with working electrodes in order to decrease its surface resistance and to focus the reaction on working electrode.
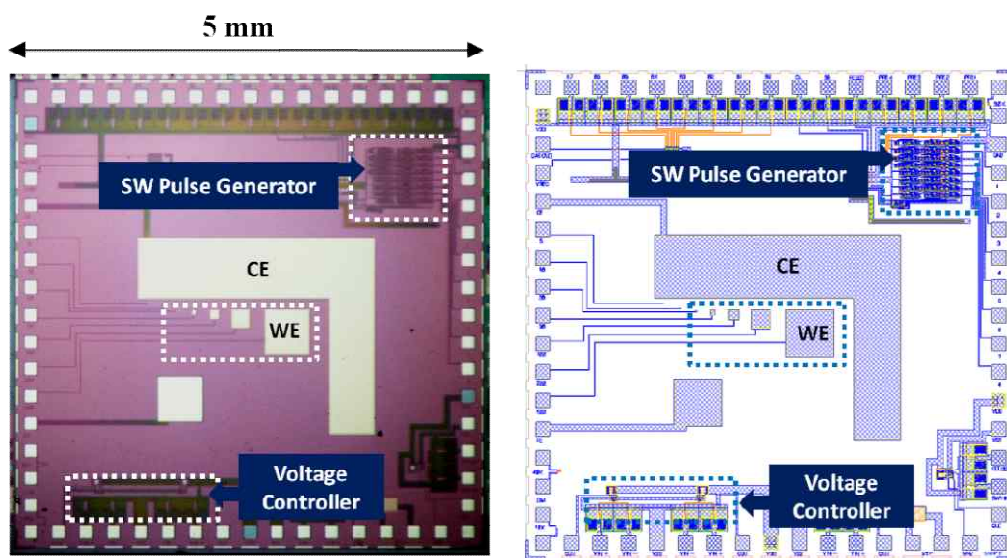
Figure 3.1 The photograph and the layout of the integrated square wave voltammetric redox sensor.

The chip also has a reference electrode, but we used the external reference electrode for more stable potential. We designed the potentiostat using these three electrodes, working electrodes (WEs), counter electrode (CE), and external reference electrode (RE) for electrochemical measurement. There is a square wave pulse generator circuit upper right-hand side of the chip, and the composition of the circuit is described in the next section.

3.2.2   Design of the Square Wave Pulse Generator Circuit

In this section, the principle of square wave pulse generation is explained. Figure 3.2 shows the diagram of a square wave pulse generator. For the magnitude of each pulse, low side and high side, two counters are prepared. This magnitude is called square wave amplitude. The values of counter A and counter B is increased, then a selector pick out the values from two counters alternately. It also can control square wave frequency and step increment by using system clock (CL) and the reference voltage of DAC (Vref), respectively. We already explained about the component of the square wave voltammetry in 2.4.1. The D flip flop (DFF) is made for deglitch.

Figure 3.3 shows the structure of the presetter. Square wave amplitude shown in figure 2.3 is decided by this presetter. Initial value of a counter B is set 0, and initial value of a counter A is decided by the last 4-digit, as shown in figure 3.4. The differential values between counter A and counter B are square wave amplitude of the system. The four presetter is set in front of the counter A for last 4-digit.
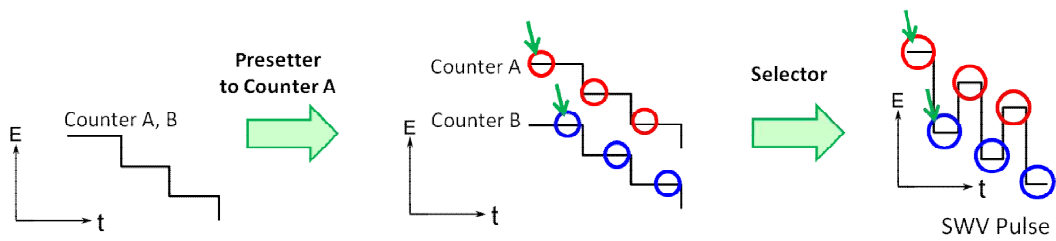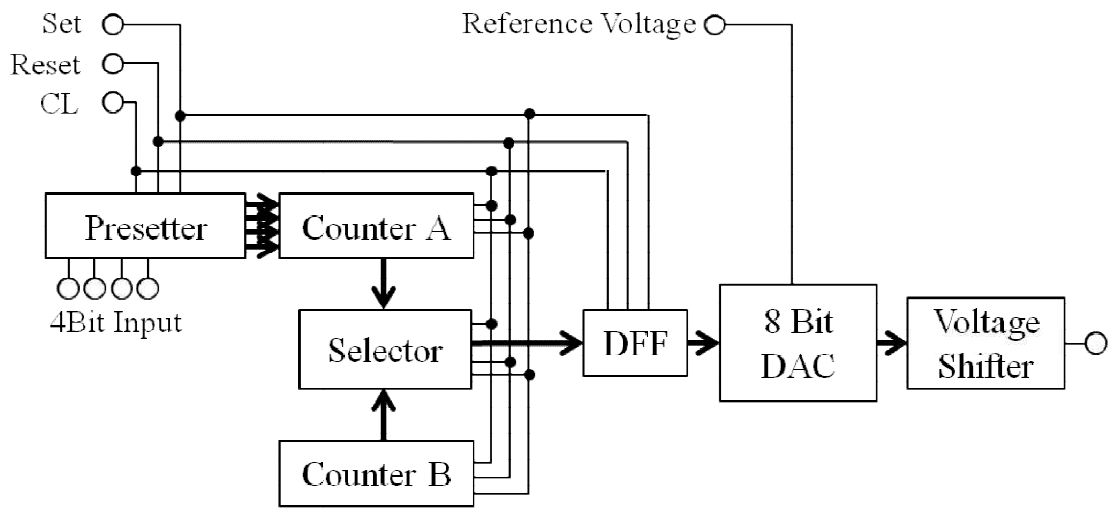
Figure 3.2 Block diagram of the square wave pulse generator.
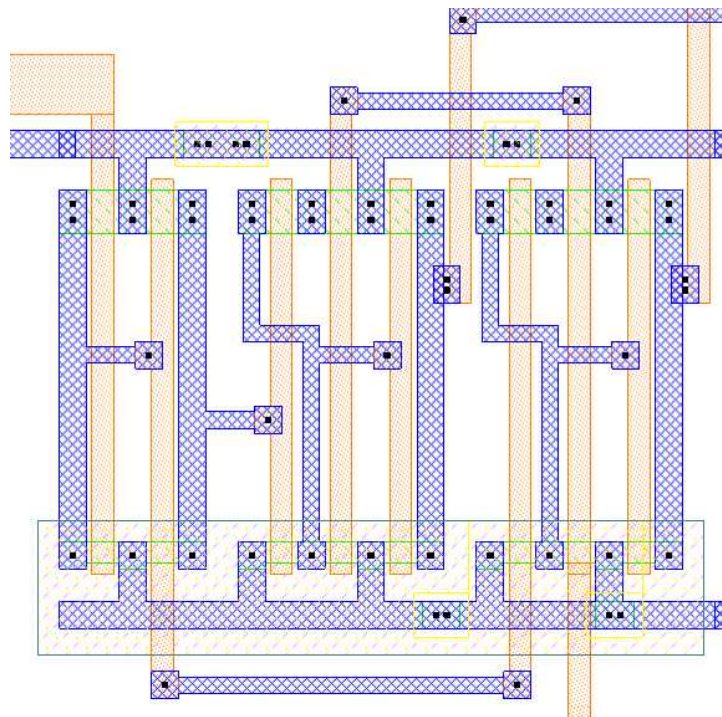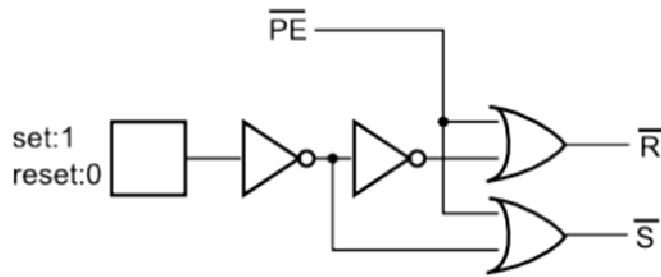
Figure 3.3 Design and layout of the presetter.
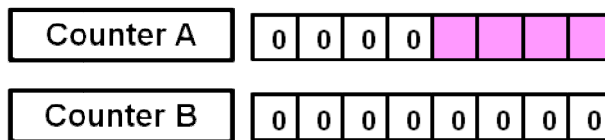
Figure 3.4 Initial value of a counter A and a counter B. The last 4-digit of the counter A

(pink color) is decided by the presetter.
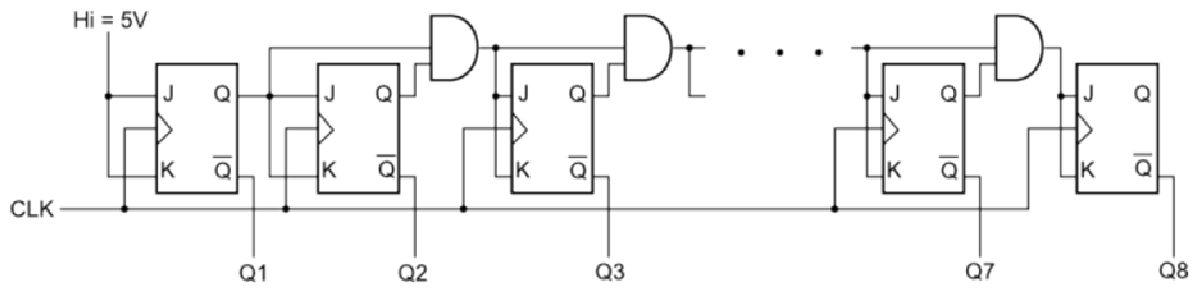
Figure 3.5 The 8-bit synchronous counter.
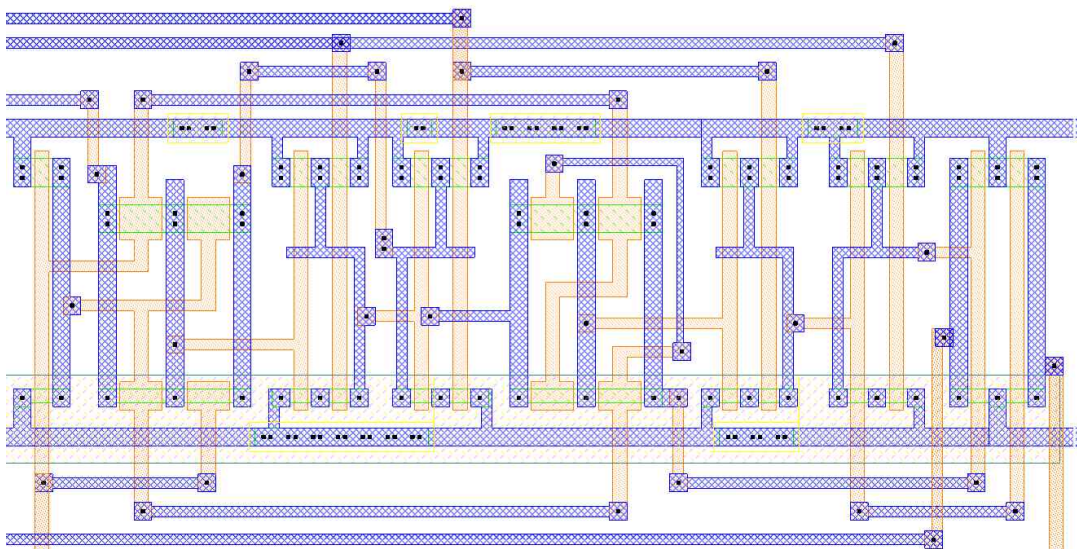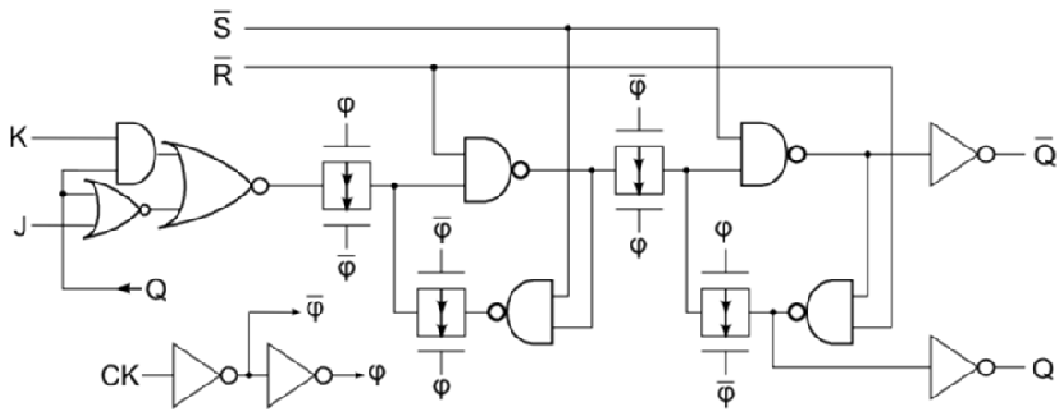
Figure 3.6 Design and layout of the JK flip flop.

Counter is designed as an 8-bit synchronous counter using JK flip flop as shown in figure 3.5. The bit number of counter determines the number of the square wave steps. In other words, square wave steps show the limit of the potential sweep range. If the potential step assume to be $\Delta E = 10$ mV, we can fulfill 2.52 V of the potential range using 8-bit counter. This is the sufficient potential range compared with the potential window of Pt as shown in figure 2.2. For different initial values, two counters are prepared. Figure 3.6 shows the design and layout of the JK flip flop, and figure 3.7 shows a simulation result of an 8-bit counter.
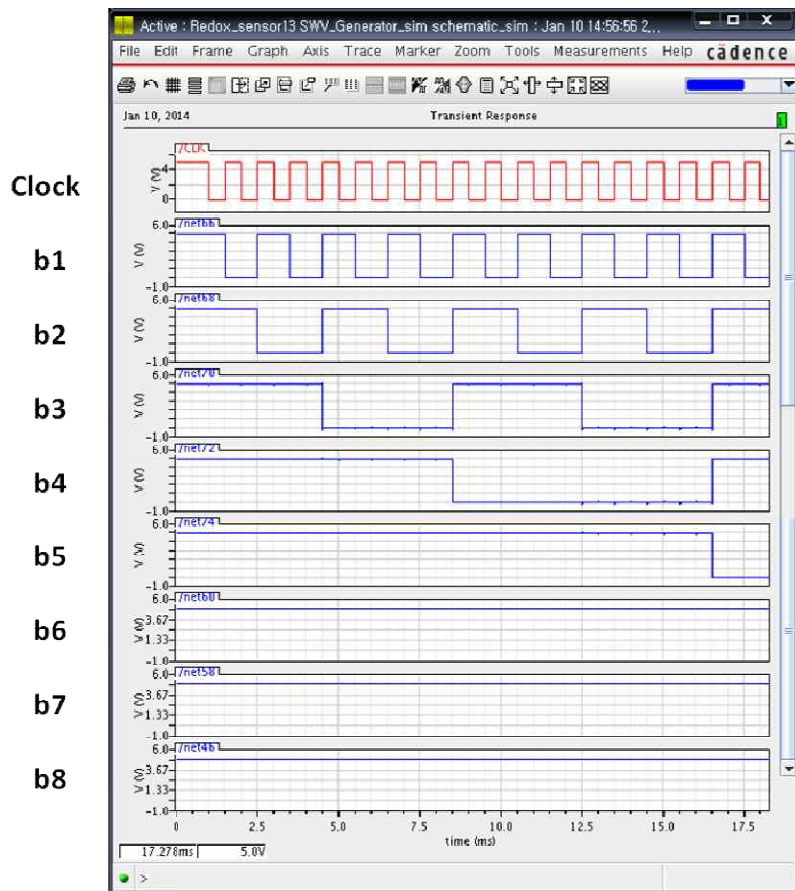
Figure 3.7 Simulation of an 8-bit counter.
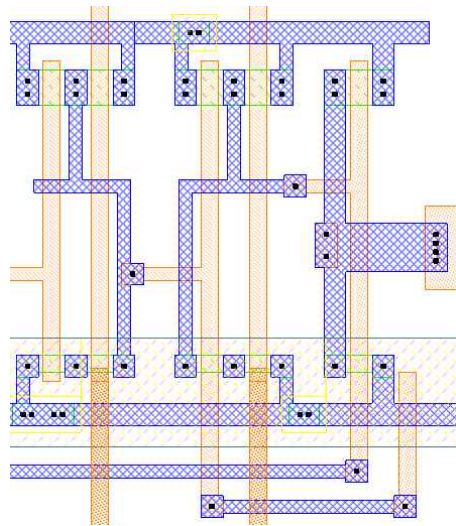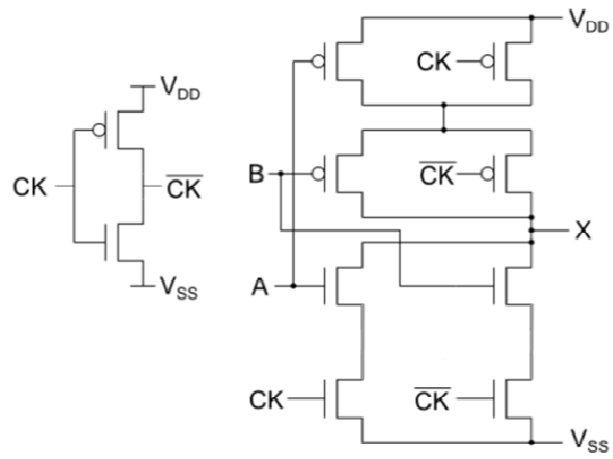
Figure 3.8 Design and layout of the selector.

Selector is composed of logic gate. Figure 3.8 shows the circuit design and layout of the selector. A clock (CK) is used at alternative signal. During the high clock the selector selects A node value, then "A bar" comes out as a output signal. During the low clock the selector selects B node value, then "B bar" comes out as a output signal. After the select gate, the D flip flop (DFF) comes out. Figure 3.10 shows the DFF circuit. DFF is a deglitch circuit which removes the spike occurring from digital logic circuit.

Figure 3.9 Simulation of a selector.
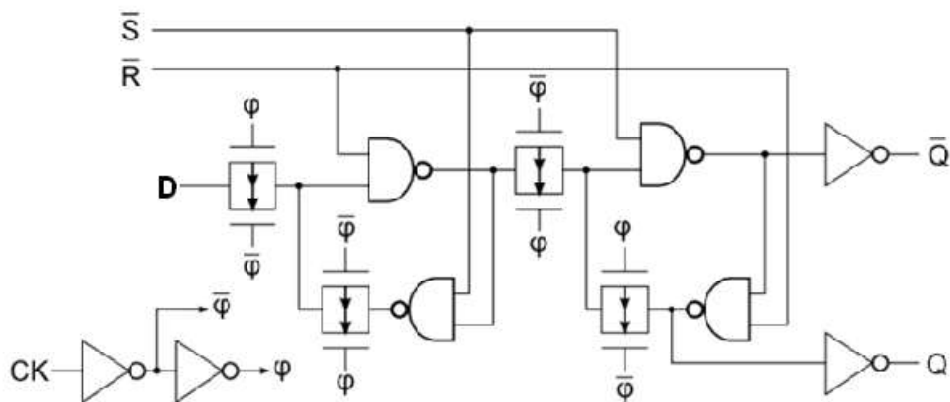
Figure 3.10 Design of the D flip flop.

The 8-bit digital to analog converter (DAC) is designed using R-2R ladder. Figure 3.11 shows the circuit design and the layout of the 8-bit R-2R ladder DAC. The lower part of the layout of figure 3.11 is resistors made of poly-silicon. The value of R is 10 kΩ. The resistance of DAC is determined as controlling the amount of ion injection into the poly-silicon layer. Figure 3.13 is a block diagram from two counters to DAC. This shows the mechanism of the selecting each bit and the flow to DAC.

Figure 3.14 shows the voltage shifter. Voltage shifter is located after the 8-bit DAC for determination of start potential of square wave voltammetry. An output potential Vout equals V2-V1. Square wave pulse enters V2. The offset voltage for shifting potential enters V1.
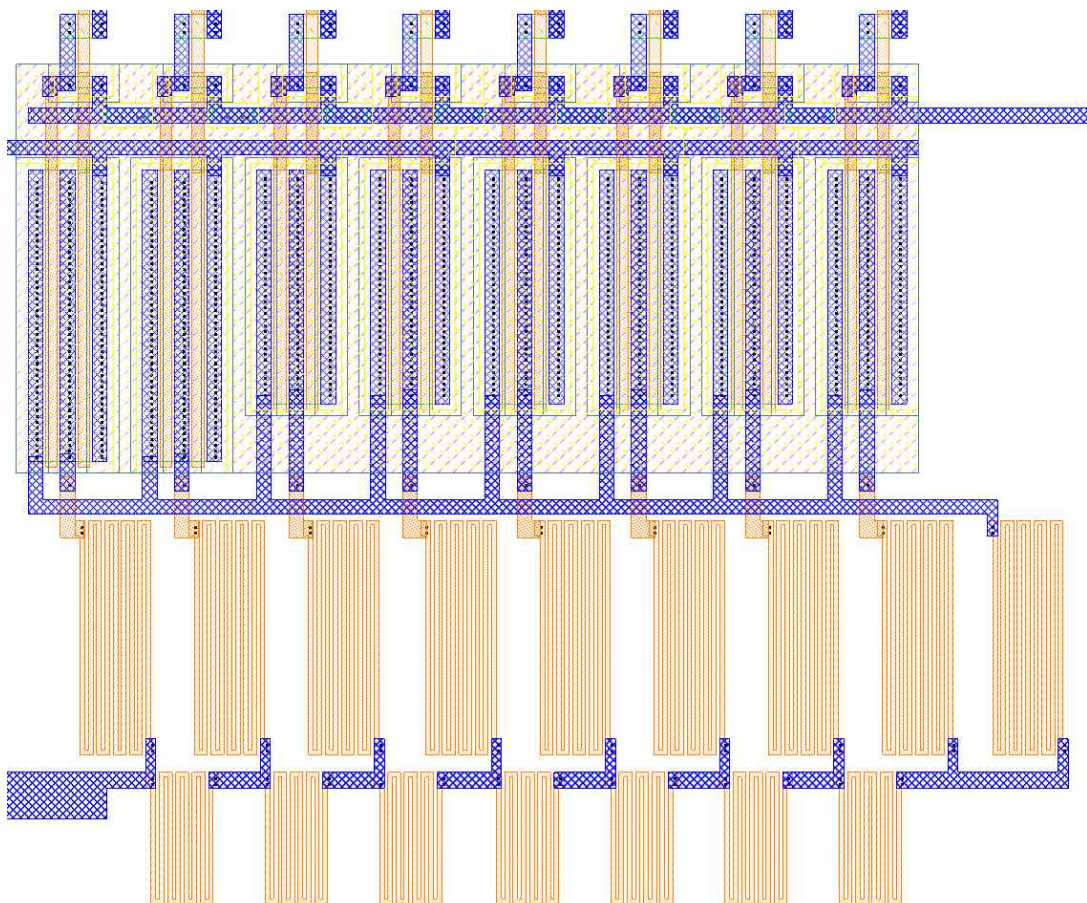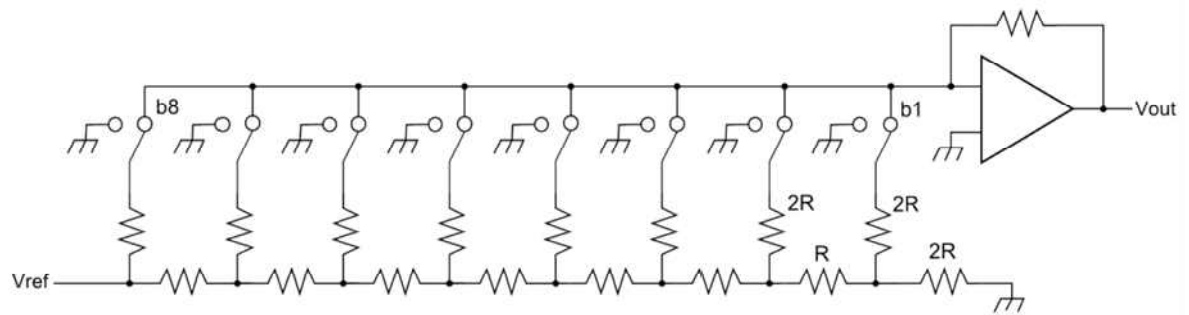
Figure 3.11 Design and layout of the 8-bit R-2R ladder DAC. (R = 10 kΩ)
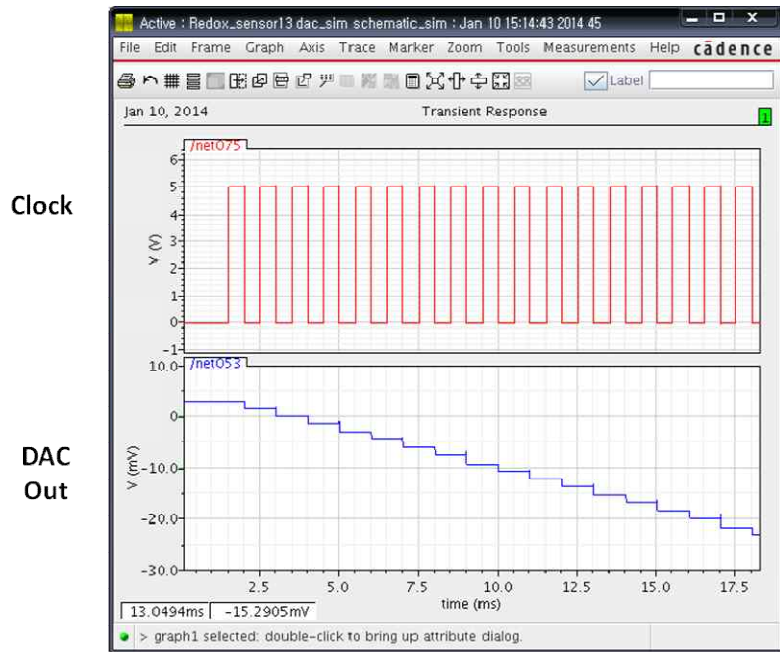
Figure 3.12 Simulation of a DAC.
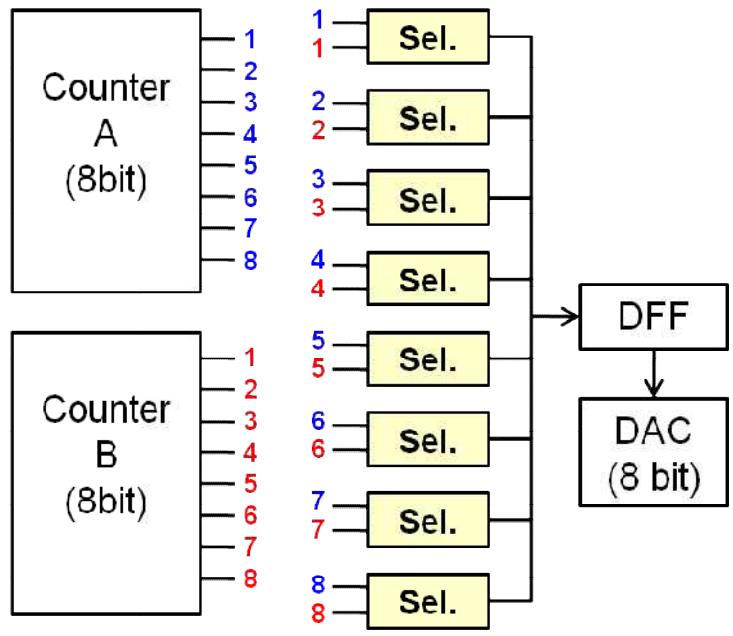
Figure 3.13 Block diagram from counter to DAC.
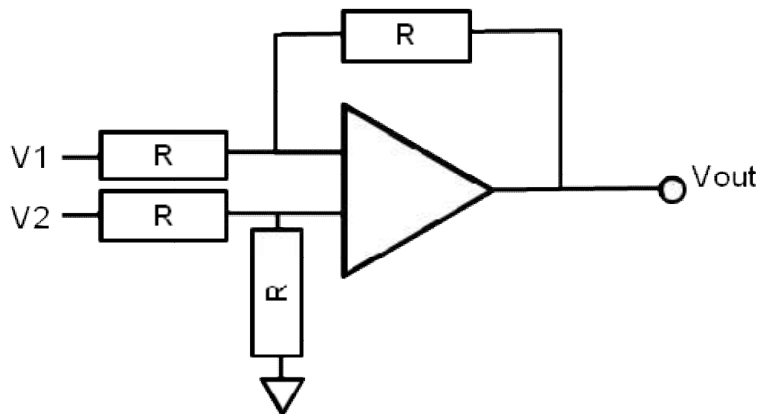
Figure 3.14 A voltage shifter for deciding initial potential.

3.2.3 Design of the OPAMP

In this section, a two-stage operational amplifier (OPAMP) for use as a voltage controller of potentiostat, voltage shifter, and current-voltage converter was designed. The designed bias circuit was of the simple diode-type MOS, and the start-up circuit was achieved using a current mirror for operating the differential amplifier [9-11]. Figure 3.15 show the structure of the OPAMP. The amplification of two-stage OPAMP is easier than one-stage OPAMP. Table 3.1 lists the parameters of n-MOS and p-MOS transistors, capacitor, and resistor.
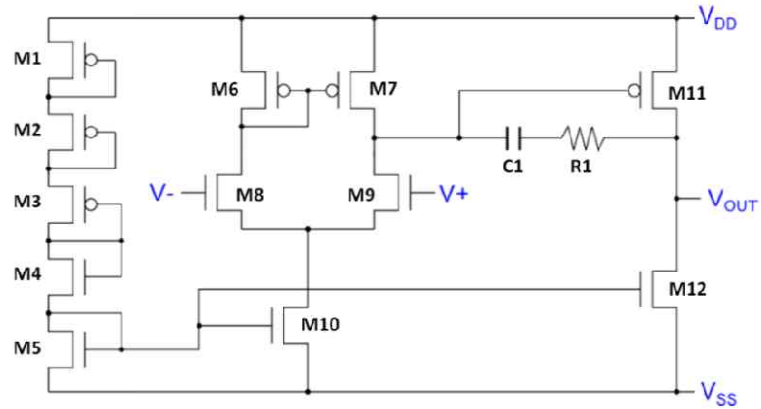
Figure 3.15 The structure of the OPAMP

Component Values (L/W)			
M1	4/12	M8	2/3
M2	4/12	M9	2/3
M3	4/12	M10	4/6
M4	4/6	M11	4/62
M5	4/6	M12	4/26
M6	2/6	C1	3 pF
M7	2/6	R1	80 Ω

Table 3.1 The size of the MOSFET, capacitor, and resistor of the OPAMP.

Figure 3.16 shows the layout of the designed OPAMP. The size is 170 x 130 μm^2. The OPAMP is designed by 2-μm rule.
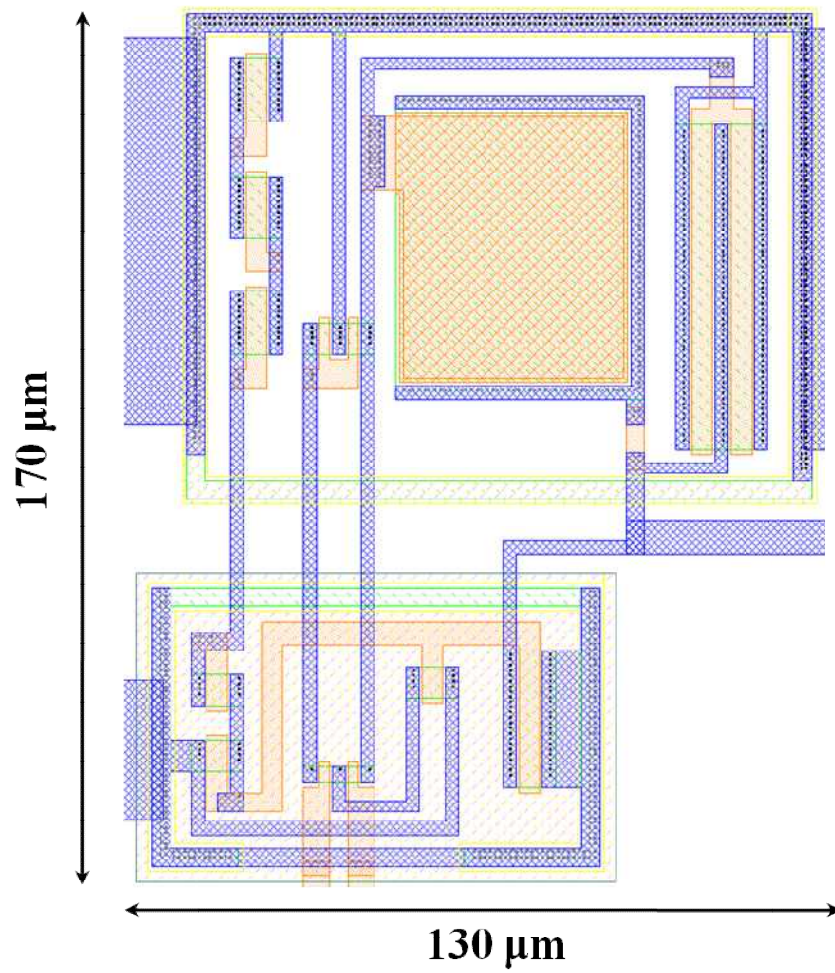
Figure 3.16 Layout of the designed OPAMP
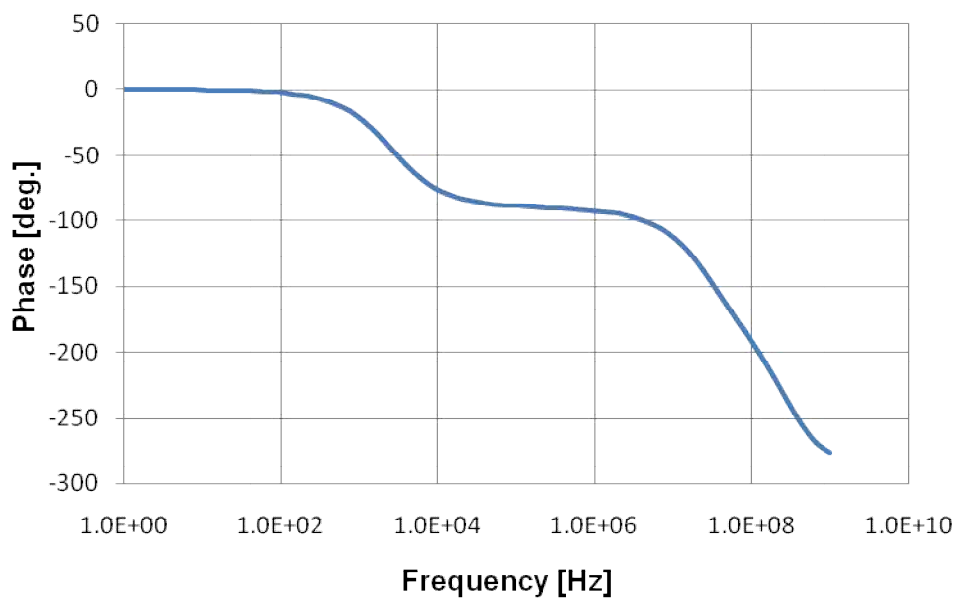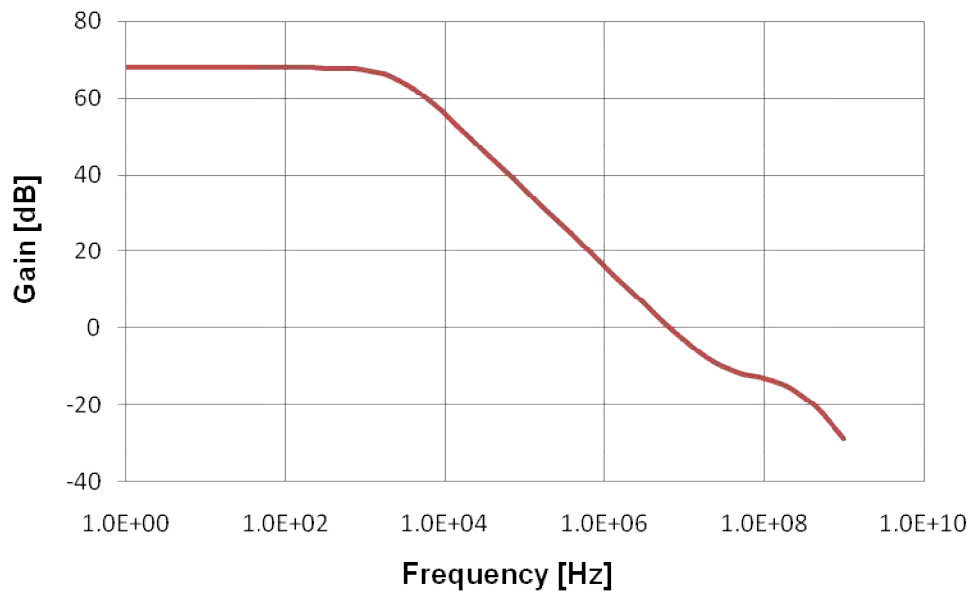
Figure 3.17 Simulation result of the OPAMP. Open loop gain 68 dB, Unity gain

frequency 5 MHz.

3.2.4 Potentiostat for Electrochemical Measurement

A Potentiostat is the equipment that is maintained the constant value of setup potential between a working electrode and a counter electrode. The potentiostat is needed for electrochemical measurement [12-16].
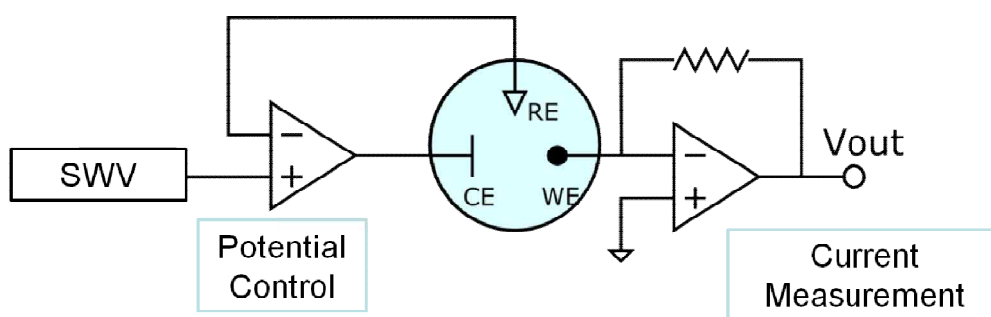
Figure 3.18 The potentiostat.

The concept of electrochemical measurement system in this study is shown in figure 3.18. There are three electrodes, which are counter electrode, reference electrode, and working electrode. Two OPAMPs are also needed. The first stage OPAMP can control the potential which enters the counter electrode, thus the characteristic of voltage follower is important. The second stage OPAMP is conducted as the current to voltage converter. Sufficient phase margin is needed with respect to signal oscillation, and is also needed several kHz of unity gain frequency, because limit frequency of SWV is about 2 kHz. The designed OPAMP has 98 degree of phase margin and has 5 MHz of unity gain. Square wave pulse enters the input (Vin+) of the first stage OPAMP. Then, the output signal is appeared after the output node of second stage OPAMP. The sizes of the working electrodes are from 5

μm □ to 500 μm □. The size of the counter electrode is 2.5 mm^2 which is 100 times larger than working electrode of 500 μm □. The counter electrode must be a wider area compared with working electrodes in order to decrease its surface resistance and to focus the reaction on working electrode. Working electrode is virtual short, and square wave pulse enters the potentiostat. The differential value between reference electrode and working electrode equals the inverse of the input square wave pulse.

3.3   Experiment Setup and Procedures

Figure 3.19 shows the block diagram of the redox sensor system. Figure 3.20 shows a fully packaged redox sensor chip. After packaging, the surface of the chip was cleaned using piranha solution (H2SO4:H2O2 = 4:1). Then, an external Ag/AgCl reference electrode (ALS RE-1B) is connected to the sample well as shown in figure 3.20. The sample solution was dropped onto the chip. 50 μl of the sample solution was sufficient for measurement. The output current flows on WE when a square wave enters the solution. Then, we can measure the output voltage through an external current-voltage converter. Potassium ferricyanide ($K_3[Fe(CN)_6]$) in 1 M potassium nitrate (KNO_3) solution was measured to obtain the characteristics of the proposed chip.

3.4   Measurement Results of Integrated Square Wave Voltammetric Circuit

Figure 3.21 (a) shows an output voltage signal from the square wave pulse generator. Step increment is 4 mV by adjusting reference voltage (Vref) of DAC into 1.3 V. Square

wave amplitude is 75 mV by controlling the value of presetters. When the step increment is 4 mV and the start voltage is -0.6 V, the sweep range of this system is from -0.6 V to +0.7 V. This waveform is totally a good match with a general square wave pulse, but there are unstable waveforms around the points of 5 seconds. This comes from a little difference among the resistors of DAC in figure 3.11, during CMOS process. If we increase the resistor at the next process, the square wave could be stable. In this study, however, the peak current at the point of redox potential could obtain using designed square wave voltammetric pulse generator circuit.

The square wave pulse enters the potentiostat. Then, we can see the output current from the working electrode, as shown in figure. 3.21 (b). From this result which is the current response vs. scanning time plot, the two current values from the end of each half cycle are subtracted. These two currents are the reduction and oxidation current. The subtracted values are plotted. Then, the square wave voltammogram (current vs potential) is obtained.
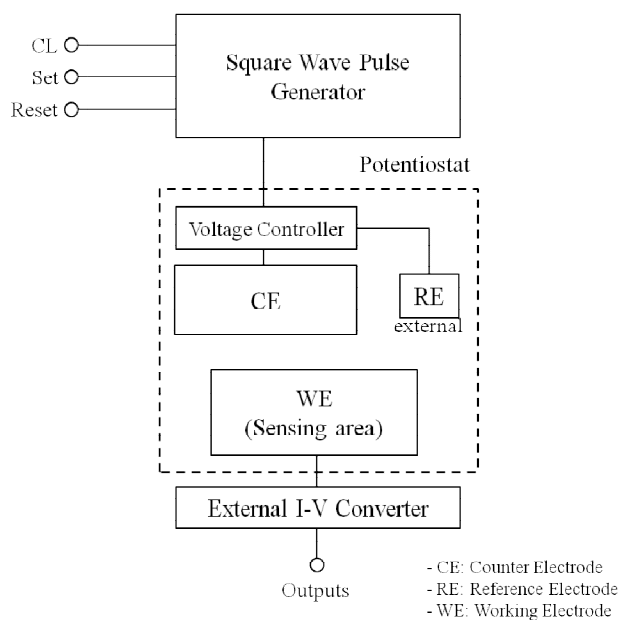
Figure 3.19 Block diagram of the redox sensor system with a square wave pulse generator.

57
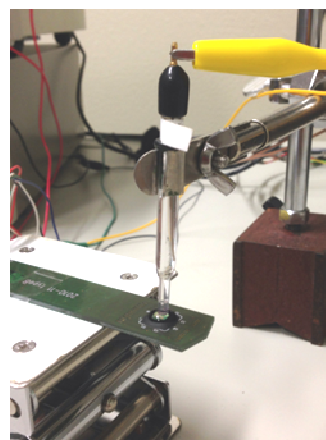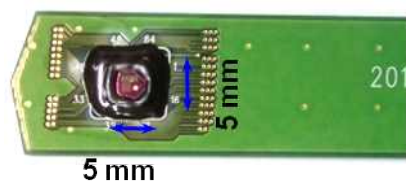
Figure 3.20 Packaged redox sensor chip and the experimental setup of the chip with external Ag/AgCl reference electrode.
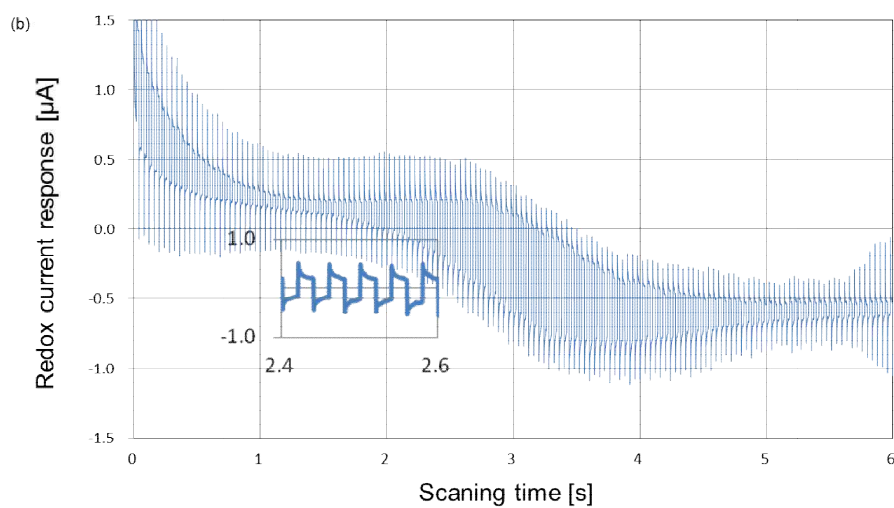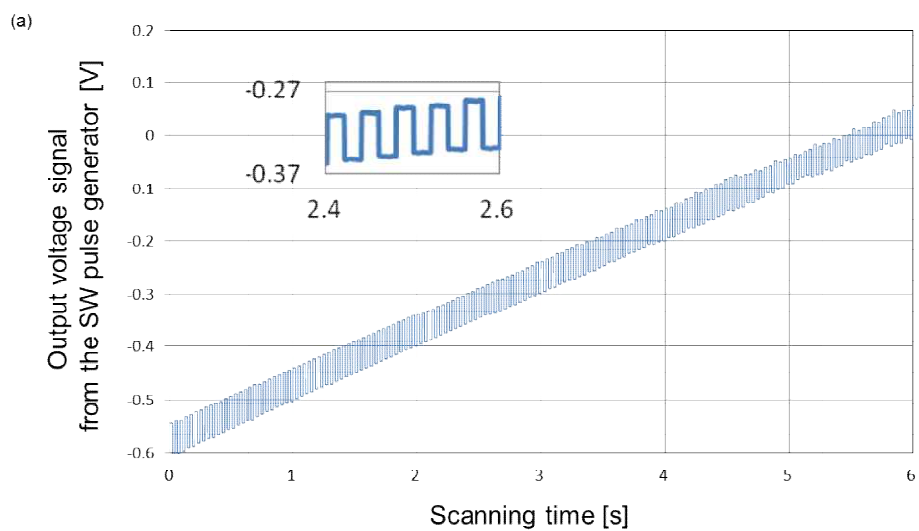
Figure 3.21 (a) Output voltage signal of SW pulse. (b) Reduction-oxidation current response.

The current characteristics can obtain from the differential value between the reduction and oxidation currents, and can also determine the kind of material by its redox potential, as shown in figure 3.22. Figure 3.23 is a comparison of the peak current between potassium ferricyanide and potassium chloride. The peak current of potassium ferricyanide is appeared depends on its concentration, but that of potassium chloride does not.
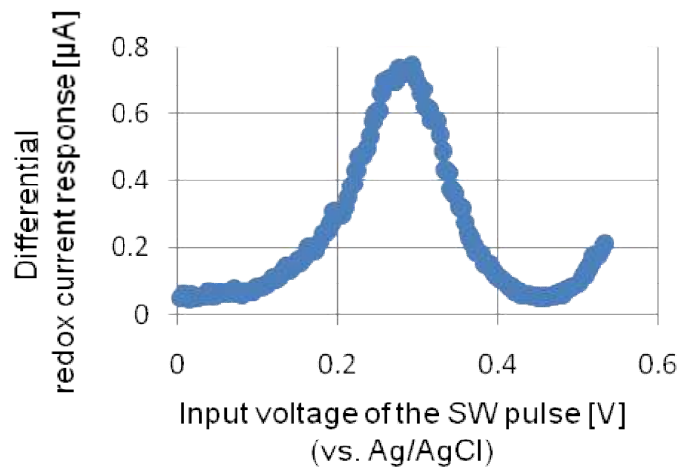
Figure 3.22 current-voltage plot of potassium ferricyanide.
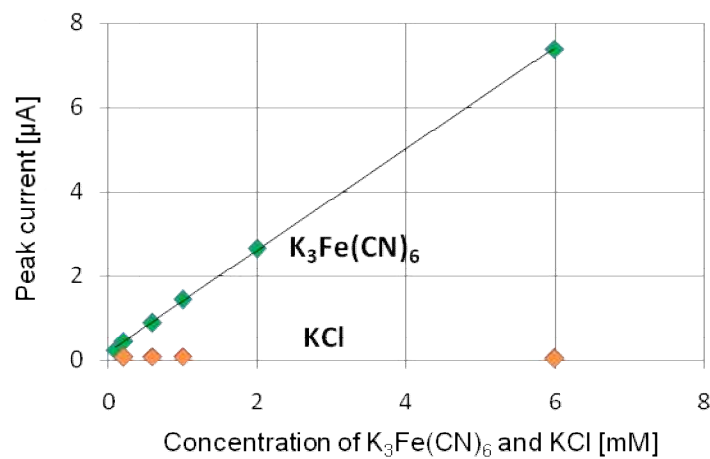
Figure 3.23 Comparison of peak current between potassium ferricyanide and potassium chloride.

To verify the accuracy of the peak current and redox potential of the fabricated chip, we compared the proposed sensor and an electrochemical analyzer (ALS 760EP). Figure 3.24 shows the current response result under the condition of 6 mM potassium ferricyanide at a 200 x 200 μm^2 of working electrode area. Figure 3.24 (a) shows the result of the fabricated chip, and figure 3.24 (b) shows the result of the electrochemical analyzer. The values of the fabricated chip and the electrochemical analyzer are shown in table 3.2. From this result, we can confirm that the fabricated chip can detect potassium ferricyanide with good performance.

Figure 3.25 (a) shows the square wave frequency dependence of the peak Faraday current, and figure 3.25 (b) shows the potassium ferricyanide concentration dependence of the peak Faraday current for the 500 x 500 μm^2 of working electrode. The peak Faraday current means a subtracted capacity current from the net peak current. The peak Faraday current depends linearly on the square root of the SW frequency and the concentration of materials according to the current equation of square wave voltammetry as described in chapter 2.

Frequency (Hz)	Fabricated chip		Electrochemical analyzer	
	Peak current (A)	Redox potential (V)	Peak current (A)	Redox potential (V)
20	8.20×10^{-7}	0.291	8.42×10^{-7}	0.290
50	1.16×10^{-6}	0.292	1.25×10^{-6}	0.295
100	1.57×10^{-6}	0.291	1.84×10^{-6}	0.295
200	2.02×10^{-6}	0.292	2.40×10^{-6}	0.295
500	3.10×10^{-6}	0.292	3.21×10^{-6}	0.295

Table 3.2 Peak current and redox potential between fabricated chip and electrochemical analyzer for 6 mM of potassium ferricyanide.
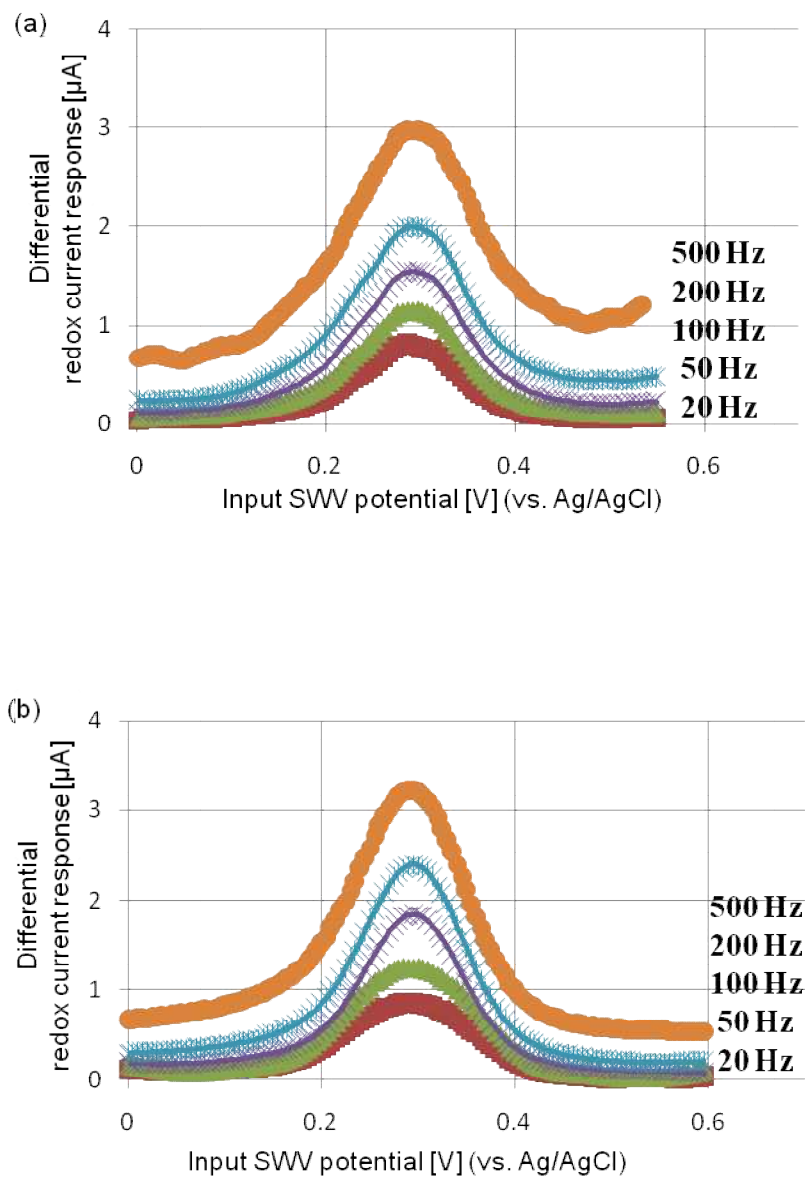
Figure 3.24 Comparison of peak current and redox potential between (a) fabricated chip and (b) electrochemical analyzer for 6 mM of potassium ferricyanide.
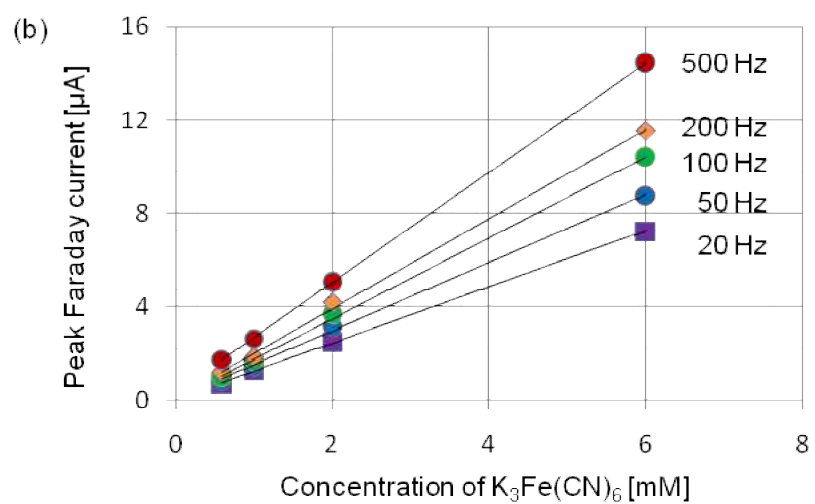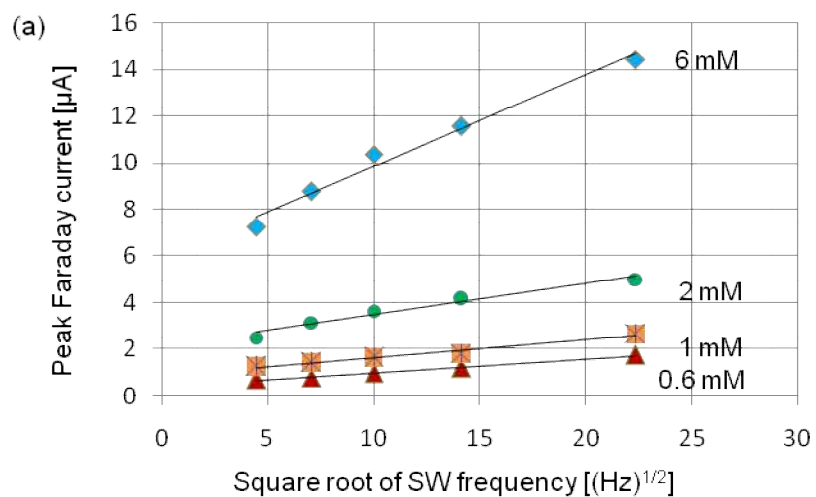
Figure 3.25 (a) SW frequency dependence of the peak Faraday current. (b) Potassium ferricyanide concentration dependence of the peak Faraday current.

This sensor showed a strong linearity in the plots of the peak Faraday current versus the square root of the SW frequency with accuracy of over 96% and in the plots of the peak Faraday current versus concentration with an accuracy of over 99% in the range of 0.6 to 6 mM and 20 to 500 Hz, respectively.

Then, we can think about the limitation of scan speed of this sensor, this is decided by frequency. Figure 3.26 shows the current responses of each frequency from 20 Hz to 2 kHz. Figure 3.27 shows the current characteristics which are current values at peak point, current values at base line, and current-voltage plot of each frequency. If the frequency is increased, capacitive current is increased as already explained in chapter 2. When capacitive current is quite large compared with the faraday current, peak current of SWV measurement does not observe. This point can decide the limitation of frequency. In the figure 3.26, the peak current can confirm until 1 kHz, but it cannot see at 2 kHz measurement. By the way, at 1 kHz of the figure 3.27 the current-time plot, the current value of each cycle is unstable because of the harmonic wave. I supposed that this harmonic wave comes from the designed SWV pulse generator circuit. Thus, the limitation of frequency of the proposed sensor is 500 Hz. At 500 Hz, sampling of the stable current value is enabled, and the peak current also can observe. In the future, if we modified the harmonic wave of the circuit, limitation of frequency could be improved.
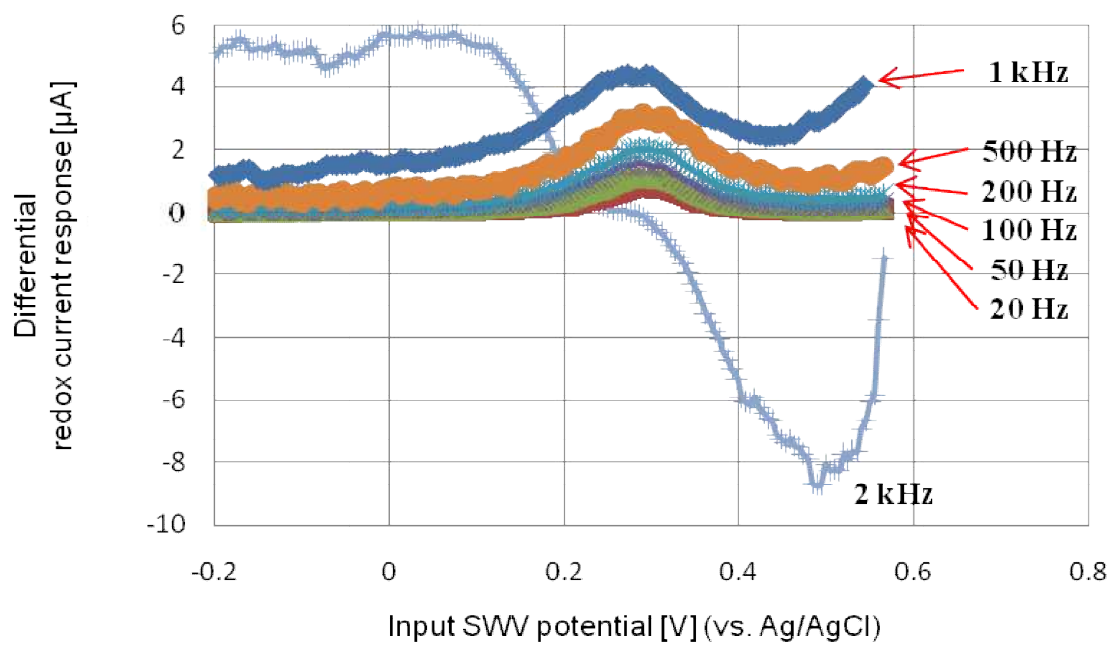
Figure 3.26 Current characteristics from 20 Hz to 2 kHz of the proposed sensor.

Current-time plot at peak point

Current-time plot at base line

Current-voltage plot
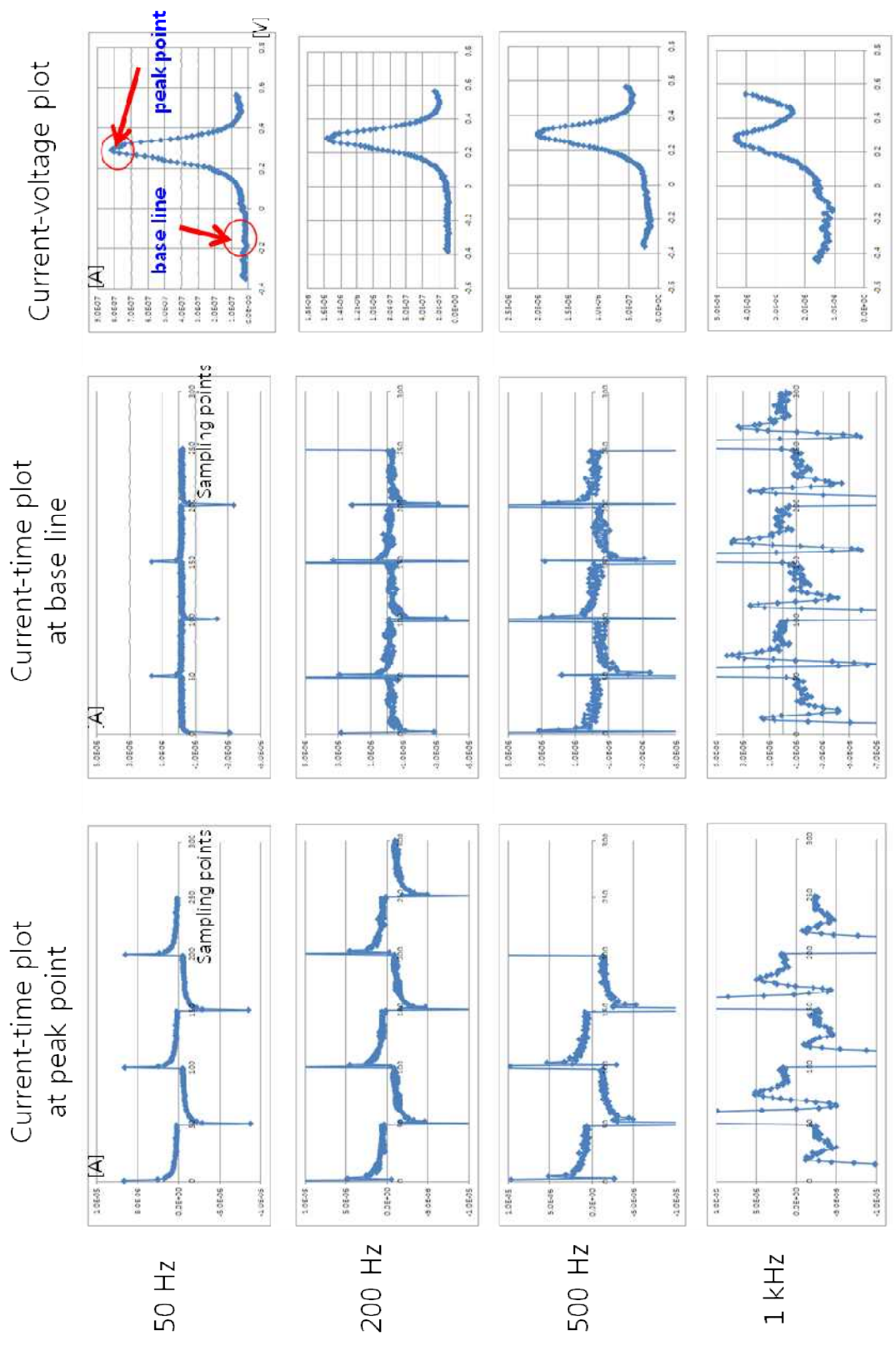
Figure 3.27 Current characteristics of proposed sensor

66

3.5 Conclusion

In this chapter, we introduced the redox sensor with on-chip square wave voltammetry circuit. An integrated redox sensor chip was successfully designed and fabricated. The square wave pulse was observed as expected. We confirmed that the proposed sensor system can detect potassium ferricyanide with good performance by comparison with an electrochemical analyzer. We can control the scan rate, square wave amplitude, and the step increment as purposes of measurement. This sensor shows a good linearity in the range of 0.6 to 6mM and 20 to 500 Hz. We also successfully obtained the detection limit as low as 0.6 mM under the condition of a higher scan rate than cyclic voltammetry employing the first integrated SWV redox sensor system. We also described each part of the square wave pulse generator. The OPAMP is made for voltage control and current measurement. From these results, the proposed sensor can apply the other biomaterials and array sensors.

References

[1] V. Mirceski, S. Komorsky-Lovric, and M. Lovric, "Square-Wave Voltammetry: Theory and application", Springer-Verlag Berlin Heidelberg, 2007.

[2] M. Lambrechts and W. Sansen, "Biosensors: microelectrochemical devices", IOP Publishing, Bristol UK, 1992.

[3] E. T. Smith and B. A. Feinberg, "Redox properties of several bacterial ferredoxins using square wave voltammetry", Journal of Biological Chemistry, Vol. 265, pp.14371-14376, 1990.

[4] J. J. O'Dea, J. Osteryoung, and T. Lane, "Determining kinetic parameters from pulse voltammetric data", Journal of Physical Chemistry, Vol. 90, No. 12, pp. 2761-2764, 1986.

[5] J. J. O'Dea, K. Wikiel, and J. Osteryoung, "Square-wave voltammetry for ECE mechanisms", Journal of Physical Chemistry, Vol. 94, No. 9, pp. 3628-3636, 1990.

[6] J. J. O'Dea, J. Osteryoung, and R. A. Osteryoung, "Theory of square wave voltammetry for kinetic systems", Analytical Chemistry, Vol. 53, No. 4, pp. 695-701, 1981.

[7] J. Zhang, Y. Huang, N. Trombly, C. Yang, and A. Mason, "Electrochemical array microsystem with integrated potentiostat", Proceeding of IEEE Sensors, p. 385, 2005.

[8] P. M. Levine, P. Gong, K. L. Shepard, and R. Levicky, "Active CMOS Array for Electrochemical Sensing of Biomolecules", IEEE 2007 Custom Integrated Circuits Conference, p. 825, 2007.

[9] P. R. Gray and R. G. Meyer, "MOS operational amplifier design-a tutorial overview", IEEE Journal of Solid-State circuits, Vol. 17, Issue. 6, pp. 969-982, 2003.

[10] D. Johns, and K. Martin, "Analog Integrated Circuit Design", John Wiley and Sons, New York, 1997.

[11]R. Jaeger, "Microelectronic Circuit Design", McGraw Hill, 1997.

[12]M. D. Steinberg and C. R. Lowe, "A micropower amperometric potentiostat", Sensors and Actuators B, Vol. 97, pp. 284-289, 2004.

[13]H. S. Narula and J. G. Harris, "VLSI potentiostat for Amperometric measurements for electrolytic reactions", ISCAS 2004. Proceedings of the 2004 International Symposium on Circuits and Systems, pp. I-457 – I-460, 2004.

[14]Erik Lauwers, Jan Suls, Walter Gumbrecht, David Maes, Georges Gielen, and Willy Sansen, "A CMOS Multiparameter Biochemical Microsensor With Temperature Control and Signal Interfacing", IEEE Journal of Solid-State Circuits, Vol. 36, No. 12, pp. 2030-2038, 2001.

[15]Kwang-Seok Yun, Joonho Gil, Jinbong Kim, Hong-Jeong Kim, Kyunghyun Kim, Daesik Park, Myeung su Kim, Hyungcheol Shin, Kwyro Lee, Juhyoun Kwak, and Euisik Yoon, "A miniaturized low-power wireless remote environmental monitoring system based on electrochemical analysis", Sensors and Actuators B, Vol. 102, pp. 27-34, 2004.

[16]M. Stanacevic, K. Murari, A. Rege, G. Cauwenberghs, and N. Thakor, "VLSI Potentiostat Array with Oversampling Gain Modulation for Wide-Range Neurotransmitter Sensing", IEEE Transactions on Biomedical Circuits and Systems, Vol. 1, Issue 1, pp. 63-72, 2007.

CHAPTER 4

Studies on Array Sensor Employing Integrated Square Wave Voltammetry Redox Sensor

4.1 Introduction

The integration and miniaturization of an electrochemical sensor on Si technology have appeared in recent years [1-5]. Portable diagnosis and high speed measurement system are developed with the demands for the point of care testing, the simple detecting, and on-site measurements in agriculture, environmental field, and medical science. Huge and external instruments should be miniaturized for simple and fast measurement. Electrochemical sensors based on complementary metal-oxide-semiconductor (CMOS) technology would be possible to solve these requirements. Recently, there are some reports for electrochemical array sensor for bioimaging. The location information and amount of biomaterials can be monitored using array sensor system as in-vivo and in-vitro measurement. In 2005, an electrochemical array microsystem without integrated potentiostat is published [6]. In 2012, an amperometric sensor for multi-point biosensing with integrated I-V converter has been worked using external cyclic voltammetry pulse generator [7]. For miniaturization and simple measurement, integration of pulse generator, potentiostat, and readout circuit is required.

In chapter 3, we already have been worked using an on-chip square wave voltammetric redox sensor system for high speed measurement and miniaturization [8]. Potassium ferricyanide was detected by using the on-chip square wave voltammetric method on a

single working electrode instead of using cyclic voltammetry. In this chapter, we report an integrated 8 x 8 array redox sensor system using on-chip square wave pulse generator circuit for multi-point and high speed measurement.

4.2 Design of Array Sensor Employing Integrated Square Wave Voltammetry Circuit

4.2.1 Overview of the Chip Layout
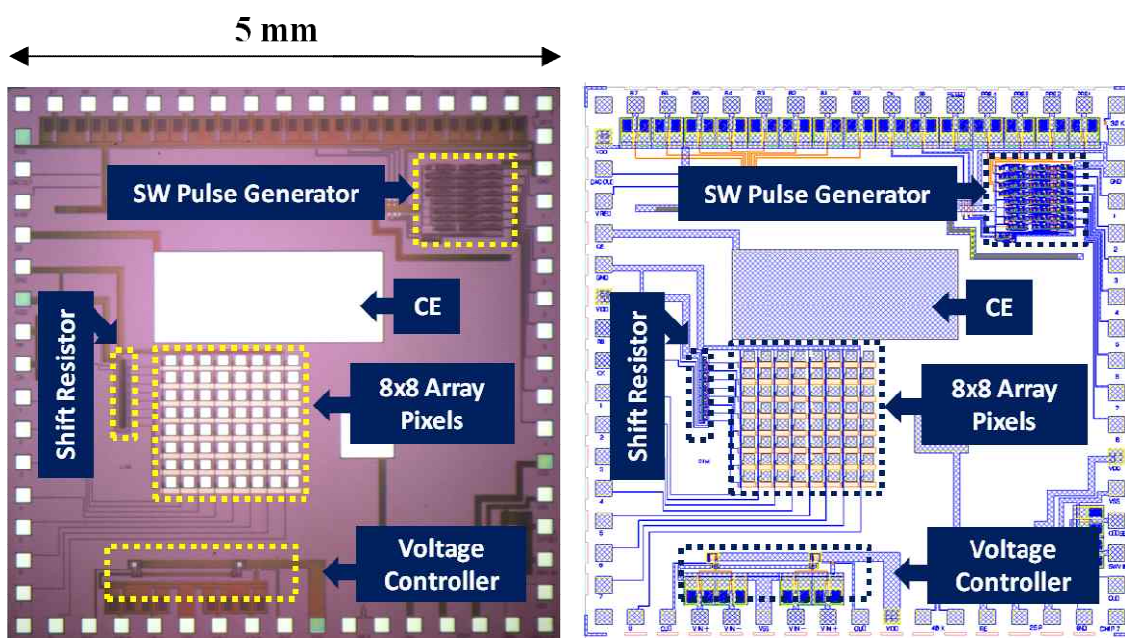
Figure 4.1 Top view of the sensor chip (Design and layout). Square wave pulse generator, an 8 x 8 array sensing area, counter electrode, shift resistor, and voltage controller circuit are integrated.

Figure 4.1 shows the photograph and the layout of the integrated square wave voltammetric redox sensor with array working electrodes. This chip consists of square wave pulse generator, and 8 x 8 array working electrodes (or array pixels), counter electrode, shift resistor, and voltage controller. The 8 x 8 array working electrodes were made of platinum whose size is 100 μm x 100 μm for a reduction-oxidation reaction between array electrodes and biomaterials. Counter electrode whose size is 1.6 mm^2 was also made of platinum because of its stability for a wide range of potentials. Counter electrode must be wider than working electrodes in order to decrease its surface resistance and to focus the reaction on working electrodes. Square wave pulse generator circuit is already explained in chapter 3.2.2.

4.2.2   Shift Resistor Circuit

A shift resistor consists of D flip flop (DFF). In this study, an 8-bit shift resistor is used to measure an 8 x 8 array sensors. Figure 4.2 shows the 8-bit shift resistor using reset signal, and figure 4.3 shows the circuit of the inside of the DFF. When a reset signal and a low clock signal are applied, the output of the DFF is maintained by present value, because a latter part of the DFF is maintained by a present value. By the way, when high clock signal is applied, a fore part of the DFF is maintained by a present value and a latter part of the DFF is changed the value. As a result, during the high clock signal, the output value of the DFF is changed. Figure 4.4 show the layout of the fabricated shift resistor. Figure 4.5 show the simulation result of the shift resistor.
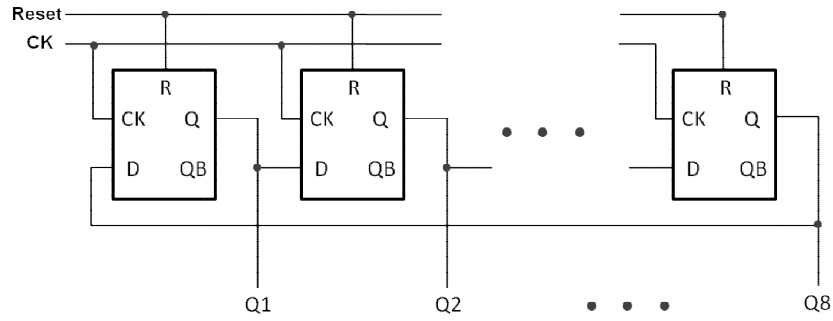
Figure 4.2 The structure of the shift resistor.
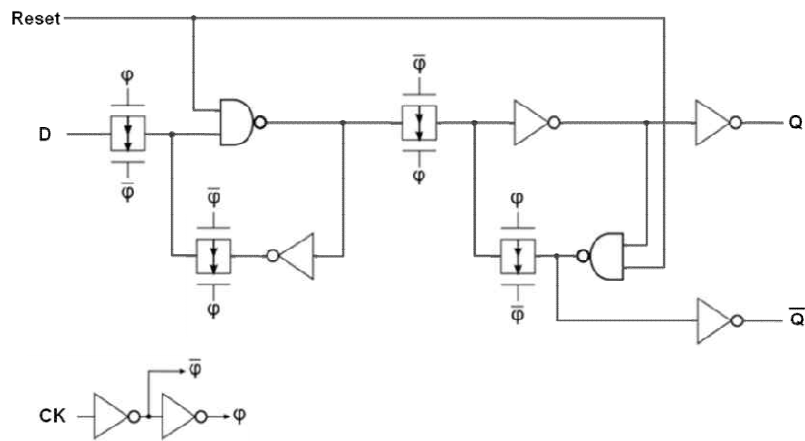
Figure 4.3 Each cell of the shift resistor using D flip flop.

74
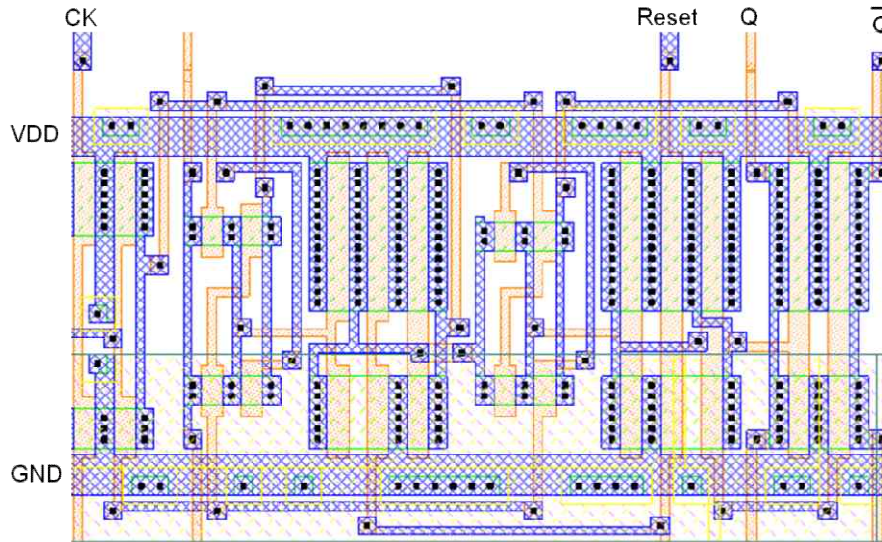
Figure 4.3 Layout of the shift resistor.
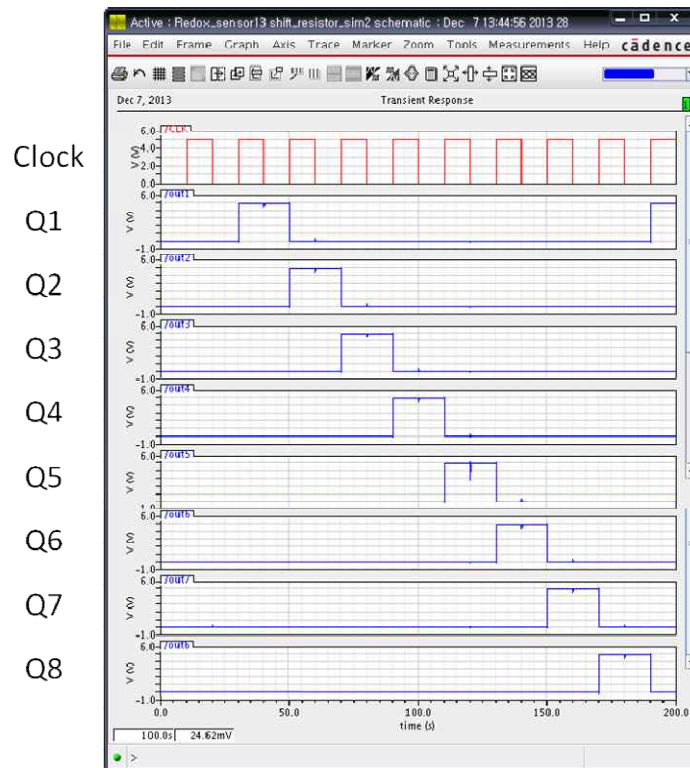
Figure 4.5 Simulation of an 8-bit shift resistor. Clock and 8 output signals (Q1 ~ Q8).

4.3   Experimental Setup and Procedure

   Figure 4.2 shows a block diagram of the proposed 8 x 8 array redox sensor system. The redox sensor chip consists of the square wave pulse generator, a counter electrode, 8 x 8 array working electrodes, a voltage controller. Pulse generator (Tektronix DG 2020A) is used for applying system clock, set and reset clock. An Ag/AgCl reference electrode and 8 I-V converter is used as an external unit. The square wave which comes from square wave pulse generator in a chip enters the counter electrode through the voltage controller.
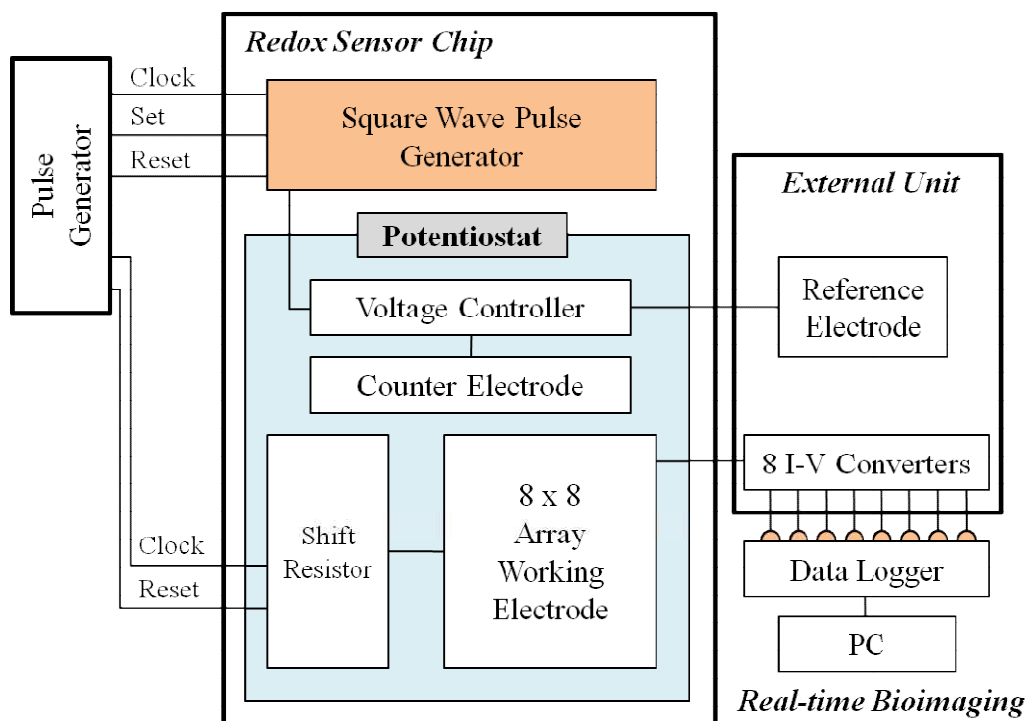
Figure 4.2 Block diagram of the proposed redox sensor system.

The Ag/AgCl reference electrode is connected to a sensor to monitor the potential of the solution. The output current flows on each 8 x 8 array WE when a square wave enters the solution. The shift resistor can read each current signal of 8 x 8 array pixels in order. Then, we can measure the output voltage of each pixel through an external current-voltage converter and a data logger (Keyence NR-500, NR-HA08).

The result is shown on a monitor through a data logger. Step increment can control by the reference voltage of the 8 bit DAC. When 2.6 V and 5.2 V of the reference voltage enter the DAC, the step increment is 10 mV and 20 mV, respectively. The square wave frequency can control by the input system clock as shown in figure 4.2. If we know the square wave frequency, the step increment, and the measurement potential range, we can calculate a frame rate of the system. Figure 4.3 shows the entire measurement system for 8 x 8 array redox sensor.

Figure 4.4 shows the mechanism of a measurement method and readout order. Each electrode has its own nMOS switch. When this nMOS switch is on by the shift resistor, the signal goes to the readout circuit which is I-V converter. There are 8 times sweep of square wave pulse at each column. An 8 pads and I-V converter are needed for obtaining the output signals of each line. In this system, the frame rate equals to 8 times scan rate of square wave. The scan rate is determined by the square wave frequency and square wave amplitude.

We already confirmed that the sensor was operated until 500 Hz of square wave frequency in figure 3.22. This proposed redox sensor system was designed to operate 400 ms/frame under the condition of 20 mV and 500 Hz of step increment and square wave frequency, respectively.
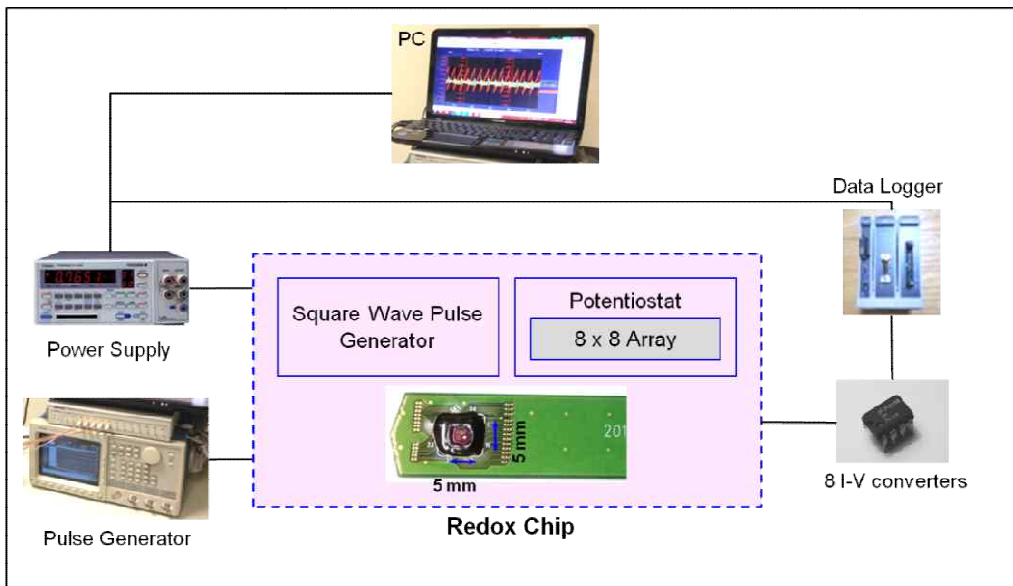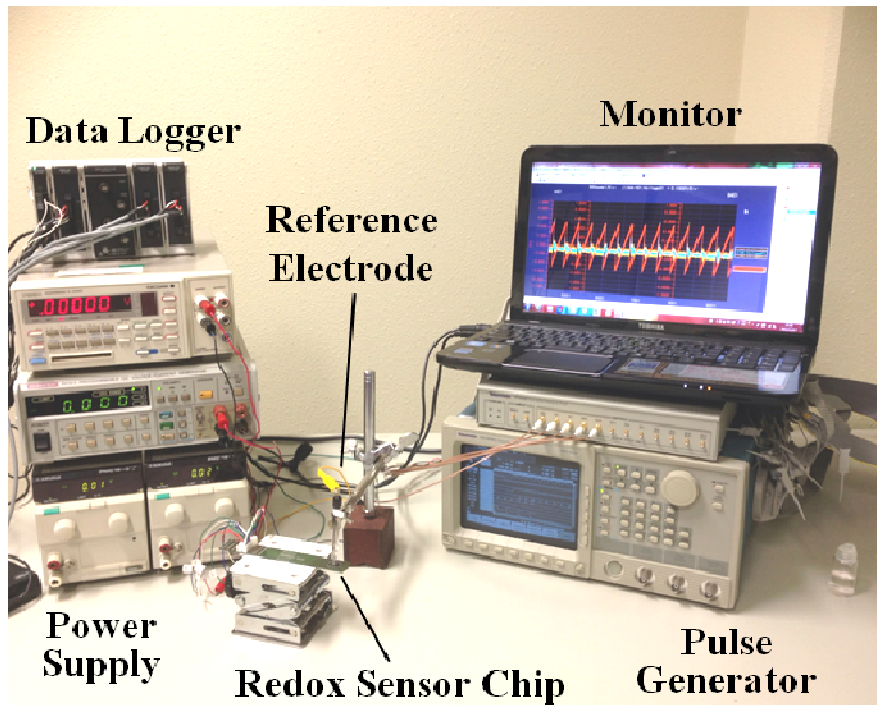
Figure 4.3 Entire measurement system for 8 x 8 array sensor.
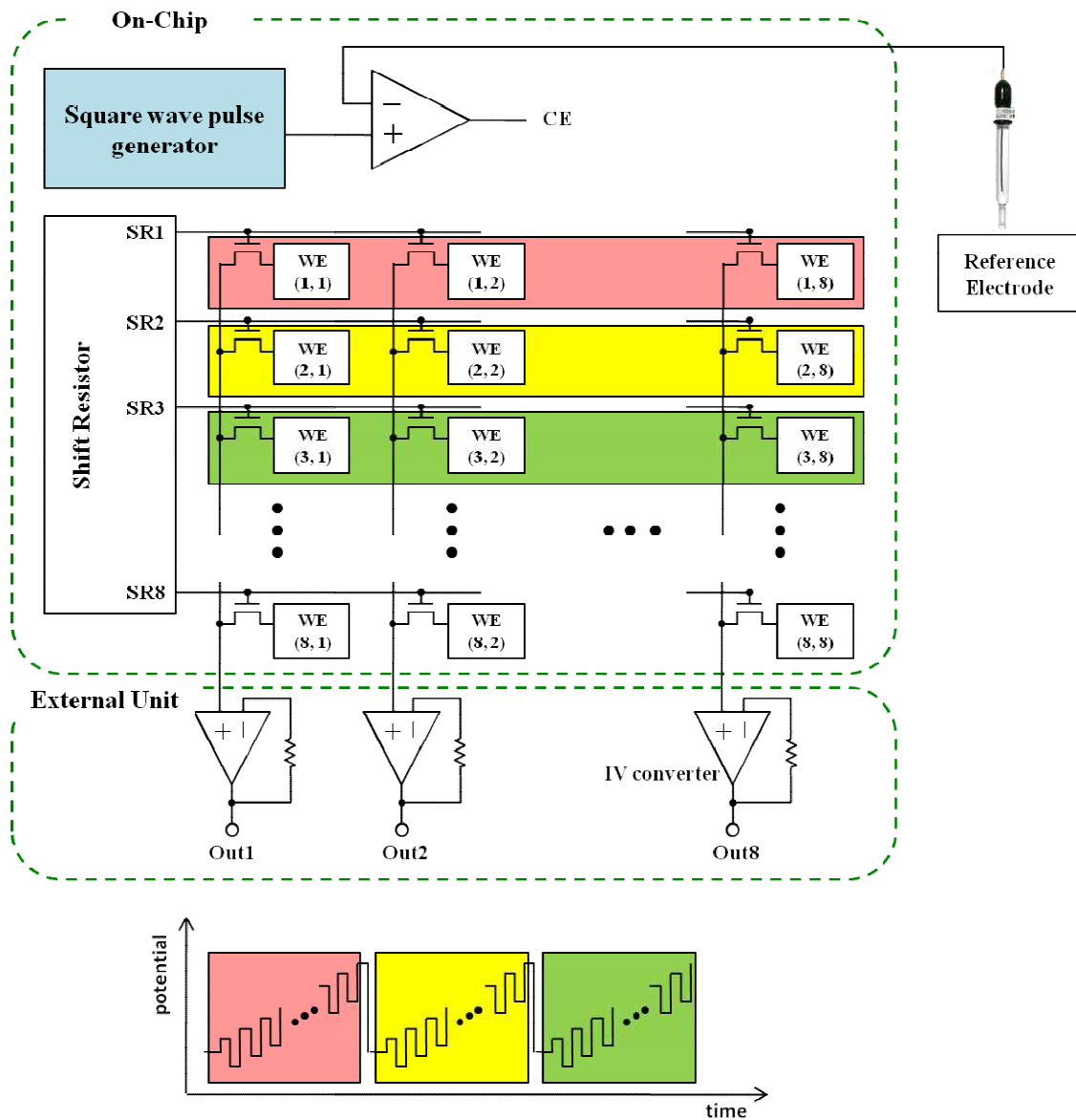
Figure 4.4 Conceptual diagram of square wave voltammetry measurement.

4.4   Implementation and Experimental Results

Figure 4.5 shows the current responses of the square wave voltammograms from 8 x 8 array pixels at 6 mM of potassium ferricyanide in 1 M potassium nitrate (KNO3) solution. Step increment is 4 mV, square wave amplitude is 75 mV, and square wave frequency is 50 Hz. The average peak current of 64 pixels is 301 nA, and the standard deviation is 59.8 nA. The peak currents among the pixels are somewhat different. There are two reasons with regard to peak currents variation.
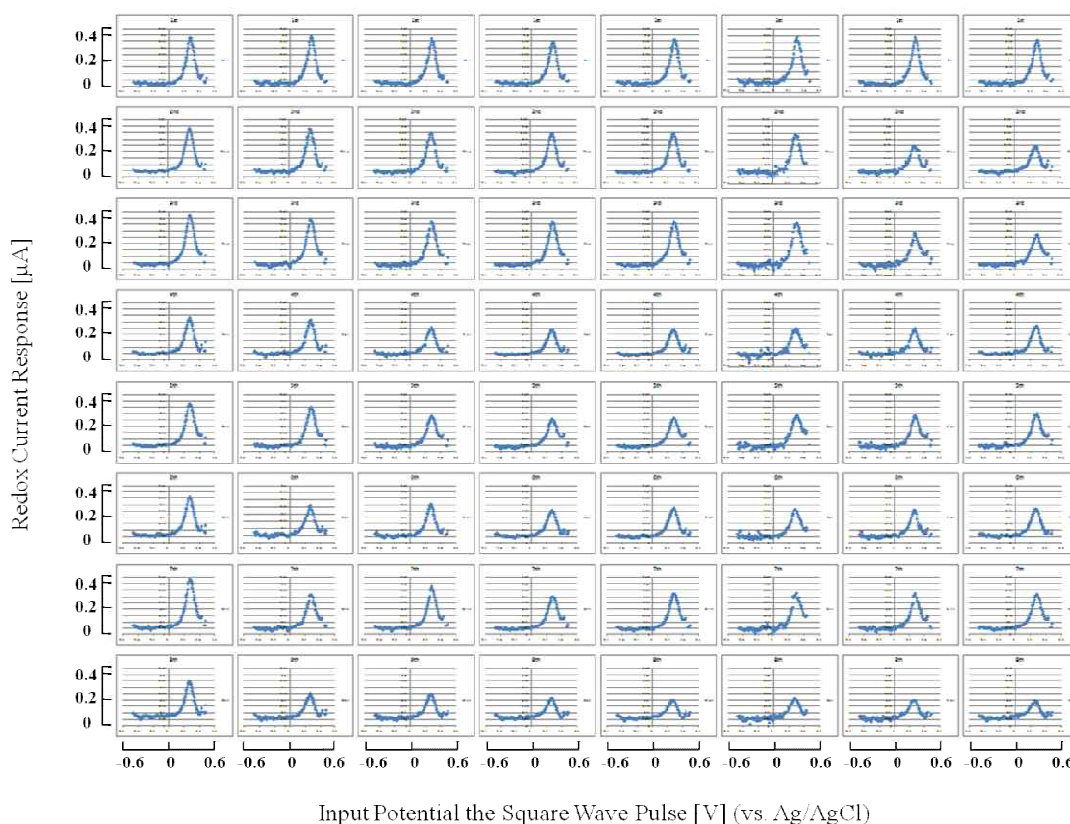
Figure 4.5 Current responses of the square wave voltammetry from 8 x 8 array pixels. 50 Hz of Square wave frequency. 6 mM Potassium ferricyanide (K3[Fe(CN)6]) in 1 M potassium nitrate (KNO3) solution.

The first reason is comes from the area differentials of working electrodes. During the lift-off process for the formation of working electrodes, the variation of working electrodes area is occurred removing the edge of the working electrodes. The peak current is a function of concentration, electrode area, and square wave frequency from the equation 2.9. Square wave frequency and concentration of the material is fixed. Thus, we can think that an effective area of working electrodes is asymmetry.

The second reason of peak currents variation is in the diffusion layer of working electrodes. The diffusion layer is the region in the vicinity of the electrode where the mass transportation is occurred because of the concentration difference. If the distance between the working electrodes is smaller than the diffusion layer length, the peak current is also influenced by this overlapped diffusion layer. The distance between the working electrodes of the fabricated chip is 60 μm. The equation of the diffusion layer is as in the following.

$$\delta = \sqrt{\pi D t} \qquad\qquad (4.1)$$

where δ is the diffusion layer, D is diffusion coefficient, and t is relaxation time. The diffusion layer is the function of time and diffusion coefficient. In SWV technique, higher and lower potential is alternately changed in a cycle. The t which is the time of a higher or lower potential is quite smaller than cyclic voltammetry. In this study, t is 20 ms (50 Hz). The diffusion coefficient of potassium ferricyanide is 7.6 x 10-6 cm^2s^{-1}. Thus, the diffusion layer is 6.91 μm under the condition of 50 Hz of square wave frequency. We confirmed that the distance between the working electrodes which is 60 μm is larger than the diffusion layer of this measurement condition. In the proposed sensor, there is no cross talk between the working electrodes because the diffusion layer does not overlap as theoretically.

By the way, I also thought about the diffusion layer at the actual measurement, not the theoretical calculation. In other words, we need to confirm the decreasing oxidants in the

vicinity of the sensing area during the reaction. A measurement is conducted inserting the "waiting time". The waiting time is sited after one cycle of SWV pulse for the charging oxidants. The waiting time between the SWV pulses is 4 times longer than a cycle of SWV pulse, which is sufficient time to charge the oxidant. Table 4-1 shows the average peak current and standard deviation of each frame with or without waiting time at 50 Hz of square wave frequency. The average peak current is large in case of inserting waiting time as shown in figure 4.6. This is because the oxidant is charged during the waiting time. The standard deviation with regard to the average peak current is small in case of inserting waiting time. The sensor shows equable distribution because of charging oxidant during the waiting time. Thus, the reason of appearing the different peak current distribution in figure 4.5 is that the decreasing oxidants during reaction are affected to the next reaction.

Table 4-1. Average peak current and standard deviation of each frame with or without waiting time (50 Hz square wave frequency).

No waiting time I

	1st frame	2nd frame	3rd frame
Average peak current [μA]	0.436	0.544	0.554
Standard deviation [μA]	0.034	0.051	0.050
$\dfrac{\text{Average peak current}}{\text{Standard deviation}}$ x 100 [%]	7.75	9.30	9.02

No waiting time II

	1st frame	2nd frame	3rd frame
Average peak current [μA]	0.556	0.582	0.575
Standard deviation [μA]	0.050	0.045	0.058
$\dfrac{\text{Average peak current}}{\text{Standard deviation}}$ x 100 [%]	9.01	7.75	10.14

Waiting time

	1st frame	2nd frame	3rd frame
Average peak current [μA]	0.680	0.694	0.708
Standard deviation [μA]	0.047	0.035	0.046
$\dfrac{\text{Average peak current}}{\text{Standard deviation}}$ x 100 [%]	6.95	5.07	6.56
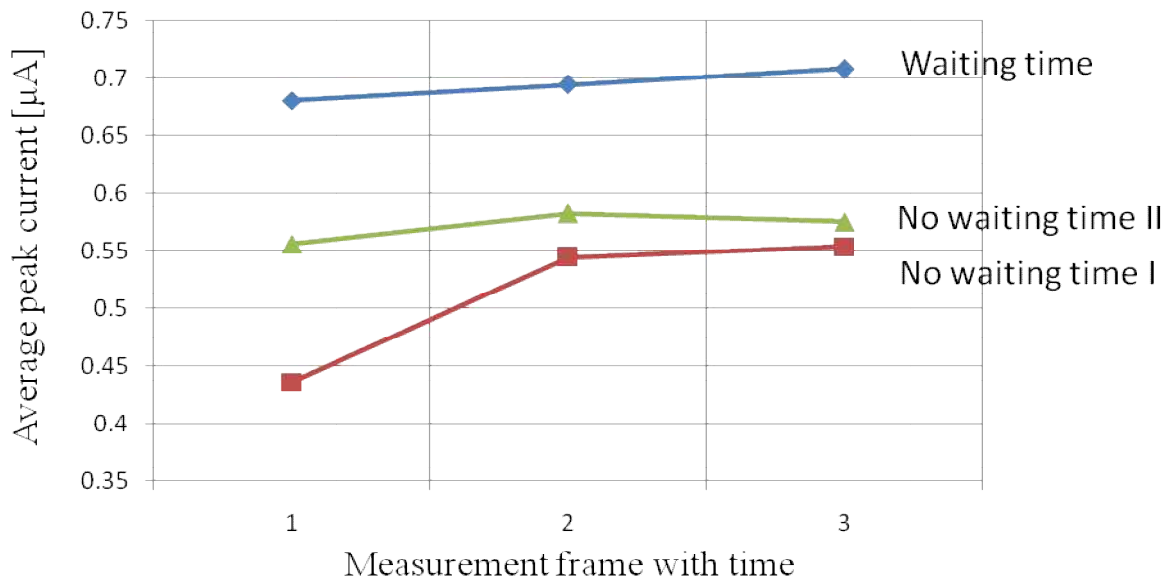
Figure 4.6 Average peak current with or without waiting time.
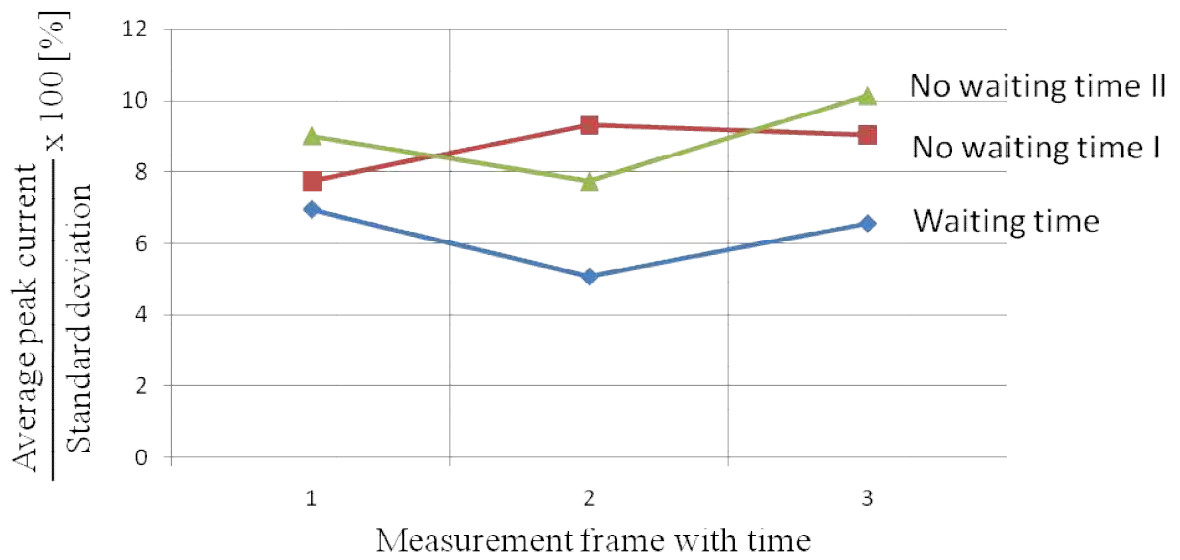
Figure 4.7 Percentage of standard deviation with or without waiting time.

Figure 4.8 shows the histogram of the number of redox potential at 64 pixels. The average redox potential of 64 pixels is 280 mV. Standard deviation of 64 pixels is 7.2 mV. The redox potential variation of the proposed sensor is small from the result. 59 of 64 pixels (92.2 %) are in the range of 20 mV of redox potential. Whole redox potential distribution of 64 pixels is in the range of 50 mV. Therefore, the proposed sensor can detect multi-ion with at least 50 mV difference of redox potential. Peak currents of 8 x 8 array pixels at each concentration are measured to obtain the qualitative information of target material, potassium ferricyanide.

Figure 4.9 show the peak current response at each concentration on a coordinate (5, 5), the center of the 8 x 8 array pixels. We carried out the peak current calibration of all 64 pixels. Figure 4.9 shows the measured ferricyanide concentration result versus concentration of a ferricyanide standard solution plot of the 8 x 8 array pixels.
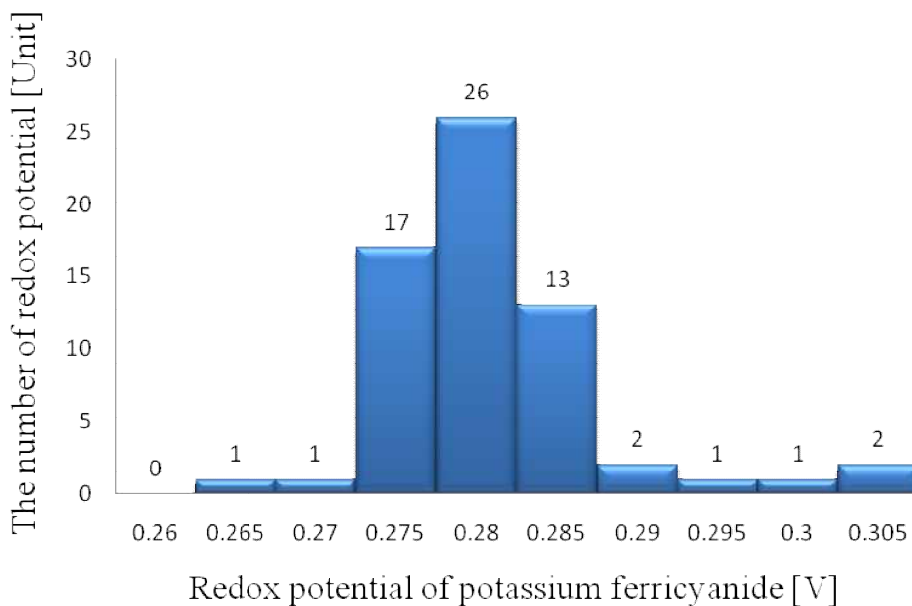
Figure 4.8 Histogram of a number of redox potential at 64 pixels.
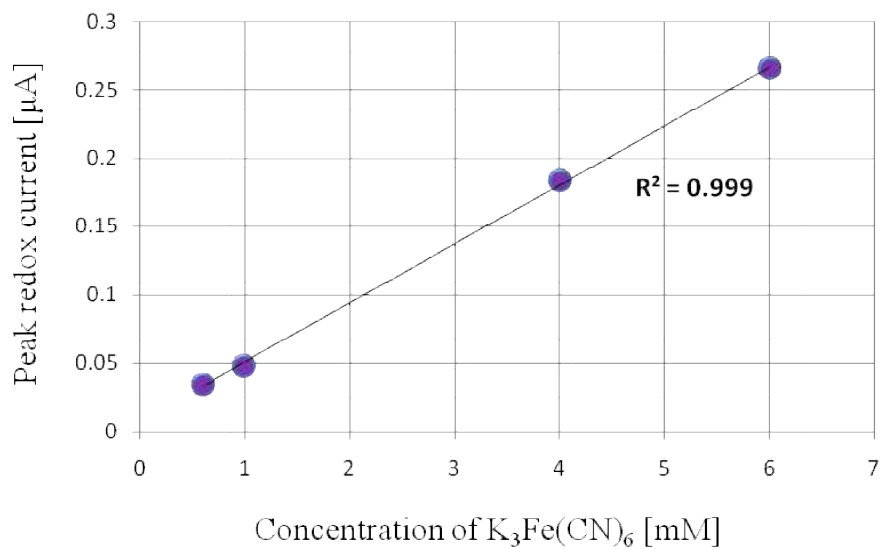
Figure 4.9 Concentration dependence of the peak redox current on a coordinate (5, 5)

single pixel, the center of the 8 x 8 array pixels.
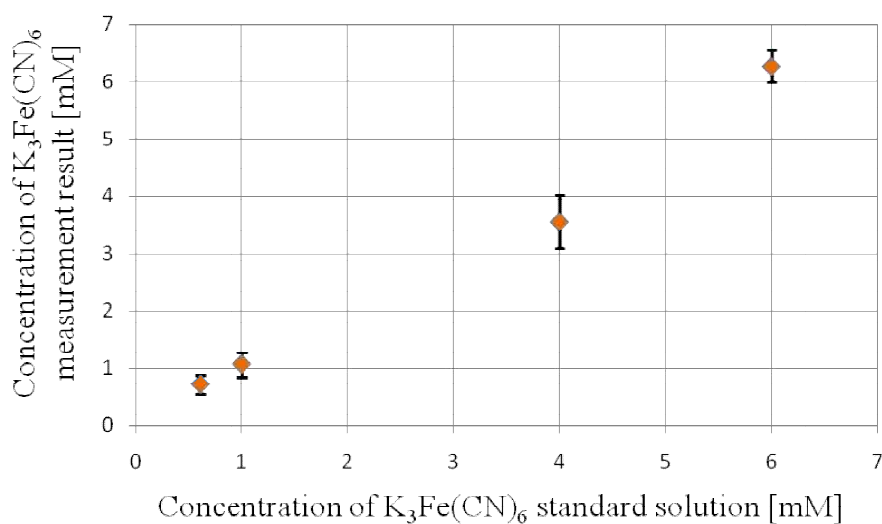
Figure 4.10 Measured ferricyanide concentration result versus concentration of a

ferricyanide standard solution.

From the result of the current responses of 64 array pixels, the peak current is somewhat difference among the pixels. The peak current is a function of concentration, electrode area, and square wave frequency. Square wave frequency and concentration of the material is fixed. Therefore, we can think that an effective area of electrodes is asymmetry. It can be minimize the effective area of electrodes by piranha cleaning or by applying the voltage to the electrodes for removing organic materials. Nevertheless, if the peak current differences are remaining, it can be possible to improve the deviation by conducting current calibration.

The points of each concentration as shown in figure 4.10 are average values of 64 pixels. An error bar of the figure 4.10 shows the range of 2σ. Concentration of measurement result increases linearly as concentration of standard solution increases. The square of correlation coefficient (R^2) is 0.985.

The redox imaging using the proposed sensor was measured in 24 seconds/frame. Each column takes 3 seconds under the condition of 50 Hz and -0.2 ~ 0.4 V of square wave frequency and scan range, respectively. Figure 4.11 shows the 2-dimensional images dropping the 6 mM ferricyanide onto the upper left side of the sensor. For slow down the diffusion rate of the ferricyanide, gel-type ferricyanide solution was made using agar. 5 g agar and 1 mL ferricyanide were mixed to measure. From the 1st frame, it was possible to observe the distribution of ferricyanide. From the 2nd frame, the diffusion of ferricyanide was successfully observed.
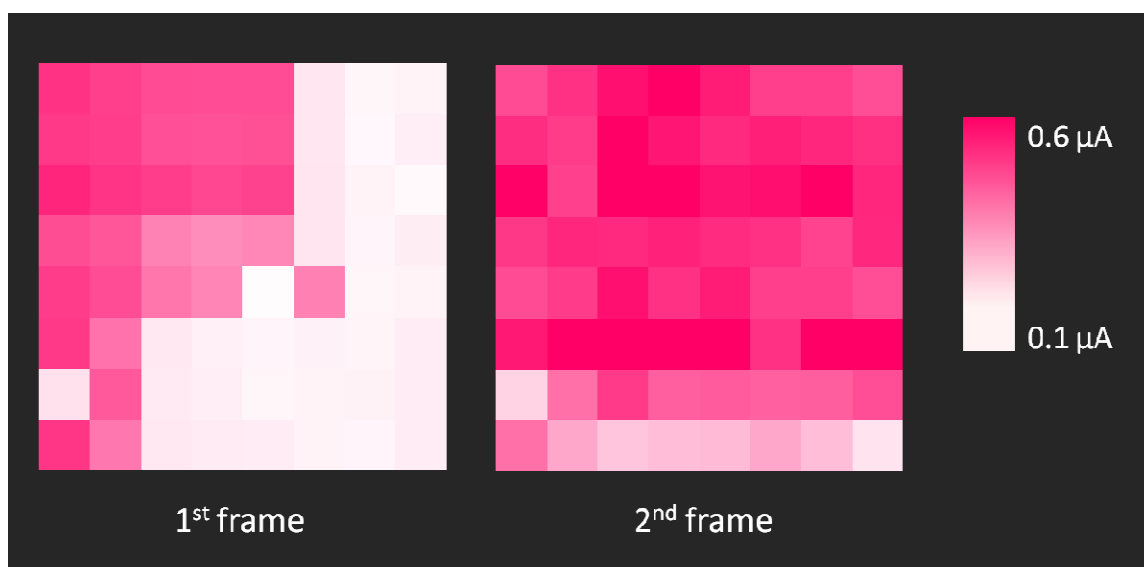
Figure 4.11 Two-dimensional redox images of potassium ferricyanide with time.

(dropping the ferricyanide onto the upper left side of the array sensor.)

4.5 Conclusion

In this chapter, the integrated square wave voltammetry redox sensor employing the 8 x 8 array working electrodes is described for the application of a redox image sensor. Using this microelectrode array sensor, distribution and diffusion of the material were possible to confirm. The results showed the possibility of bioimaging using the proposed sensor. For the next step, it is needed to obtain output results of array pixels at the same time for more rapid measurement, and increasing pixels is also needed to improve the accuracy of the location information.

References

[1] T. Tokuda, K. Tanaka, M. Matsuo, K. Kagawa, M. Nunoshita, and J. Ohta, "Optical and electrochemical dual-image CMOS sensor for on-chip biomolecular sensing applications", Sensors and Actuators A , Vol. 135, Issue 2, pp. 315-322, 2007.

[2] A. L. Ghindilis, M. W. Smith, K. R. Schwarzkopf, K. M. Roth, K. Peyvan, S. B. Munro, M. J. Lodes, A. G. Stover, K. Bernards, K. Dill, and A. McShea, "CombiMatrix oligonucleotide arrays: Genotyping and gene expression assays employing electrochemical detection", Biosensors and Bioelectronics, Vol. 22, Issues 9-10, pp. 1853-1860, 2007.

[3] S. B. Prakash, M. Urdaneta, M. Christophersen, E. Smela, and P. Abshire, "In situ electrochemical control of electroactive polymer films on a CMOS chip", Sensors and Actuators B, Vol. 129, Issue 2, pp. 699-704, 2008.

[4] P. M. Levine, P. Gong, R. Levicky, and K. L. Shepard, "Real-time, multiplexed electrochemical DNA detection using an active complementary metal-oxide-semiconductor biosensor array with integrated sensor electronics", Biosensors and Bioelectronics, Vol. 24, Issue 7, pp. 1995-2001, 2009.

[5] X. Zhu and C. H. Ahn, "On-Chip Electrochemical Analysis System Using Nanoelectrodes and Bioelectronic CMOS Chip", IEEE Sensors Journal, Vol. 6, Issue 5, pp. 1280-1286, 2006.

[6] K. Sawada, T. Shimada, T. Ohshina, H. Takao, and M. Ishida, "Highly sensitive ion sensors using charge transfer technique", Sensors and Actuators B, Vol. 98, Issue 1, pp. 69-72, 2004.

[7] Kumi Y. Inoue, Masahki Matsudaira, Reyushi Kubo, Masanori Nakano, Shinya Yoshida, Sakae Matsuzaki, Atsushi Suda, Ryota Kunikata, Tatsuo Kimura, Ryota Tsurumi, Toshihito Shioya, Kosuke Ino, Hitoshi Shiku, Shiro Satoh, Masayoshi

Esashi, and Tomokazu Matsue, "LSI-based amperometric sensor for bio-imaging and multi-point biosensing", Lab on a Chip, Vol. 12, pp. 3481-3490, 2012.

[8] B. Lim, M. Futagawa, S. Takahashi, F. Dasai, M. Ishida, and K. Sawada, "Integrated Square Wave Voltammetry Redox Sensor System for Electrochemical Analysis", Japanese Journal of Applied Physics, Vol. 52, p. 116502, 2013.

CHAPTER 5

Thesis Conclusions

Over the past 20 years, development of integrated electrochemical sensors was improved dramatically by using silicon technology. This dissertation is about the electrochemical redox image sensor employing integrated square wave voltammetric circuit. Electrochemical sensor is capable of analyzing quantitative and qualitative information. Square wave voltammetry technology is generally high speed and high sensitivity method than cyclic voltammetry which is conventional method, and microelectrode array sensor chip is capable of observing biomaterials in 2-dimensional chemical imaging. The advantages of integration which are electrochemical cells, square wave pulse generator circuit, and readout circuit is described in this thesis.

The principle of the electrochemical analysis and basic information is explained in chapter 2. It is also explained about various voltammetry techniques. One of the disadvantages of square wave voltammetry technique is the complexity of the measuring equipment. Because of this problem, in-site measurement was generally difficult. Thus it is not often used in spite of its high sensitivity and high speed measurement. However, if square wave voltammetry technology is integrated on a single chip, huge equipment does not needed so that in-situ and simple measurement can be possible.

Chapter 3 showed the research using on-chip square wave voltammetry circuit. The square wave pulse generator which is the key point of this thesis is integrated on a chip, and the electrical characteristic is evaluated. It is designed that square wave amplitude, step increment, and square wave frequency can control by adjusting presetter circuit,

reference voltage, and system clock, respectively. These three are important components of the square wave voltammetry. We can calculate the scan rate using these three components. Other elements such as electrodes, readout circuit, and OPAMP which is needed at the electrochemical measurement is integrated on the same chip. Therefore, simple electrochemical measurement can be possible to use the proposed chip. The characteristic of the on-chip redox sensor showed the general results of an electrochemical sensor. Potassium ferricyanide which is generally used in the electrochemical field is employed to evaluate the characteristics of the chip. These results show the possibility of detecting other biomaterials using fabricated sensor. There are seven chips of 5-μm-rule process, and two chips of 2-μm-rule process.

In chapter 4, the array electrodes are designed and evaluate the characteristics of on-chip square wave voltammetry. For the array measurement, the readout circuit is needed. In this study, 8-bit shift resistor is proposed as a signal readout circuit for 8 x 8 array pixels in sequence. The shift resistor is integrated on the chip. The characteristics of the 8 x 8 pixels are also confirmed. Each pixel has somewhat difference peak current, however if a current calibration is carried out, there is no problem to conduct imaging. The results of this chapter will open up the possibility of chemical imaging. In the near future, it is needed to obtain output results of array pixels at the same time for more rapid measurement, and increasing pixels is also needed to improve the accuracy.

This research evaluates the various biomaterials using integrated electrochemical array sensor, and enables to conduct high speed measurement by integrating square wave voltammetry pulse generator. To our best knowledge, the proposed sensor chip is the first sensor to integrated square wave voltammetry circuit. From this study, the results show the possibility of real-time chemical imaging. This thesis will open up the development of the smart medical sensor for the human beside us.

Acknowledgements

I would like to express my heartfelt gratitude to my Professor Kazuaki Sawada. He gave me all the opportunities to study here in Toyohashi University of Technology (TUT). Thanks to his advices and mentorship, I have completed safely my doctoral study and arrived at the end of the doctoral course. I also appreciate to Professor Makoto Ishida for his consideration and advices of my research. Without their guidance and persistent help, this dissertation would not have been possible.

I wish to express my sincere thanks to Professor Jang-Kyoo Shin who always gave me the moral support and research guidance, as well as the advices of the course of my life.

I am extremely thankful to Dr. Masato Futagawa for being able to initiate the overall experiment and to advise the theory of my work. I am also deeply thankful to Mr. Sou Takahashi of his great team work and collaboration as my co-worker.

During my doctoral course in Japan, I have received benefits of financial support from Global COE program "Frontiers of Intelligent Sensing" and MEXT (Japanese Ministry of Education, Culture, Sports, Science and Technology) Scholarship program, and I sincerely appreciated it.

I would like to thank to Dr. Byunghyun Cho and Dr. Min-Woong Seo. I have a great memory with them here in Japan sharing a lot of experiences, and we also did help each other about our study and our life as a co-worker and as a friend.

I am grateful to Dr. Sang Baie Shin for his consideration and advices of my research.

Finally, I would like to thank my mother, father, brother, and sister-in-law all of my family for their unconditional love and support during the past four years. I would not have been able to complete this thesis without their love and encouragement.

마지막으로, 일본에서 혼자 생활하고 공부해온 지난 몇 년간 아버지, 어머니, 내 동생 그리고 우리 가족이 된 제수씨, 모두에게 받은 큰 애정과 격려, 말로 표현할 수 없는 내 가족의 희생과 지원이 없었다면, 박사 학위까지의 과정이 불가능 했을 것입니다. 소중한 나의 가족에게 감사의 마음 전합니다.

July   2014   Byounghyun LIM

List of Publications

International Paper
"Integrated Square Wave Voltammetry Redox Sensor System for Electrochemical Analysis", <u>Byounghyun Lim</u>, Masato Futagawa, Sou Takahashi, Fumihiro Dasai, Makoto Ishida, and Kazuaki Sawada, Japanese Journal of Applied Physics, Vol. 52 (2013) 116502.

"Integrated 8 x 8 Array Redox Sensor System Employing On-chip Square Wave Voltammetric Circuit for Multi-point and High-speed Detection", <u>Byounghyun Lim</u>, Masato Futagawa, Sou Takahashi, Fumihiro Dasai, Makoto Ishida, and Kazuaki Sawada, Japanese Journal of Applied Physics, Vol. 53 (2014) 046502.

"Smart Integrated Sensor for Multiple Detections of Glucose and L-Lactate Using On-Chip Electrochemical System", Tomoyuki Yamazaki, Takaaki Ikeda, <u>Byounghyun Lim</u>, Koichi Okumura, Makoto Ishida, and Kazuaki Sawada, Journal of Sensors, Vol. 2011 (2011) Article ID 190284.

"Monolithic Integration of Surface Plasmon Detector and Metal-Oxide-Semiconductor Field-Effect Transistors", Takuma Aihara, Masashi Fukuhara, Ayumi Takeda, <u>Byounghyun Lim</u>, Masato Futagawa, Yuya Ishii, Kazuaki Sawada, and Mitsuo Fukuda, IEEE Photonics Journal, Vol. 5, No. 4 (2013) 6800609.

International Conference
"Fabrication of an Integrated Square Wave Voltammetry (SWV)-Redox Sensor", <u>Byounghyun Lim</u>, Masato Futagawa, Sou Takahashi, Fumihiro Dasai, Makoto Ishida, and Kazuaki Sawada, 2013 International Conference on Solid State Devices and Materials, Fukuoka, Japan (2013)

"Integrated SWV Redox Array Sensor Chip with 64 Pixels for Multi-point and High-speed Detection", <u>Byounghyun Lim</u>, Masato Futagawa, Sou Takahashi, Fumihiro Dasai, Makoto Ishida, and Kazuaki Sawada, The 7th Asia-Pacific Conference on Transducers and Micro/Nano Technologies, Daegu, Korea (2014) Abstract No. E-T04-0030

Domestic Symposium
"Integrated Electrochemical Sensor System Employing on-chip Square Wave Voltammetry Pulse Generator", <u>Byounghyun Lim</u>, Masato Futagawa, Sou Takahashi, Fumihiro Dasai,

Makoto Ishida, and Kazuaki Sawada, The 30th Sensor Symposium on Sensors, Micromachines, and Application Systems, Nov. 5th 2013, Sendai International Center.

Appendix A

Process Flow (Cross sectional view)

1. P-well formation
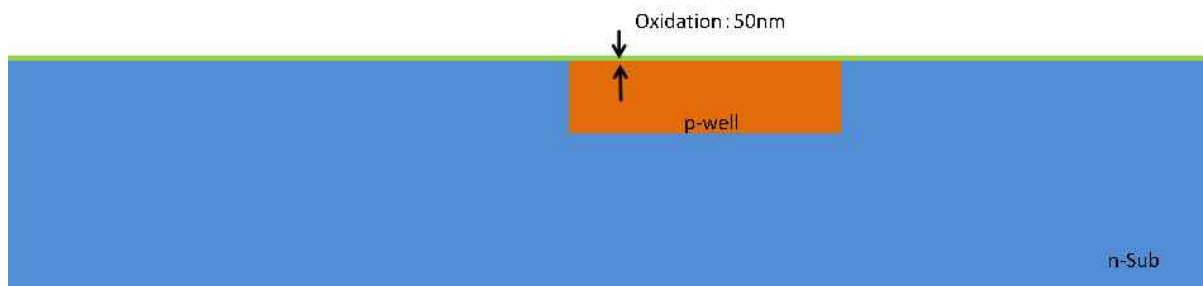
2. Active region
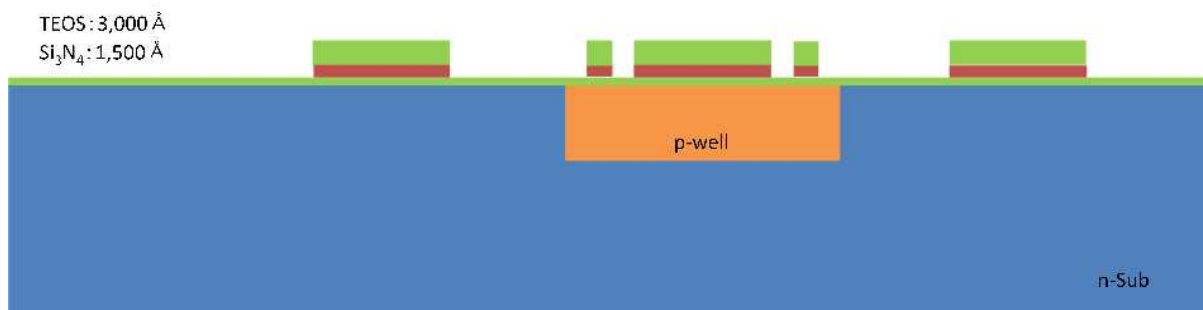
3. n channel stopper
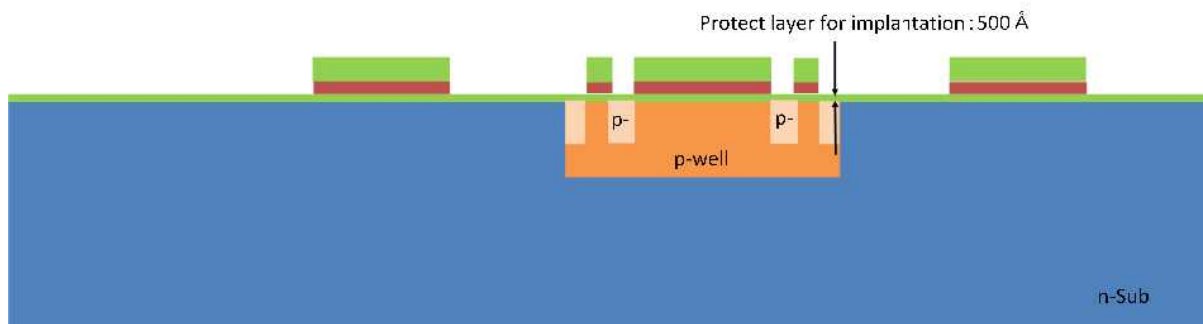
4. p channel stopper
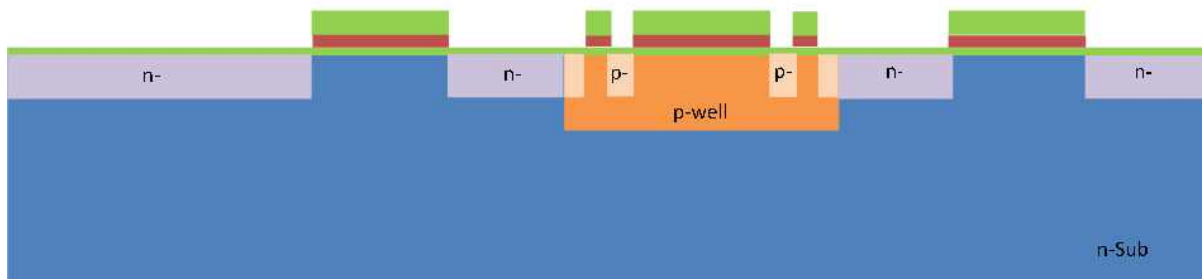
5. LOCOS

6. Poly-Si formation

7. PMOS formation

8. NMOS formation

9. Contact formation

TEOS : 5000 Å → densify 4750 Å
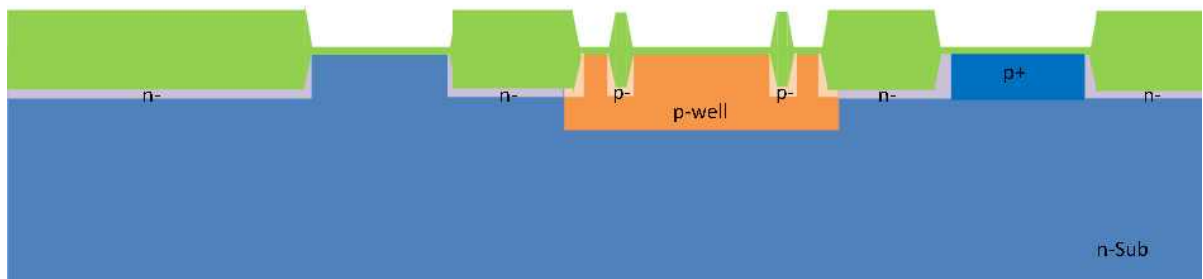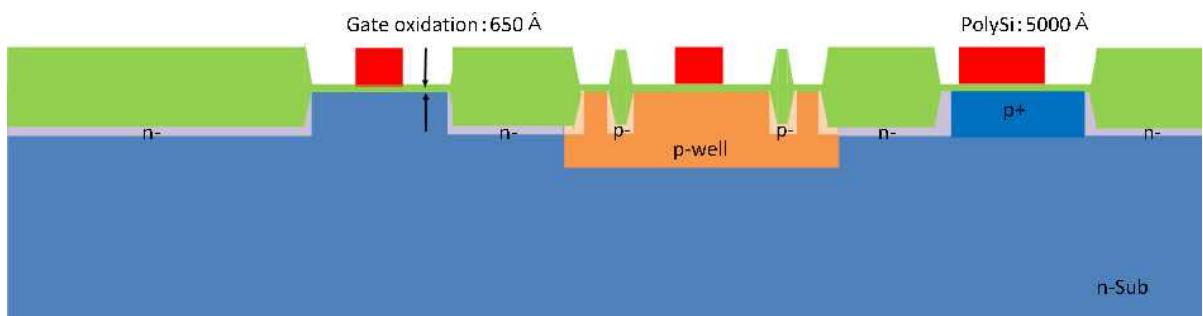
10. Al metallization
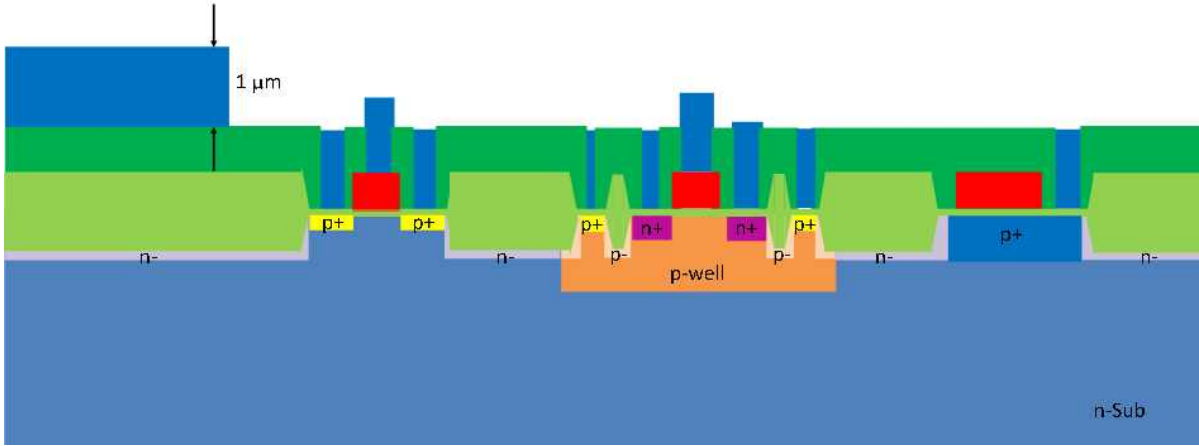
11. Pt (Pt/Ti) electrode formation
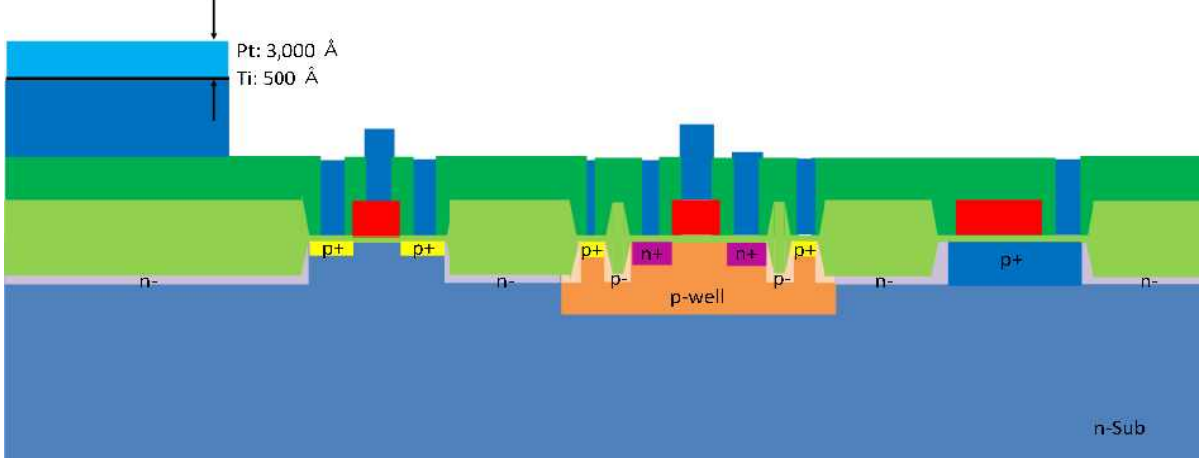
12. Silicon nitride passivation layer
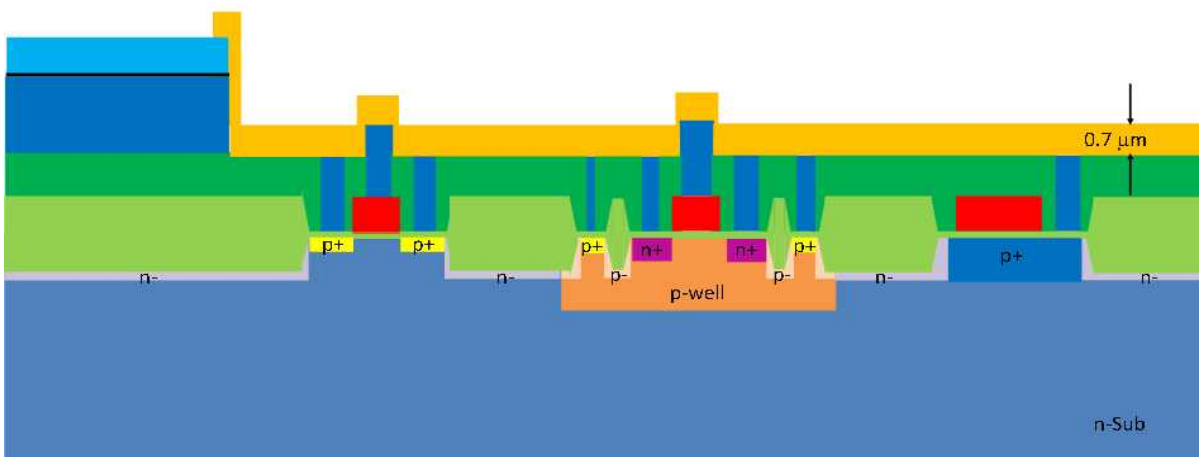
Appendix B

Process Chart

Standard CMOS Process

No.	Step	Conditions	Time	Specs
1	Wafer	N(100), 4 inch, 3.95-4.63 cm		
2	Pre clean	APM 70 deg C (1:1:6 = $NH_4OH:H_2O_2:H_2O$) DIW overflow HPM 70 deg C (1:1:6 = $HCl:H_2O_2:H_2O$) DIW overflow DHF DIW overflow Spin dry	10 min 10 min 10 min 10 min 20 s 5 min	Wet station
3	Oxidation	OX1: 1,000 deg C Dry O_2 250 l/hr Anneal N2 250 l/hr	 55 min 10 min	thickness:50nm
4	Thickness check	Optical measurement Wf No._____ Top_____ Center_____ Bottom_____ Left_____ Right_____ Average_____		T1:Pad Ox

5	AM photo
	(alignment mark)
		OAP-bake: 160 deg C
		OAP coat
		     1st 500 rpm
		     2nd 3,000 rpm
		PR coat: THMR-iP3100HS LB 15 cp
		     1st 500 rpm
		     2nd 3,000 rpm
		Coat-bake: 110 deg C
		Expose: i-Ray stepper
		Development: NMD
		Rinse: DW
		Dev-bake: 120 deg C
			90 s
			
			5 s
			30 s
			
			5 s
			25 s
			90 s
			(300 ms)
			33 s
			33 s
			5 min
				Coat recipe: No.8
				Development recipe: No.21
				
				Lazer microscope
				L/S Size: _____um
				Wf No._____
				Top_____
				Center_____
				Bottom_____
				Left_____
				Right_____
				Average_____

6	Si etch	RIE (rank A) SF6=10 sccm, 1 Pa, 100 W	5-6 min Time_____	etch:300-450 nm
7	Etch check	Optical measurement Wf No._____ Top_____ Center_____ Bottom_____ Left_____ Right_____ Average_____		Main wafer
8	PR removal	SPM 120 deg C (3:1 = $H_2SO_4:H_2O_2$) DIW	10 min 10 min	

9	PW photo	OAP-bake: 160 deg C
		OAP coat
		    1st 500 rpm
		    2nd 3,000 rpm
		PR coat: THMR-iP3100HS LB 15 cp
		    1st 500 rpm
		    2nd 3,000 rpm
		Coat-bake: 110 deg C
		Expose: i-Ray stepper
		Development: NMD
		Rinse: DW
		Dev-bake: 120 deg C
		O_2 asher
			90 s
			
			5 s
			30 s
			
			5 s
			25 s
			90 s
			(300 ms)
			33 s
			33 s
			5 min
			1 min 30 s
				Coat recipe: No.8
				Development recipe: No.21
				
				Lazer microscope
				L/S Size: _____um
				Wf No._____
				Top_____
				Center_____
				Bottom_____
				Left_____
				Right_____
				Average_____

10	P-well I/I	BF3 60 keV, 1.0×10^{13} cm^{-2}		
11	PR removal	SPM 120 deg C (3:1 = H_2SO_4:H_2O_2) DIW	10 min 10 min	
12	Pre clean	APM 70 deg C (1:1:6 = NH4OH:H2O2:H2O) DIW overflow HPM 70 deg C (1:1:6 = HCl:H2O2:H2O) DIW overflow DHF DIW overflow Spin dry	10 min 10 min 10 min 10 min 20 s 10 min	
13	Drive in	OX6: 1,150 deg C Dry O_2 250 l/hr	 9 hr	
14	SiO2 removal	BHF DIW overflow	remove all 10 min	
15	Check	hydrophobic? OK / NG		T1:Pwell
16	Sheet resistance	Top_____ Center_____ Bottom_____ Left_____ Right_____ Average_____		T1:Pwell
17	Pre clean	APM 70 deg C (1:1:6 = NH4OH:H2O2:H2O) DIW overflow HPM 70 deg C (1:1:6 = HCl:H2O2:H2O) DIW overflow DHF DIW overflow Spin dry	10 min 10 min 10 min 10 min 20 s 5 min	
18	Pad Oxidation	OX1: 1,000 deg CDry O_2 250 l/hrAnneal N2 250 l/hr	55 min10 min	thickness:50nm
19	Thickness check	Optical measurement Wf No._____ Top_____ Center_____ Bottom_____ Left_____ Right_____ Average_____		T1:Pad Ox
20	Pre clean	APM (1:1:6) 70 deg C DIW overflow HPM (1:1:6) 70 deg C DIW overflow Spin dry	10 min 10 min 10 min 10 min	
21	Si3N4 depo.	LPCVD	Time_____	thickness:150 nm

22	TEOS depo.	LPCVD 708 deg C, 0.3 Torr, B.G. 0.035 Torr TEOS/O$_2$ = 30 sccm/0.3 (l/min)	Time_____	thickness:300 nm Add Ref. wafer
23	Thickness check	Optical measurement Wf No._____ Si3N4 Top_____ Center_____ Bottom_____ Left_____ Right_____ Average_____ TEOS Top_____ Center_____ Bottom_____ Left_____ Right_____ Average_____		T1:Pad + Si3N4 T3:Si3N4 Ref:TEOS
24	AC photo (Active area)	OAP-bake: 160 deg C OAP coat 1st 500 rpm 2nd 3,000 rpm PR coat: THMR-iP3100HS LB 15 cp 1st 500 rpm 2nd 3,000 rpm Coat-bake: 110 deg C Expose: i-Ray stepper Development: NMD Rinse: DW Dev-bake: 120 deg C O2 asher	90 s 5 s 30 s 5 s 25 s 90 s (300 ms) 33 s 33 s 5 min 1 min 30 s	Coat recipe: No.8 Development recipe: No.21 Lazer microscope L/S Size: _____um Wf No._____ Top_____ Center_____ Bottom_____ Left_____ Right_____ Average_____
25	TEOS etch	BHF DIW overflow	Time_____ 10 min	etch rate:Ref.
26	Etch check	Optical measurement Wf No._____ Top_____ Center_____ Bottom_____ Left_____ Right_____ Average_____		Main Wafer :Pad + Si3N4
27	Si$_3$N$_4$ etch	RIE (Si) CF$_4$/O$_2$ = 20/5 sccm, 10 Pa, RF 100 W	2 min 45 s Time_____	etch rate:T1
28	Etch check	Optical measurement Wf No._____ Top_____ Center_____ Bottom_____ Left_____ Right_____ Average_____		
29	PR removal	SPM 120 deg C (3:1 = H2SO4:H2O2) DIW	10 min 10 min	
30	NStop photo (for N-ch Stopper) Pwell mask	OAP-bake: 160 deg C OAP coat 1st 500 rpm 2nd 3,000 rpm PR coat: THMR-iP3100HS LB 15 cp 1st 500 rpm 2nd 3,000 rpm Coat-bake: 110 deg C Expose: i-Ray stepper Development: NMD Rinse: DW Dev-bake: 120 deg C O2 asher	90 s 5 s 30 s 5 s 25 s 90 s (300 ms) 33 s 33 s 5 min 1 min 30 s	Coat recipe: No.8 Development recipe: No.21 Lazer microscope L/S Size: _____um Wf No._____ Top_____ Center_____ Bottom_____ Left_____ Right_____ Average_____

31	N Ch stop I/I	Boron 50 keV, 3.0×10^{13} cm^{-2}		
32	PR removal	SPM 120 deg C (3:1 = H2SO4:H2O2) DIW	10 min 10 min	

33	PStop photo
	(for P-ch Stopper)
	inverted Pwell mask
		OAP-bake: 160 deg C
		OAP coat
		    1st 500 rpm
		    2nd 3,000 rpm
		PR coat: THMR-iP3100HS LB 15 cp
		    1st 500 rpm
		    2nd 3,000 rpm
		Coat-bake: 110 deg C
		Expose: i-Ray stepper
		Development: NMD
		Rinse: DW
		Dev-bake: 120 deg C
		O2 asher
			90 s
			
			5 s
			30 s
			
			5 s
			25 s
			90 s
			(300 ms)
			33 s
			33 s
			5 min
			1 min 30 s
				Coat recipe: No.8
				Development recipe: No.21
				
				Lazer microscope
				L/S Size: _____ um
				Wf No._____
				Top_____
				Center_____
				Bottom_____
				Left_____
				Right_____
				Average_____

34	P Ch stop I/I	Phosphorus 60 keV, 3.0×10^{13} cm^{-2}		
35	PR removal	SPM 120 deg C (3:1 = H2SO4:H2O2) DIW	10 min 10 min	
36	Pad SiO$_2$ etch	BHF DIW overflow	(45 s)	
37	Etch check	Optical measurement Wf No._____ Top_____ Center_____ Bottom_____ Left_____ Right_____ Average_____		
38	Pre clean	APM (1:1:6) 70 deg C DIW overflow HPM (1:1:6) 70 deg C DIW overflow Spin dry	10 min 10 min 10 min 10 min	
39	LOCOS Oxidation	OX1: 1,000 deg C Wet H$_2$/O$_2$ 250/250 (l/hr) Dry O$_2$ 250 l/hr Anneal N2 250 l/hr	6 hr 40 min 10 min 10 min	
40	Thickness check Sheet resistance	Optical measurement Wf No._____ Si3N4 Top_____ Center_____ Bottom_____ Left_____ Right_____ Average_____ Sheet resistance Top_____ Center_____ Bottom_____ Left_____ Right_____ Average_____		T1:LOCOS T1:Nch Stopper T2:Pch Stopper
41	TEOS removal	BHF DIW overflow	10 min	Ref. rate check
42	Si$_3$N$_4$ removal	H$_3$PO$_4$ 160 deg C DIW 80 deg C DIW Overflow	10 min 10 min	
43	Etch check	Optical measurement Wf No._____ Top_____ Center_____ Bottom_____ Left_____ Right_____ Average_____		T3:Si3N4

44	Pad SiO2 removal	BHF DIW overflow	(25 sec)	
45	Etch check	Optical measurement Wf No._____ Top_____ Center_____ Bottom_____ Left_____ Right_____ Average_____		Main wafer
46	Cleaning	APM 70 deg C (1:1:6 = NH4OH:H2O2:H2O) DIW overflow HPM 70 deg C (1:1:6 = HCl:H2O2:H2O) DIW overflow DHF DIW overflow Spin dry	10 min 10 min 10 min 10 min 20 s 5 min	
47	Oxidation (for CP I/I)	OX1: 1000 deg C Dry O2 250 l/hr Anneal N2 250 l/hr	 55 min 10 min	thickness:50 nm
48	Thickness check	Optical measurement Wf No._____ Top_____ Center_____ Bottom_____ Left_____ Right_____ Average_____		T3:Pad Ox

49	CP photo	OAP-bake: 160 deg C
		OAP coat
		    1st 500 rpm
		    2nd 3,000 rpm
		PR coat: THMR-iP3100HS LB 15 cp
		    1st 500 rpm
		    2nd 3,000 rpm
		Coat-bake: 110 deg C
		Expose: i-Ray stepper
		Development: NMD
		Rinse: DW
		Dev-bake: 120 deg C
		O2 asher
			90 s
			
			5 s
			30 s
			
			5 s
			25 s
			90 s
			(300 ms)
			33 s
			33 s
			5 min
			1 min 30 s
				Coat recipe: No.8
				Development recipe: No.21
				
				Lazer microscope
				L/S Size: _____um
				Wf No._____
				Top_____
				Center_____
				Bottom_____
				Left_____
				Right_____
				Average_____

50	CP I/I	Boron 50 keV, 5.0×10^{13} cm^{-2}		
51	PR removal	SPM 120 deg C (3:1 = H2SO4:H2O2) DIW	10 min 10 min	
52	SiO$_2$ removal	BHF DIW overflow	40 s	
53	Etch check	Optical measurement Wf No._____ Top_____ Center_____ Bottom_____ Left_____ Right_____ Average_____		T3:PadOx
54	Cleaning	APM (1:1:6) 70 deg C DIW overflow HPM (1:1:6) 70 deg C DIW overflow Spin dry	10 min 10 min 10 min 10 min	
55	Oxidation (for GATE)	OX3: 1,000 deg C Dry O$_2$ 250 l/hr Anneal N$_2$ 250 l/hr	 75 min 10 min	thickness:65 nm
56	Thickness check	Optical measurement Wf No._____ Top_____ Center_____ Bottom_____ Left_____ Right_____ Average_____		T4:Gate oxide

57	Poly-Si depo.	LPCVD 625 deg C, 0.5 Torr SiH$_4$ 0.2 slm		thickness:350 nm
58	Thickness check	Optical measurement Wf No._____ Top_____ Center_____ Bottom_____ Left_____ Right_____ Average_____		T4:GateOx + Poly
59	Resistance I/I	As 80keV 6.0e14 cm^{-2}		1-3 kOhm/sheet
60	RE photo mask:protected high-RES.	OAP-bake: 160 deg C OAP coat 1st 500 rpm 2nd 3,000 rpm PR coat: THMR-iP3100HS LB 15 cp 1st 500 rpm 2nd 3,000 rpm Coat-bake: 110 deg C Expose: i-Ray stepper Development: NMD Rinse: DW Dev-bake: 120 deg C O2 asher	90 s 5 s 30 s 5 s 25 s 90 s (300 ms) 33 s 33 s 5 min 1 min 30 s	
61	Poly-Si I/I	As 85keV 4.5e15 cm^{-2}		10~20 Ohm/sheet
62	PR removal	O2 ashing SPM	30 min 10 min	
63	PS photo	OAP-bake: 160 deg C OAP coat 1st 500 rpm 2nd 3,000 rpm PR coat: THMR-iP3100HS LB 15 cp 1st 500 rpm 2nd 3,000 rpm Coat-bake: 110 deg C Expose: i-Ray stepper Development: NMD Rinse: DW Dev-bake: 120 deg C O2 asher	90 s 5 s 30 s 5 s 25 s 90 s (300 ms) 33 s 33 s 5 min 1 min 30 s	Coat recipe: No.8 Development recipe: No.21 Lazer microscope L/S Size: _____um Wf No._____ Top_____ Center_____ Bottom_____ Left_____ Right_____ Average_____
64	Poly-Si etch	RIE (Si) SF$_6$ = 10 sccm, 1 Pa, RF 100 W	3.5 to 4.3 min	
65	PR removal	SPM DIW	10 min 10 min	
66	Etch check	Optical measurement Wf No._____ Top_____ Center_____ Bottom_____ Left_____ Right_____ Average_____		Main wafer

67	PD photo (GATE & RA masked)	OAP-bake: 160 deg C
		OAP coat
		    1st 500 rpm
		    2nd 3,000 rpm
		PR coat: THMR-iP3100HS LB 15 cp
		    1st 500 rpm
		    2nd 3,000 rpm
		Coat-bake: 110 deg C
		Expose: i-Ray stepper
		Development: NMD
		Rinse: DW
		Dev-bake: 120 deg C
		O2 asher
			90 s
			
			5 s
			30 s
			
			5 s
			25 s
			90 s
			(300 ms)
			33 s
			33 s
			5 min
			1 min 30 s
				Coat recipe: No.8
				Development recipe: No.21
				
				Lazer microscope
				L/S Size: _____um
				Wf No._____
				Top_____
				Center_____
				Bottom_____
				Left_____
				Right_____
				Average_____

68	PD I/I	B 30 keV, 4.0×10^{15} cm^{-2}		implant Cap contact (p+)
69	PR removal	O2 ashing SPM	30 min 10 min	

70	ND photo (pMOS GATE & RA masked)	OAP-bake: 160 deg C
		OAP coat
		    1st 500 rpm
		    2nd 3,000 rpm
		PR coat: THMR-iP3100HS LB 15 cp
		    1st 500 rpm
		    2nd 3,000 rpm
		Coat-bake: 110 deg C
		Expose: i-Ray stepper
		Development: NMD
		Rinse: DW
		Dev-bake: 120 deg C
		O2 asher
			90 s
			
			5 s
			30 s
			
			5 s
			25 s
			90 s
			(300 ms)
			33 s
			33 s
			5 min
			1 min 30 s
				Coat recipe: No.8
				Development recipe: No.21
				
				Lazer microscope
				L/S Size: _____um
				Wf No._____
				Top_____
				Center_____
				Bottom_____
				Left_____
				Right_____
				Average_____

71	ND I/I	As 85 keV, 4.0×10^{15} cm^{-2}		
72	PR removal	O2 ashing SPM	30 min 10 min	
73	Cleaning	APM (1:1:6) 70 deg C DIW overflow HPM (1:1:6) 70 deg C DIW overflow Spin dry	10 min 10 min 10 min 10 min	

74	TEOS depo.	LPCVD
		    706 deg C, 0.3 Torr
		    TEOS = 30 sccm, O$_2$ = 0.3 l/min
				thickness:500 nm

75	Thickness check	Optical measurement Wf No._____ Top_____ Center_____ Bottom_____ Left_____ Right_____ Average_____		T7:TEOS
76	TEOS densify anneal	OX4: 1,000 deg C Anneal N$_2$:250 l/hr	20 min	
77	Thickness check Sheet resistance	Optical measurement Wf No._____ Si3N4 Top_____ Center_____ Bottom_____ Left_____ Right_____ Average_____ Sheet resistance Top_____ Center_____ Bottom_____ Left_____ Right_____ Average_____		T7:TEOS T1:nMOS S-D T3:Capacitor T6:pMOS S-D

78	Cont. photo	OAP-bake: 160 deg C
		OAP coat
		    1st 500 rpm
		    2nd 3,000 rpm
		PR coat: THMR-iP3100HS LB 15 cp
		    1st 500 rpm
		    2nd 3,000 rpm
		Coat-bake: 110 deg C
		Expose: i-Ray stepper
		Development: NMD
		Rinse: DW
		Dev-bake: 120 deg C
		O2 asher
			90 s
			
			5 s
			30 s
			
			5 s
			25 s
			90 s
			(300 ms)
			33 s
			33 s
			5 min
			1 min 30 s
				Coat recipe: No.8
				Development recipe: No.21
				
				Lazer microscope
				L/S Size: _____um
				Wf No._____
				Top_____
				Center_____
				Bottom_____
				Left_____
				Right_____
				Average_____

79	SiO$_2$ removal	RIE (rank A) + BHF		T7:Etch rate
80	Etch check	Optical measurement Wf No._____ Top_____ Center_____ Bottom_____ Left_____ Right_____ Average_____		Main wafer
81	PR removal	SPM 120 deg C (3:1 = H2SO4:H2O2) DIW	10 min 10 min	
82	Cleaning	APM (1:1:6) 120 deg C DIW overflow HPM (1:1:6) 120 deg C DIW overflow DHF (1:50) DIW overflow Spin dry	10 min 10 min 10 min 10 min 20 s 5 min	
83	Al depo.	target: Al-1% Si Ar 0.5 Pa (50 sccm), RF 1 kW	16 min	thickness: 1um
84	Thickness check	Optical measurement Wf No._____ Top_____ Center_____ Bottom_____ Left_____ Right_____ Average_____		T8:Al

85	Al photo	OAP-bake: 160 deg C
		OAP coat
		    1st 500 rpm
		    2nd 3,000 rpm
		PR coat: THMR-iP3100HS LB 15 cp
		    1st 500 rpm
		    2nd 3,000 rpm
		Coat-bake: 110 deg C
		Expose: i-Ray stepper
		Development: NMD
		Rinse: DW
		Dev-bake: 120 deg C
		O2 asher
			90 s
			
			5 s
			30 s
			
			5 s
			25 s
			90 s
			(300 ms)
			33 s
			33 s
			5 min
			1 min 30 s
				Coat recipe: No.8
				Development recipe: No.21
				
				Lazer microscope
				L/S Size: _____um
				Wf No._____
				Top_____
				Center_____
				Bottom_____
				Left_____
				Right_____
				Average_____

86	Al etch (+ O2 Asher)	RIE (rank B)	10-13 min	etch rate:test wafer
87	Etch check	Optical measurement Wf No._____ Top_____ Center_____ Bottom_____ Left_____ Right_____ Average_____		Main wafer
88	PR removal	O$_2$ asher	30 min	
89	check characteristics			

Post CMOS Process

No.	Step	Conditions	Time	Specs
1	Al-1%Si removal	RIE (Metal) SF_6 = 10sccm, 5 Pa, 100 W	1 min	
2	H_2 anneal	H2 Anneal furnace 400 deg. C, H_2 = 120 ml/min, N_2 3l/min	30 min	for sintaring
3	SiN depo.	P-CVD SiH4/N2 = 117 sccm, NH3 = 6 sccm, N2 = 183 sccm, 100 W, depo = 100Pa, 300 deg. C	27 min	thickness 1.0 um

4	SiN photo	OAP-bake: 160 deg C
		OAP coat
		    1st 500 rpm
		    2nd 3,000 rpm
		PR coat: THMR-iP3100HS LB 15 cp
		    1st 500 rpm
		    2nd 3,000 rpm
		Coat-bake: 110 deg C
		Expose: i-Ray stepper
		Development: NMD
		Rinse: DW
		Dev-bake: 120 deg C
		O_2 asher
			90 s
			
			5 s
			30 s
			
			5 s
			25 s
			90 s
			(300 ms)
			33 s
			33 s
			5 min
			1 min 30 s
				Coat recipe: No.8
				Development recipe: No.21

5	SiN etch	RIE (Metal) CF4 20sccm 10 Pa, 100 W		
	etch check			T1:etch rate
6	PR removal	O2 asher	30 min	
7	H2 anneal	H2 Anneal furnace 400 deg. C, H_2 = 120 ml/min, N_2 3l/min	30 min	for Vth cure

8	Pt photo	LOR30B-bake: 170 deg C
		LOR coat
		    1st 500 rpm
		    2nd 4,500 rpm
		Coat-bake: 170 deg C
		
		PR coat: THMR-ip3100HS LB 15 cp
		    1st 500 rpm
		    2nd 3,000 rpm
		Coat-bake: 110 deg C
		Expose: i-Ray stepper
		Development: NMD
		Rinse: DW
		Dev-bake: 120 deg C
		O2 asher
			5 min
			
			5 sec
			45 sec
			5 min
			
			5 s
			25 s
			90 s
			(300 ms)
			33 s
			33 s
			5 min
			1 min 30 s	

9	Ti sputter	multi-target sputter 0.2 Pa, 0.2 kW, Rot	20 min	
10	Pt sputter	Pt sputter 0.5 Pa, 50 kW	100 min	ステージ温度が上がり過ぎないように注意
	thickness check			T2:Pt
11	Lift off	Remover PG IPA rinse		

12	Au Photo	LOR30B-bake: 170 deg C
		LOR coat
		    1st 500 rpm
		    2nd 4,500 rpm
		Coat-bake: 170 deg C
		
		PR coat: THMR-ip3100HS LB 15 cp
		    1st 500 rpm
		    2nd 3,000 rpm
		Coat-bake: 110 deg C
		Expose: i-Ray stepper
		Development: NMD
		Rinse: DW
		Dev-bake: 120 deg C
		O2 asher
			5 min
			
			5 sec
			45 sec
			5 min
			
			5 s
			25 s
			90 s
			(300 ms)
			33 s
			33 s
			5 min
			1 min 30 s	

13	Ti sputter	multi-target sputter 0.2 Pa, 0.2 kW, Rot	20min	
14	Au Depo.	Au Deposition machine	(6 min)	thickness 250-300nm
15	Lift off	Remover PG IPA rinse		Don't use ultrasonic cleaner
16	SiO passivation	PECVD (rank C)		聞く 800nm
17	SiN passivation	PECVD (rank C)		聞く 300nm T3:etch rate
	thickness check			T3:SiN,SiO

18	PR WP
	(Waterproof)
		PR coat: THMR-ip3100HS LB 15 cp
		    1st 500 rpm
		    2nd 2,500 rpm
		Coat-bake: 110 deg C
		Expose: i-Ray stepper
		Development: NMD
		Rinse: DW
		Dev-bake: 120 deg C
		O2 asher
			5 s
			25 s
			90 s
			(300 ms)
			33 s
			33 s
			5 min
			1 min 30 s	

19	SiN etch	RIE (samco, rank C)		聞く
20	SiO etch	RIE (samco, rank C)		聞く T3:etch rate
21	PR removal	O2 asher	30 min	
22	dicing	Lazer dicer		

Appendix C

Device Fabrication and Chip Layout

1. Fabrication:

The proposed sensor chips are fabricated at the LSI fabrication center of Toyohashi University of Technology and the LAPIS Semiconductor Co., Ltd. The device was fabricated on the basis of the standard CMOS process and post CMOS process. The post CMOS process includes the formation of a sensing area and passivation layers. It was fabricated as an n-type silicon wafer. The CMOS circuits were fabricated by ion implantation, oxidation, and photolithography. Then, a platinum layer was sputtered, followed by titanium sputtering. The titanium layer was used as an adhesive layer. Electrodes were patterned using a lift-off method. Finally, all the chip surfaces except the electrodes were covered with silicon nitride and silicon oxide to protect the circuits from the solution under investigation. The chip was mounted and wire-bonded to a 64-pin package. The pads and package were connected through 20-μm-diameter gold wires. The wires were encapsulated with epoxy to avoid unwanted contacts and create a sample well of about 50 μl.

2. Chip Layout:
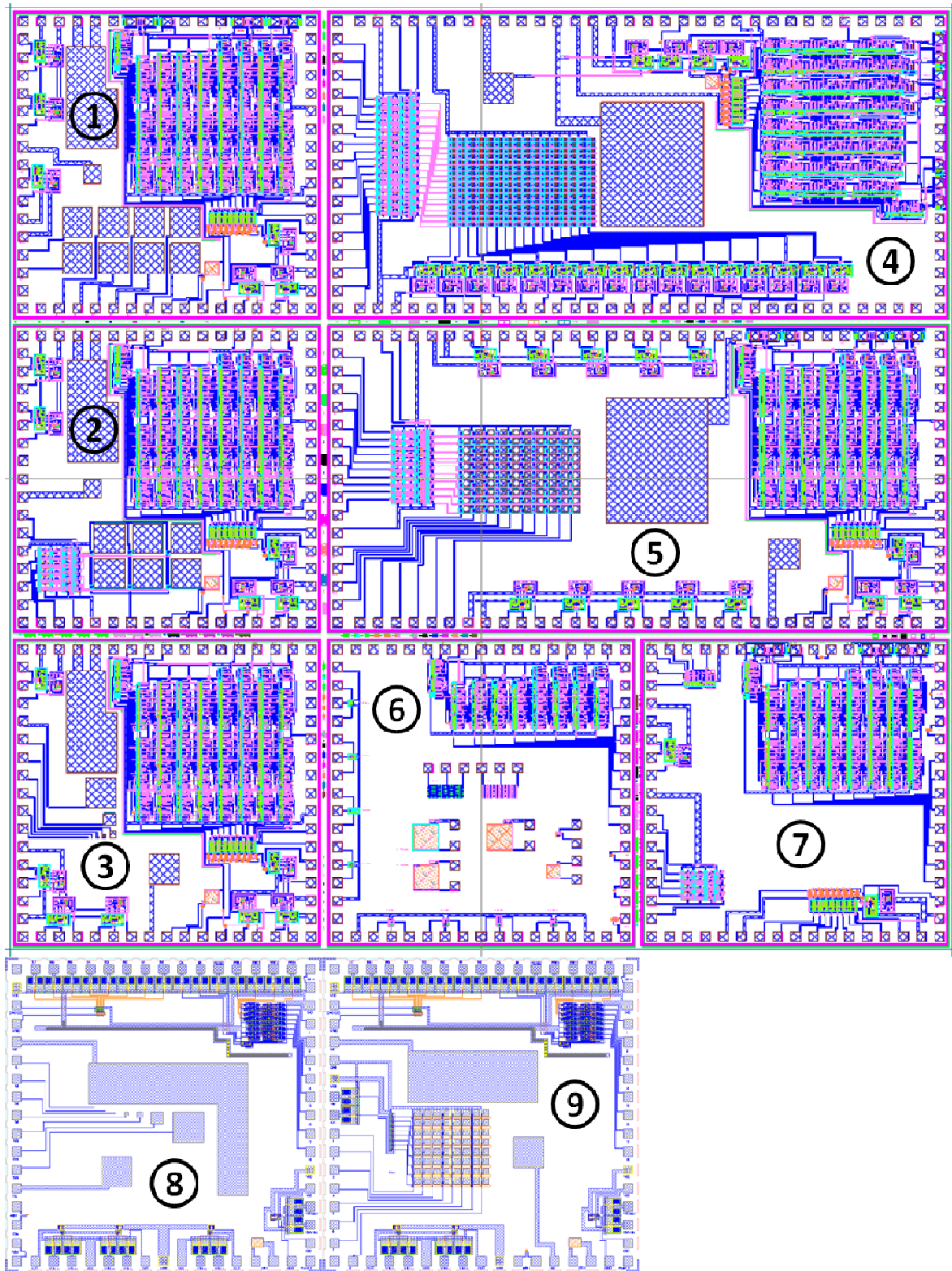
The chip sizes are 5 x 5 mm^2 and 5 x 10 mm^2. From chip 1 to chip 7, it is designed by 5-μm-rule process which is fabricated at the LSI fabrication center of Toyohashi University of Technology. Chip 8 and 9, 2-μm-rule is used which is fabricated at the LAPIS Semiconductor Co., Ltd.

Chip 1: Multi-target and low concentration measurement. Each size of 8 working electrodes is 500 x 500 μm^2. Square wave pulse generator with six OPAMPs.

Chip 2: A 2 x 3 array sensor chip with shift resistor. Only one output pad is needed by using the shift resistor. The size of the working electrode is 500 x 500 μm^2. For low concentration measurement.

Chip 3: Single electrode chip. Each working electrode is divided according to the size. The size of the working electrode is from 5 x 5 μm^2 to 500 x 500 μm^2. It might be applied to EC sensor.

Chip 4: A 16 x 16 array sensor chip. This chip has all of the components to conduct square wave voltammetric measurement, so that it does not need any external connecting line. The size of the working electrode is 50 x 50 μm^2. Each 16 lines of array pixels are connected to their own I-V converters. There are 16 I-V converters on this chip, and 16-bit shift resistor.

Chip 5: A 10 x 10 array sensor chip. Analog circuit and digital circuit are separated. External connecting wire is needed to connect the whole circuit. There are 10 I-V converters for read out. This chip can check the characteristics of analog and digital circuits, separately.

Chip 6 and Chip 7: TEG chip for the evaluation and the feedback of the fabricated sensor. This chip consists of a counter A, a shift resistor, OPAMP, D flip flop, DAC, square wave pulse generator, nMOS, pMOS, and MOSCAP.

Chip 8: Single electrode chip. Each working electrode is divided according to the size. The size of the working electrode is from 5 x 5 μm^2 to 500 x 500 μm^2. There are four OPAMPs which are fabricated by 2-μm-rule.

Chip 9: An 8 x 8 array sensor. There are 8-bit shift resistor and 8 output pads. External read out circuit of 8 I-V converters is needed. There are two OPAMPs as a voltage shifter and a voltage controller at the potentiostat.